N73-14217
NASA CR-121114

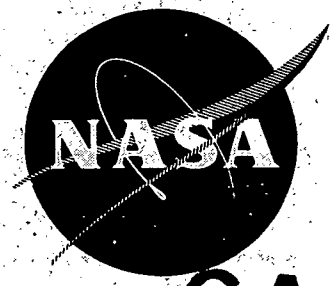

REFOCUSING OF THE SPENT AXISYMMETRIC BEAM IN KLYSTRON TUBES

by

Dr. G. M. Branch and W. Neugebauer

GENERAL ELECTRIC COMPANY

prepared for

NATIONAL AERONAUTICS AND SPACE ADMINISTRATION

NASA Lewis Research Center
Contract NAS3-8999
Dr. H. G. Kosmahl, Project Manager

NOTICE

This report was prepared as an account of Government-sponsored work. Neither the United States, nor the National Aeronautics and Space Administration (NASA), nor any person acting on behalf of NASA:

A.) Makes any warranty or representation, expressed or implied, with respect to the accuracy, completeness, or usefulness of the information contained in this report, or that the use of any information, apparatus, method, or process disclosed in this report may not infringe privately-owned rights; or

B.) Assumes any liabilities with respect to the use of, or for damages resulting from the use of, any information, apparatus, method or process disclosed in this report.

As used above, "person acting on behalf of NASA" includes any employee or contractor of NASA, or employee of such contractor, to the extent that such employee or contractor of NASA or employee of such contractor prepares, disseminates, or provides access to any information pursuant to his employment or contract with NASA, or his employment with such contractor.

Requests for copies of this report should be referred to

National Aeronautics and Space Administration
Scientific and Technical Information Facility
P.O. Box 33
College Park, Md. 20740

NASA CR- 121114

FINAL REPORT

REFOCUSING OF THE SPENT AXISYMMETRIC BEAM IN KLYSTRONS

by

Dr. G. M. Branch
and
W. Neugebauer

GENERAL ELECTRIC COMPANY
Tube Products Department
Microwave Tube Operation
Schenectady, New York

prepared for

NATIONAL AERONAUTICS AND SPACE ADMINISTRATION

June 30, 1972

CONTRACT NAS3-8999

NASA Lewis Research Center
Cleveland, Ohio
Dr. H. G. Kosmahl, Project Manager
Spacecraft Technology Division

FOREWORD

The work described herein was performed by the General Electric Microwave Tube Operation under NASA Contract NAS3-8999 with Dr. G. M. Branch and Mr. Wendell Neugebauer as principal investigators, assisted by Dr. E. J. Craig. Dr. H. G. Kosmahl, Spacecraft Technology Division, NASA-Lewis Research Center, was Project Manager.

TABLE OF CONTENTS

	Page
SUMMARY	1
INTRODUCTION	3
DIGITAL COMPUTER METHODS FOR SPENT-BEAM TRAJECTORY ANALYSIS	6
Ring Model of the Electron Beam	6
Kinematic Equations and Normalized Variables	7
Computation of Space-Charge Forces for the Ring Model	9
Test of Space-Charge Model	14
Test of Ring Model in Klystron Bunching Calculation	17
Gap Field Formulas	20
Description of Fortran Program for Spent-Beam Trajectory Computations	22
Ring Location and Trajectory Plotting Program	23
ANALOG COMPUTER PROGRAM FOR SPENT-BEAM ANALYSIS	28
Magnetic-Field Model	28
Equations of Motion	32
Evaluation of the Electric Field	33
Axial Motion	34
Evaluation of a Simple Magnetic Lens for Refocusing	35

Page

STUDY OF REFOCUSING METHODS 37

Development of Tables of Initial Disk Velocities and Locations 37

Ring-Model Study of Output Gap Interaction 38

Quadrupole-Doublet Refocusing Lens 42

Conical-Grid Refocusing Lens 47

Permanent-Magnet-Wedge Refocusing System 47

Beam Expansion in a Shaped-Axial Magnetic Field . . 53

Refocusing in Tapered-Axial-Magnetic Fields 56

Refocusing in Tapered-Axial-Magnetic Fields Combined with Theta Fields 59

STATISTICAL EVALUATION AND DISCUSSION OF RESULTS 64

Selection of Refocusing Methods 64

Statistical Comparison of Hybrid and Tapered-Field Refocusing Systems 64

Physical Design Refocusing Systems 69

GENERAL PARAMETRIC SURVEY OF REFOCUSING CHARACTERISTICS 71

Development of Basic Satellite-Borne Klystron Designs at 12 GHz 71

Statistical Analysis of the Refocused Trajectories . . 75

CONCLUSIONS 96

Appendix A - Calculation of the Space-Charge Forces in a Klystron Beam A-1

Appendix B - Table of Final Radii, Velocities, Angles and Energies B-1

Appendix C - Statistical Tables of Beam Properties Before and After Refocusing C-1

SYMBOLS

REFERENCES

ABSTRACT

Analytic methods were developed and employed to optimize the magnetic field transition region between the output interaction gap of a klystron and a multi-stage depressed potential electrostatic beam collector, in order to enhance the power conversion efficiency of satellite-borne broadcast transmitters. Permanent magnet structures were designed to provide the magnetic field distributions required to expand and recollimate the spent electron beam of the power amplifier klystron for proper entry into the beam collector. These design criteria for magnetic field distributions for expanding and recollimating spent-beam electrons for optimal entry into a multi-stage depressed potential collector are generally applicable to traveling-wave tubes as well as klystrons.

SUMMARY

In order to enhance the power-conversion efficiency of a satellite-borne broadcast transmitter klystron by means of an optimized magnetic field transition between the output cavity and a multi-electrode depressed potential beam collector, analytic methods were developed and used in a detailed study of electron trajectories in the output transition region of klystrons. Both analog and digital computer programs are described and the application of these programs to the study of klystrons with parameters typically of interest for satellite-borne transmitter applications is reported. Although a novel method of generating a refocusing transverse axisymmetric magnetic field was conceived and studied during this investigation, it was found that a more easily developed tapered magnetic field distribution with only radial and axial components can lead to equally effective beam expansion and recollimation for low-angle injection of the expanded spent beam into a multi-stage depressed collector. A specific tapered magnetic field configuration was developed which gives good refocusing characteristics for both high-efficiency and low-efficiency klystrons. The proposed methods of beam expansion and recollimation for entry into a multi-stage collector are generally applicable to traveling-wave tubes as well as klystrons.

Page Intentionally Left Blank

INTRODUCTION

An analytic study of the problem of expanding and recollimating the spent electron beam in klystron amplifiers was begun on December 19, 1969 by the Microwave Tube Operation of the General Electric Company under NASA Contract NAS3-8999. Both analog and digital computer methods were developed for the detailed study of electron trajectories in a transition region between the output gap and final beam collector of a klystron. The computer programs were subsequently employed to study methods of refocusing the spent electron beam in a klystron with design parameters lying in the range of interest for satellite-borne broadcast transmitters. Although the specific objective of this study was to develop methods for designing the optimum transition region between the output cavity and a multi-stage depressed collector in a space-borne klystron, the techniques reported here may be used to improve the design of power amplifier klystrons and traveling-wave tubes for any land-based, ship-based or airborne microwave system.

In previous studies of multi-stage depressed potential collectors for klystrons carried out both at NASA-LeRC and at the General Electric Company under NASA Contracts NAS3-11530 and NAS3-11532, it was found that improved operating characteristics could be expected in such collectors if the spent electron beam could be expanded to a larger diameter to reduce its space charge density and also recollimated with the elimination of radial components of velocity before injection into the collector.[1,2,3] Because high power conversion efficiency is paramount in satellite-borne transmitters, the development of an effective magnetic field transition region between the active rf structure of the klystron (where a strong axial field is required for beam collimation) and the final collector (where negligible magnetic fields are required) is a desirable step in a continuing program to achieve higher efficiencies in klystrons.

Both analog and digital computer methods were developed for the study of electron beam trajectories in the transition region. An analog computer is capable of rapidly and economically providing plots of electron trajectories in fields with parameters which may be quickly adjusted and the distribution may be conveniently altered as indicated by inspection of a given trajectory plot. Since the number of parameters or variables handled by analog computers is generally limited, various approximations must be made in the computer simulation of the refocusing problem. Alternatively, the digital computer can provide much greater detail and accuracy in a more complete and complex simulation of the problem, but

is considerably more expensive. Because of the anticipated time required to make an accurate trajectory computation with a digital computer, an extensive effort was applied in the early part of the contracted study to develop an accurate computer simulation that could be calculated with high speed. Although a space-charge algorithm for the ring model of the electron beam was developed that was 17 times faster in execution than the conventional Green's Function approach, it proved far more economical to use the analog computer in a screening of the refocusing properties of the various field distributions proposed for the transition region. The digital computer program employing the ring model of the electron beam was used primarily for the study of the radial and axial acceleration of electrons in traversing the output gap of a klystron and to supplement analog computations of the flight of the electron rings from the output gap through the transition region.

The General Electric Multicavity Klystron Simulation program was used to develop designs of klystrons having parameters in the range of interest for a satellite-borne broadcast transmitter.[4] The klystrons were designed to have power outputs between 1 and 4 kW at a frequency of 12.00 GHz over bandwidths of 40 to 120 MHz. Tables of typical velocity spectra at both band edges as well as at band center were prepared for use with the refocusing computer programs. The ring-model digital computer program was used to portray the radial and axial motions of electrons through the combined magnetic and electric fields in the output gap of the klystron and to generate a table of radial and axial ring velocities after traversal of the gap. The table of velocities of the spent beam electrons after traversing the output gap were then used as inputs to the analog computer which implemented the further trajectory calculation of each of the rings through the relatively long transition region to the entrance aperture of the collector.

Two types of field distributions in the transition region were considered. The first distribution, referred to as the Hybrid-Field Distribution, consists of a rapid reduction of the main collimating axial magnetic field distribution to zero amplitude, followed by a shaped region containing a circumferential or theta magnetic field component. The second field distribution, identified as the Tapered-Field Transition Distribution, was also studied in detail. It consists of a diminishing magnetic field with only axial and radial components, beginning with an axial field component having the same magnitude as the main collimating field, and decaying to an intermediate amplitude. After a short plateau at this amplitude to allow optimum collimation of the expanded beam, the field is forced to decay rapidly to a negligible amplitude at the entrance to the collector. Both long tapered beam expansion regions of the order of two or more cyclotron wavelengths, as proposed by Dr. H. G. Kosmahl of NASA-LeRC,[5] as well as short regions of less than one cyclotron

wavelength were considered. Both the hybrid- and the tapered-field distributions were found to yield good beam expansion and recollimation. The latter distribution may be preferred because it requires relatively simple pole pieces and shielding whereas the hybrid distribution requires wedges of magnetic material placed within the beam.

A representative comparison of the properties of the hybrid and tapered refocusing field distributions may be made for the klystron with a collimating field equal to the Brillouin field strength: at midband the hybrid field distribution yields an rms beam expansion ratio of 9.7 with an average injection angle into the collector of 2.0 degrees, a standard deviation of 4.1 degrees and a maximum angle of 21.3 degrees; the tapered field distribution yields a beam expansion ratio of 7.1 with an average injection angle into the collector of 3.8 degrees, a standard deviation of 3.0 degrees and a maximum angle of 12.2 degrees. The low value of standard deviation of the injection angle of all electrons shows that in both cases most electrons have injection angles near the average angle and that relatively few have large angles.

Following a demonstration by computer simulation which showed that satisfactory refocusing could be achieved with a tapered magnetic field in a beam expansion region followed by a short magnetic field plateau in a beam stabilization region, an extensive study was made of various magnetic field refocusing configurations. Twenty different field configurations for six high-efficiency klystrons and one low-efficiency klystron were investigated. Of the 40 complete cases studied, 24 yielded good refocusing with the creation of a slightly diverging beam, and 10 yielded good refocusing with the creation of a non-diverging beam. Design specifications were established for refocusing field configurations providing the required beam expansion and subsequent recollimation to produce either a slightly diverging beam or a non-diverging beam at the entrance aperture of the collector, as required.

DIGITAL COMPUTER METHODS FOR SPENT-BEAM TRAJECTORY ANALYSIS

RING MODEL OF THE ELECTRON BEAM

Since all the phenomena are cyclical in a klystron operating under steady-state conditions, the characteristics of the spent electron beam may be studied by confining attention to the electrons in one rf cycle. Before the beam is modulated, the electrons occupy a cylindrical volume of radius b (the beam radius) and length equal to one wavelength along the beam (the distance traveled by any given electron during one rf cycle). In the disk model of the electron beam, this wavelength of charge is divided equally into a number of disks, typically 20, as illustrated in Figure 1. If radial

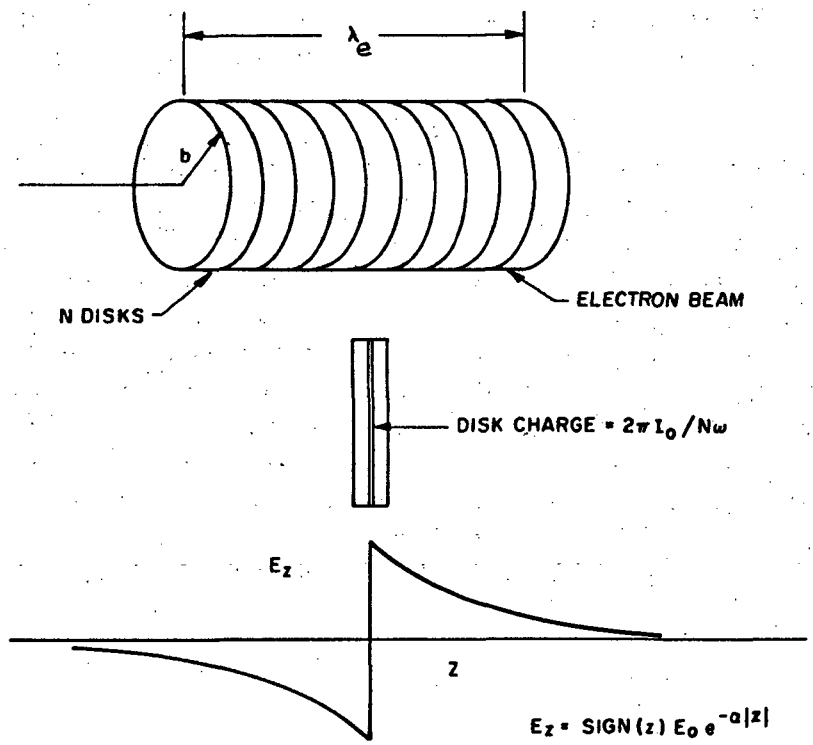

Figure 1 - Disk Model of Electron Beam (Division of One Wavelength into N Disks and Sketch of Axial Field Variation of Single Disk)

motions are not important, as in the case of a well-collimated and confined electron beam in the bunching portion of a klystron, the one-dimensional disk model provides an adequate simulation for the computation of the cascade bunching process in a multicavity klystron. In the output gap and post-output gap region where the collimating magnetic field is terminating, radial motions are very important and must be computed in the analysis of the refocusing effects of any given magnetic field distribution. Radial accelerations caused by circuit fields in the output interaction gap and space charge, must be computed and the corresponding radial velocity components and radial positions integrated. For accurate radial space charge force computations the electron disks should be further subdivided into rings. Usually each disk is divided into 3 to 5 rings, but since the time consumed in computing space charge forces is proportional to the square of the number of rings, the greater accuracy resulting from a larger number of rings is achieved at a much greater cost in terms of computer time.

KINEMATIC EQUATIONS AND NORMALIZED VARIABLES

Kinematic equations for the non-relativistic motion of electron rings were developed and a general normalization of variables was derived. Since only low power klystrons and low voltage electron beams were considered in the refocusing study, non-relativistic equations were adequate and a saving of about a factor of two in computation time ensued. The trajectories of a point lying on the radius of gyration of each ring was computed by a two-stage integration of the acceleration by a Runge-Kutta fixed time-step integration method.

The axial and radial acceleration components of an electron lying on the radius of gyration r of an electron ring are given by:

$$\ddot{z} = \frac{-e}{m} (E_z - r\dot{\theta} B_r) \tag{1}$$

$$\ddot{r} = \frac{-e}{m} (E_r + r\dot{\theta} B_z) + r\dot{\theta}^2 \tag{2}$$

where z is the axial position of the electron ring; E_z, B_z, E_r, and B_r are the axial and radial components of the local electric and collimating magnetic fields; and $r\dot{\theta}^2$ is the centrifugal force on the spinning ring. Because of the low power of the electron beam and the assumed axial symmetry of the interaction gaps, the circumferential components of both the electric and induced magnetic fields are assumed to be negligibly small. The angular

velocity of the spinning ring, $\dot{\theta}$, is computed directly from the collimating magnetic field by invoking Busch's Theorem, which states that:

$$\dot{\theta} = \frac{\frac{e}{m}}{2} \left[B_z - (r_c/r)^2 B_c \right] \tag{3}$$

where r_c is the radius of emission of the electron from the cathode and B_c is the magnitude of the magnetic field at the cathode.

These equations and the loci of the ring trajectories may conveniently be expressed in terms of normalized variables to provide more universal curves. It is useful to normalize all distances to the beam tunnel radius a and to normalize time in terms of the rf radian frequency ω. The magnetic fields are conveniently expressed in terms of the local cyclotron frequency ω_c, where

$$\omega_c = eB/m \tag{4}$$

which frequency may be normalized to the signal frequency as:

$$\Omega_c = \omega_c/\omega = eB/(m\omega) \tag{5}$$

Similarly, since both the square of the unreduced plasma frequency and the space-charge forces are proportional to the initial beam density and hence the charge contained in each ring, the space-charge forces may be normalized with respect to the square of the normalized plasma frequency Ω_p. With this normalization, the kinematic equations for electron rings in the absence of applied circuit fields become:

$$\ddot{Z} = -(E_Z/N\beta a)\, \Omega_p^2 + R\Omega_s \Omega_r \tag{6}$$

$$\ddot{R} = -(E_R/N\beta a)\, \Omega_p^2 + R\Omega_s (\Omega_s + \Omega_z) \tag{7}$$

$$\Omega_s = (\Omega_z - (R_c/R)^2 \Omega_k)/2 \tag{8}$$

where N = the total number of rings per wavelength

$\beta = \omega/u_o$

a = tunnel radius

R = r/a, normalized ring radius of gyration

$\Omega_s = \dot{\theta}/\omega$

$\Omega_r = eB_r/m\omega$

$\Omega_z = eB_z/m\omega$

R_c = normalized radius of emission at cathode

$\Omega_k = eB_k/m\omega$, where B_k is the magnetic field at the cathode

E_Z = normalized axial component of space-charge field

E_R = normalized radial component of the space-charge field

If during their trajectories the electron rings enter an interaction region where rf fields from a klystron cavity exist, E_Z and E_R above must be augmented by the corresponding local values of the time-dependent axial and radial circuit fields. The space-charge force model and the klystron interaction gap-field model will be discussed below.

COMPUTATION OF SPACE-CHARGE FORCES FOR THE RING MODEL

The ring-model computer program assumes that the radial and axial motion of electrons in an electron beam under combined space charge, cavity rf fields and superimposed dc magnetic and electric fields can be adequately represented by a ballistic calculation of the trajectories of electron rings representing annular portions of the beam. Before rf modulation, the dc electron beam is divided into N disks per wavelength and each disk is then subdivided into J annular volumes. The length of each disk or ring in terms of the average axial component of velocity $\dot{z}$ of the corresponding electrons is given by

$$w = 2\pi \dot{z}/N\omega \tag{9}$$

where ω is the angular frequency of the rf modulation. The width of the ring is thus a variable and is directly proportional to the instantaneous velocity of the ring. On the other hand, the product βw is a constant, $2\pi/N$, where β is the propagation constant $\omega/\dot{z}$. The charge enclosed is a disk is

$$Q_D = -2\pi I_o/N\omega \tag{10}$$

and the charge enclosed in the annular volume of a ring is

$$Q_R = -2\pi I_o/JN\omega \tag{11}$$

where I_o is the beam current. Since the total charge enclosed within the annular volume of the ring is a constant, the space charge density in the ring varies inversely with the volume of the ring.

Independent variables for describing the trajectories of each ring are the radius of its centroid (rms radius) and its axial position z with respect to a reference plane such as the midplane of the output circuit interaction region. For a given ring, the inner and outer radius r_i and r_o are given by constant ratios with respect to the rms radius r. Let k be an index for the rings from a given original disk, with k ranging from 1 for a central inner disk to J for the outer ring. Each of the rings will have a volume 1/J th that of the disk and hence the cross-sections of the rings will have equal areas. The centroid radius of the kth ring relative to the beam outer radius b is therefore given by

$$r_k/b = \sqrt{(2k-1)/2J} \tag{12}$$

and the ratio of the inner and outer radius of the annular volume of ring k to its rms radius r_k are given by

$$r_i/r_k = \sqrt{(2k-2)/(2k-1)} \tag{13}$$

$$r_o/r_k = \sqrt{2k/(2k-1)} \tag{14}$$

An approximate method for computing the space charge forces between rings of charge is required since the exact Green's function solution for the electric fields generated by a ring of charge is expressed in an often slowly converging infinite series of terms containing Bessel functions. An approximate solution based on more readily evaluated elliptic integrals was derived from a mirror image model.

Since no clearly defined image of a ring of charge centered in a conducting tunnel exists, an approximate mirror image had to be devised. This was done by postulating the existence of a positively-charged image at a radius greater than the tunnel radius and computing the location of a zero

equipotential in the vicinity of the actual tunnel wall. The location of this equipotential then defines a conducting surface which will provide the desired mirror image of the negatively charged ring. Figure 2 shows a sketch of the equipotential surface that defines the reflecting surface for a given charged ring. The actual location of the surface depends slightly on the radius of the ring relative to the tunnel radius; however, an average location has been found to yield sufficiently sharp images for rings of any radius. Complete analytical details are given in Appendix A.

Expressions for both the radial and axial field components generated by an electron ring in the conducting surface (shown in Figure 2) were programmed and the resulting field distributions were computed as a function of radius r and distance z from the plane of the ring. Also, the Green's function solution containing series of Bessel's functions were programmed and computed. A comparison of the field components computed by the elliptic integral expressions and by the Bessel function expressions for a ring of charge of radius equal to 0.4 times the tunnel radius is given in Table I.

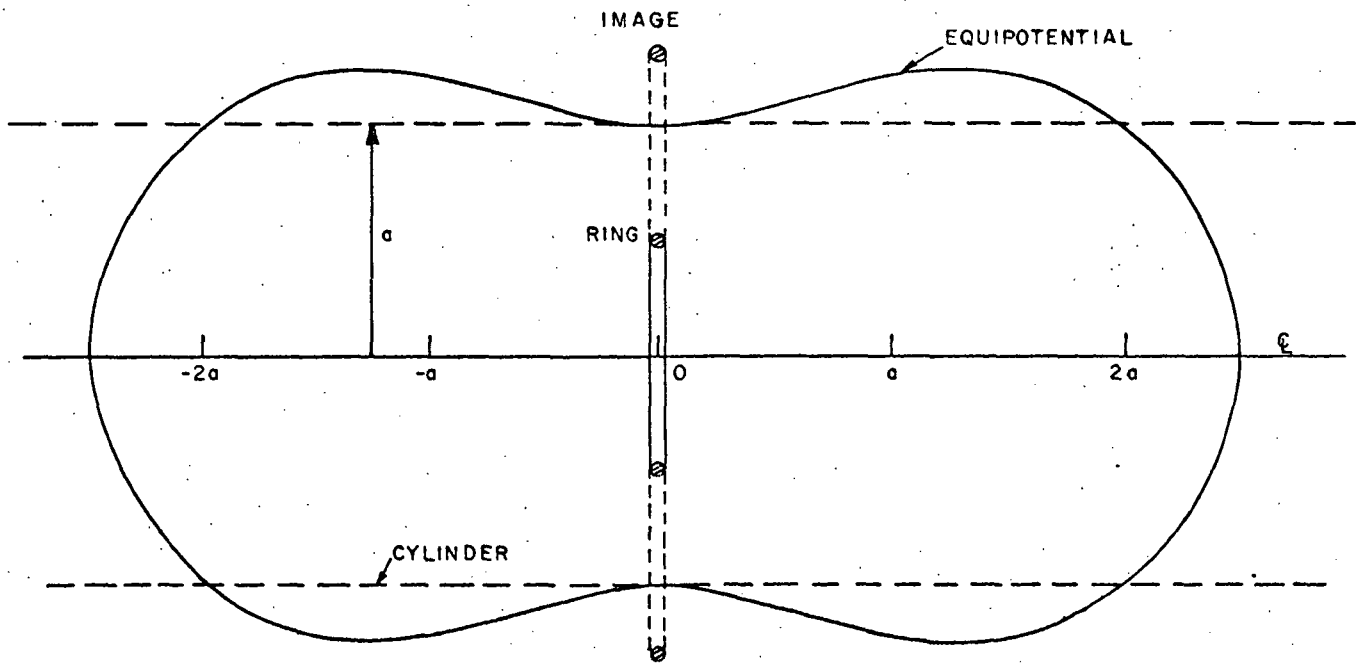

Figure 2 - Sketch of Zero Equipotential Derived from a Ring and Its Image

TABLE I - RADIAL AND AXIAL COMPONENTS OF THE ELECTRIC FIELD (NORMALIZED) DUE TO A RING OF CHARGE COAXIAL WITH A CONDUCTING CYLINDER AND CENTERED AT THE ORIGIN. THE RING RADIUS IS 40 PERCENT OF THE CYLINDER RADIUS.

r/a	z/a	E_r		E_z	
		Bessel	Elliptic	Bessel	Elliptic
0.	0.04	0.	0.	0.937	0.936
	0.2	0.	0.	3.365	3.362
	0.4	0.	0.	3.206	3.199
	0.6	0.	0.	2.157	2.163
	0.8	0.	0.	1.350	1.370
	1.0	0.	0.	0.831	0.868
	1.2	0.	0.	0.512	0.558
	1.4	0.	0.	0.316	0.366
0.2	0.04	-3.053	-3.048	1.756	1.753
	0.2	-0.326	-0.323	4.510	4.501
	0.4	0.610	0.607	3.302	3.295
	0.6	0.494	0.487	2.071	2.075
	0.8	0.318	0.309	1.274	1.296
	1.0	0.196	0.189	0.783	0.821
	1.2	0.121	0.117	0.482	0.530
	1.4	0.074	0.073	0.297	0.349
0.4	0.04	5.434	5.448	31.325	31.324
	0.2	2.816	2.823	6.314	6.297
	0.4	1.620	1.611	2.989	2.973
	0.6	0.968	0.950	1.731	1.732
	0.8	0.586	0.567	1.050	1.074
	1.0	0.358	0.344	0.645	0.687
	1.2	0.219	0.213	0.398	0.451
	1.4	0.135	0.134	0.246	0.301
0.6	0.04	6.939	6.975	0.969	0.959
	0.2	4.221	4.238	2.458	2.418
	0.4	2.154	2.135	1.792	1.755
	0.6	1.236	1.199	1.140	1.134
	0.8	0.744	0.710	0.713	0.742
	1.0	0.455	0.434	0.443	0.495
	1.2	0.280	0.271	0.275	0.336
	1.4	0.173	0.174	0.170	0.232
0.8	0.04	3.446	3.549	0.171	0.144
	0.2	2.897	2.936	0.658	0.554
	0.4	1.943	1.894	0.704	0.624
	0.6	1.228	1.155	0.517	0.510
	0.8	0.766	0.710	0.340	0.386
	1.0	0.475	0.446	0.216	0.286
	1.2	0.294	0.286	0.135	0.210
	1.4	0.182	0.187	0.084	0.154

An inspection of the table shows that for the region close to the ring ($r/a = 0.4$, $z/a \leq 0.6$), where greatest accuracy is required, the elliptic integral result agrees with the exact Bessel function result within one percent. In the remainder of the region out to $z/a = 1.4$ where the fields have decayed in amplitude by more than an order of magnitude, the agreement remains quite good.

Since the field component computation by the elliptic integral method was measured to be 17 times faster than by the Bessel function method and since for close approaches of two rings the field is calculated to within one percent of the true value, the elliptical integral approach was adopted for the computation of space-charge forces between rings.

Because the annular volume of charge is represented by a one-dimensional ring, the space-charge model breaks down when two rings become too close to each other, the elliptic functions having a logarithmic singularity for zero separation of the two rings. Experience with computing electron disk or ring trajectories by the technique of advancing time in discrete steps has shown that often the close approach of two rings will result in an abnormally large repulsive force that causes the rings to be violently ejected into the drift tube wall. Since in a distribution of charge consisting of a cloud of real electrons such violent collisions practically never occur, a method of tapering the space charge forces between the synthetic rings of charge must be employed. This is accomplished by subdividing a pair of partially overlapping rings into non-overlapping rings and a completely coincident pair of rings.

With both the annular width and the thickness of the space-charge regions being variable in a dynamical calculation, twelve types of overlap have been identified. The space-charge subroutine was expanded with programming steps to identify each type of overlap when it occurred and to compute the correctly tapered force for each type. One type is illustrated in Figure 3 which shows two rings, A and B, having a simple corner overlap. The overlapping region comprises an annular region labelled "5" in the figure. The remaining non-overlapping regions of rings A and B are each subdivided into two annular rings with a rectangular cross-section. The force on Ring B is computed by summing the following:

a) Force of Subring 1 on all of the original Ring B;

b) Force of Subring 4 on all of Ring B;

c) Force of Subring 5 on Subring 3; and

d) Force of Subring 5 on Subring 2.

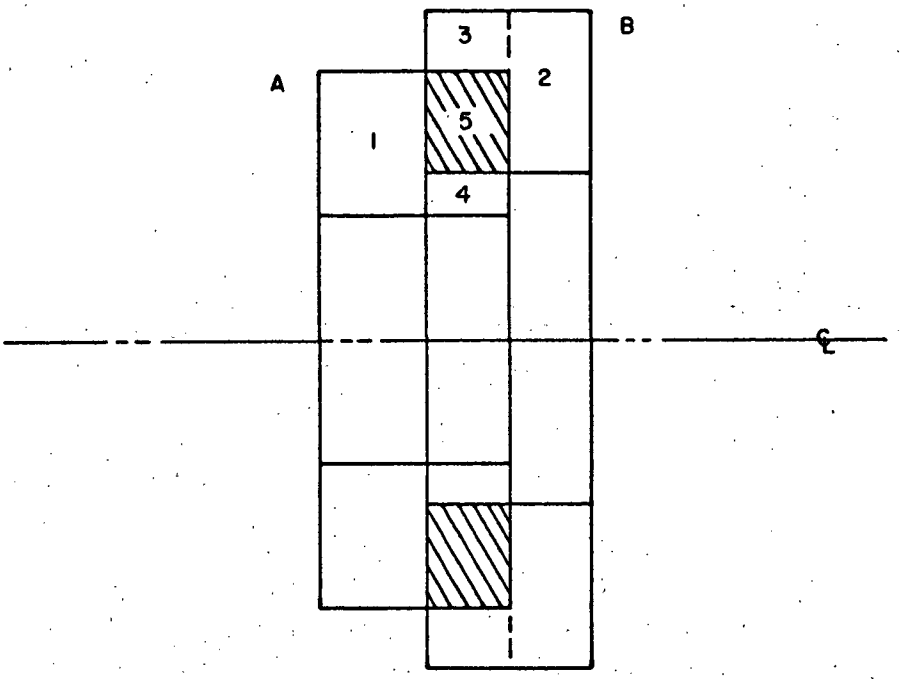

Figure 3 - Two Overlapping Rings, Showing Subdivision into Four Non-Overlapping Synthetic Rings and a Common Ring

When overlap occurs, the space charge subroutine computes the space-charge force from the non-overlapping subrings as illustrated in Figure 3 by cycling through the space-charge algorithm four times.

The radial variation of the axial component of the electric field of a ring of charge with a radius equal to 0.2 times the tunnel radius, with z/a as an independent parameter is plotted in Figure 4. Corresponding curves for the radial field variation are shown in Figure 5.

TEST OF SPACE-CHARGE MODEL

A dc test of the space-charge model and the corresponding subroutines was made by computing the components of electric force on a test ring of various widths (Δ_2 = .1a, .2a, and .4a, where a is the tunnel radius) as a function of radial position in an unmodulated electron beam. The beam was

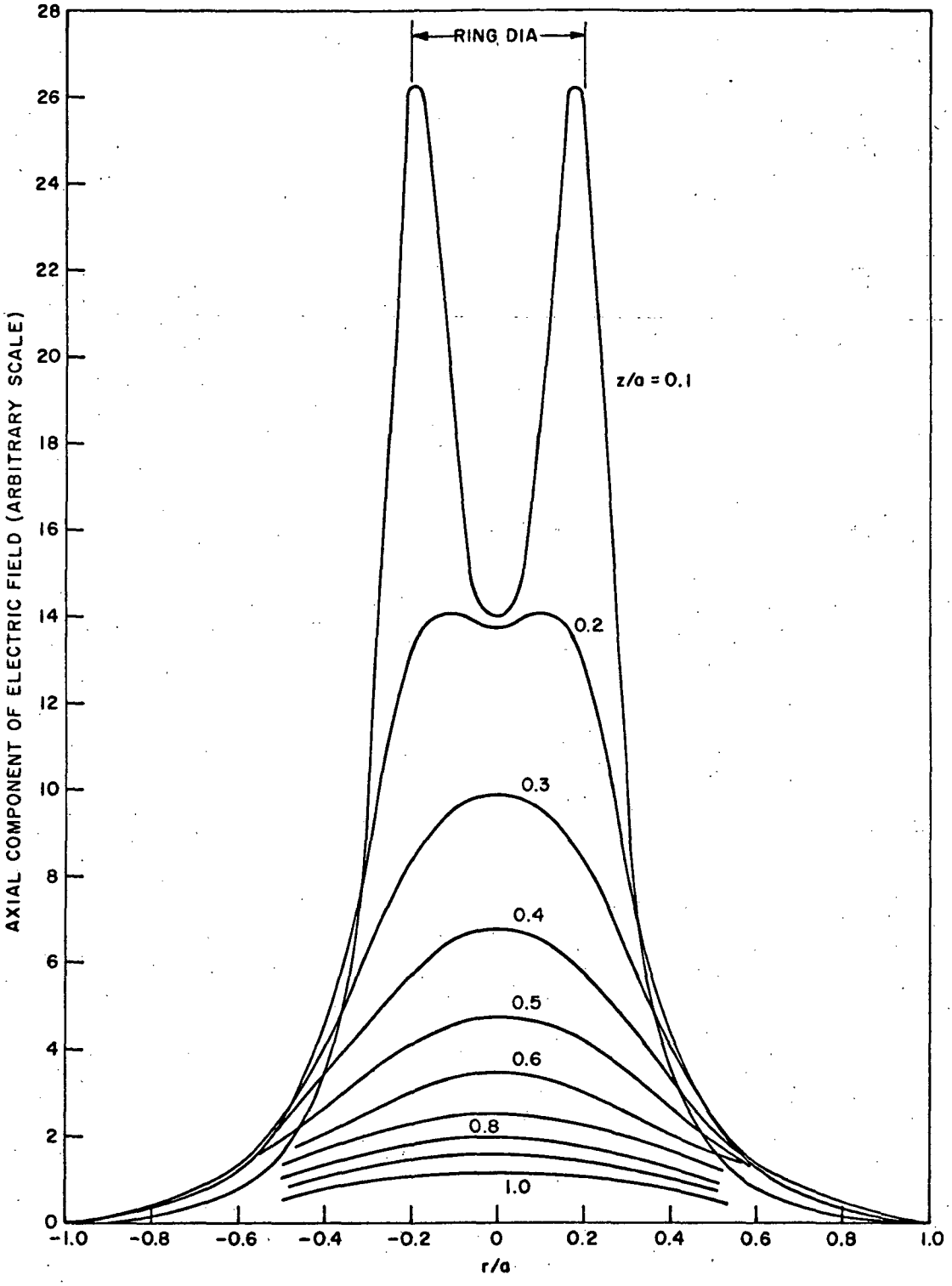

Figure 4 - Axial-Field Distribution Computed for a Charged Ring

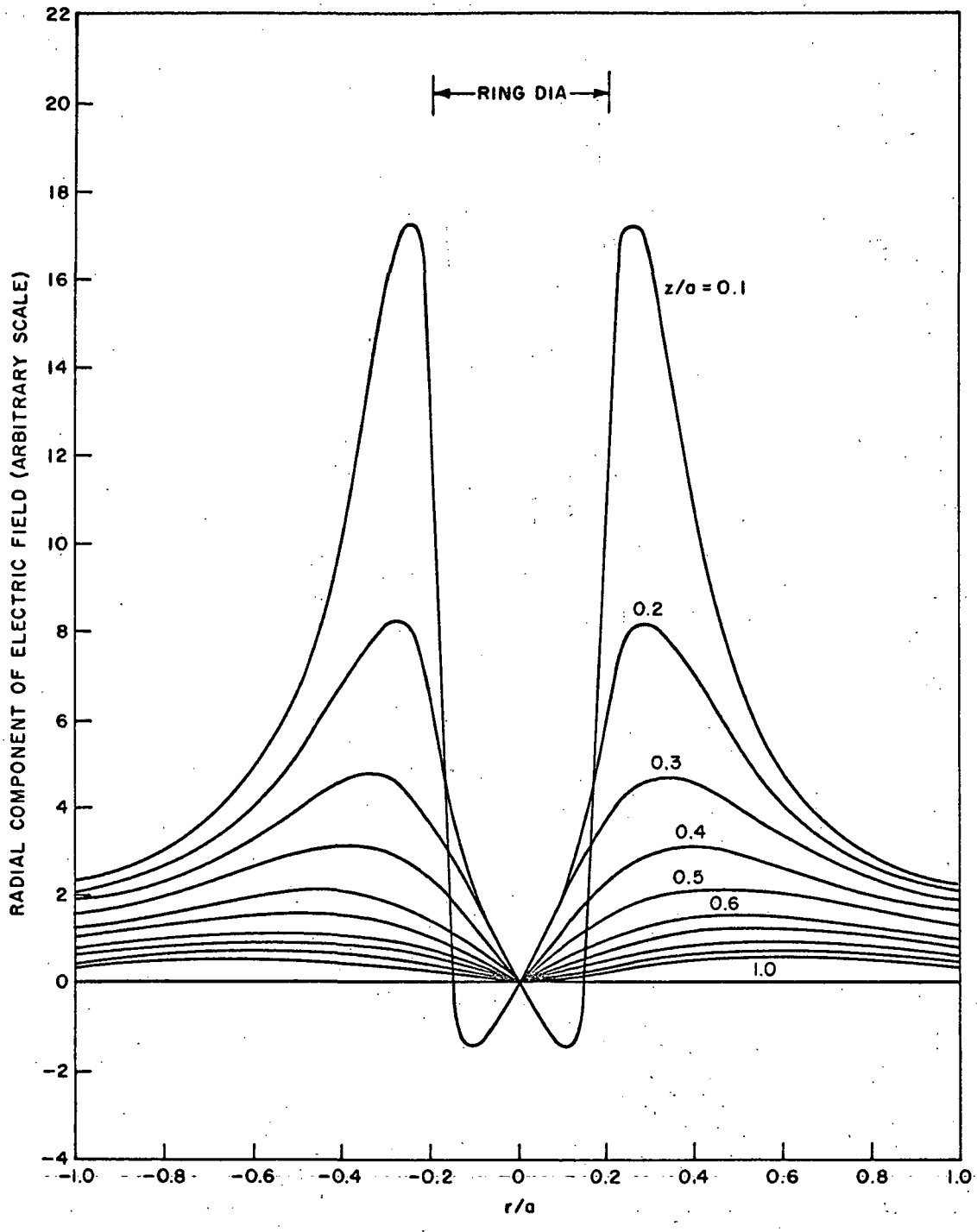

Figure 5 - Radial-Field Variation Computed for a Ring of Charge

divided into disks of width Δ_1 one-fifth the tunnel radius a, and each disk was subdivided into 3 annular regions containing equal amounts of space charge. The beam radius was 0.7a. Figure 6 illustrates the variation of the radial field of the beam as computed from the summation of space-charge forces from the 48 rings representing the beam. The model gives a field that is about 3 percent lower than the known field given by Gauss's Law, a discrepancy due to the fact that disks more than 1.5 tunnel radii in distance from the test position are ignored in the model developed from the method of images. Since in a well-bunched beam the significant interactions will occur between rings more closely space than 1.5 tunnel radii, the present model is assumed to have sufficient accuracy with errors estimated to be less than 1 percent.

TEST OF RING MODEL IN KLYSTRON BUNCHING CALCULATION

The space-charge ring model was tested by incorporating it into the GE Relativistic Multicavity Disk-Model Klystron Simulation Program for a computation of klystrons bunching with rings. An initial test was made in a computation in which each electron disk was represented by a single ring, and subject computations were made for a case in which each disk is subdivided into three rings.

The following parameters were chosen for the test cases:

Number of disk per wavelength	20
Frequency	3000 MHz
Beam voltage	10 kV
Beam current	1 A
Beam microperveance	1
Tunnel diameter	0.0635 cm
Tunnel filling ratio b/a	0.6
Collimating Field/Brillouin Field ratio	2
Cavity R/Q	100 ohms
Cavity Q (cold)	200
Cavity Q (beam loaded)	156
Plasma frequency ratio, ω_q/ω	0.101
Drive power	100 W

The results of both a small-signal space-charge wave computation of the bunching as well as of the bunching obtained with the ring-model computation are given in the following table. In the space-charge wave computation

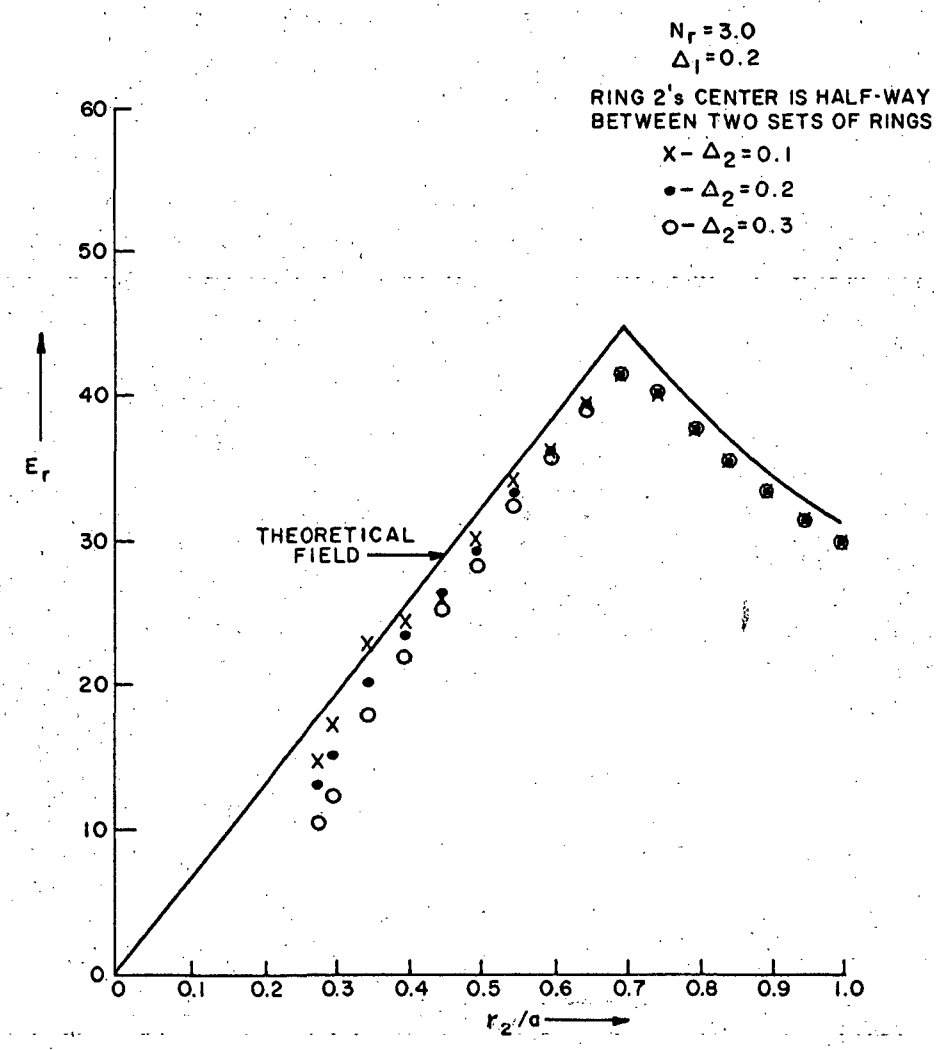

Figure 6 - Comparison of an Exact Radial Electric Field in an Electron Beam with a Field Computed by Ring Model

TABLE II - COMPARISON OF COMPUTED CURRENT MODULATION INDEX

	Space-Charge Wave Theory		Ring-Model Computation		
Drift Distance z/a	I_1/I_o	b/a	I_1/I_o	b/a Min.	b/a Max.
0	0.000	0.6	0.000	0.600	0.600
2.0	0.250	0.6	0.250	0.579	0.585
4.0	0.478	0.6	0.479	0.552	0.582
6.0	0.668	0.6	0.670	0.566	0.618
8.0	0.812	0.6	0.818	0.586	0.641
10.0	0.911	0.6	0.923	0.562	0.636
12.0	0.971	0.6	0.986	0.545	0.615
14.0	0.998	0.6	1.002	0.564	0.625
15.0	1.001	0.6			
16.0	0.998	0.6	0.965	0.581	0.643
17.0	0.969	0.6	0.876	0.553	0.618
18.0	0.908	0.6	0.738	0.544	0.598

the beam is assumed to be rigidly confined by the twice-Brillouin collimating magnetic field and the beam radius ratio b/a is confined at 0.6; whereas, in the ring-model computation the radius is allowed to vary as dictated by the combined magnetic forces and the space charge radial force. An oscillation about the initial value of 0.6 is observed and in the table the maximum and minimum ring radius at each axial position are listed.

The above data indicate that the accuracy of the ring model is adequate for the computation of klystron bunching. The predicted current modulation index maximum is the same as that predicted by the space-charge wave theory and the location of the maximum is only 7 percent shorter than that predicted. The ring-model radial force appears to be too small to hold the beam in equilibrium at the initial radius of 0.6.

The test computations for the ring-model space-charge subroutine were then extended to a consideration of the case in which each electron disk is subdivided into 3 rings. Each wavelength along the electron beam is divided into 20 disks, each of which is subdivided into 3 rings of equal volume to yield a total of 60 rings per wavelength.

The results of the computation are illustrated in Figure 7. A comparison of the current modulation index as a function of drift distance from the modulating klystron gap is shown for both the large-signal ring-model and space-charge wave calculations. Also shown in the figure is the range of radii of gyration of the three layers of rings as the rings drift in the tunnel under the combined space-charge, centrifugal and magnetic forces. Since the electron ring trajectories and the bunching action under large signal conditions prove to follow expectations, the ring model of the electron beam is presumed to be sufficiently accurate for both a qualitative and quantitative study of electron trajectories in the refocusing region of a klystron. (Because of the large current modulation developed in this case, the large-signal computation is not expected to agree with the space-charge wave computation beyond the peaks of the current modulation curves.)

GAP FIELD FORMULAS

Formulas for the radial and axial electric field components as a function of radial and axial position within the field region of a klystron interaction gap were developed by the method of zonal harmonics from a polynomial approximation to the field distribution on the axis. The axial and radial gap electric fields are evaluated by computing the gradients of the polynomial for the potential.

From an examination of both computed and experimentally observed field distributions on the axis of a klystron interaction gap, it has been previously found that the axial field can be represented to a sufficiently good approximation by the expression:

$$E_z(0, z)/E_z(0, 0) = \left[1 - (\beta z)^2\right]^3 \qquad (15)$$

where it was found empirically that in terms of an effective gap length d',

$$\beta = 1/1.008\ d'$$

The effective gap length d' is given in terms of the tunnel radius a and the actual gap length d by:

$$d' = (17\ a + 10.5\ d)/12$$

The potential function that leads to the distribution given in Equation 15 can be shown to be:

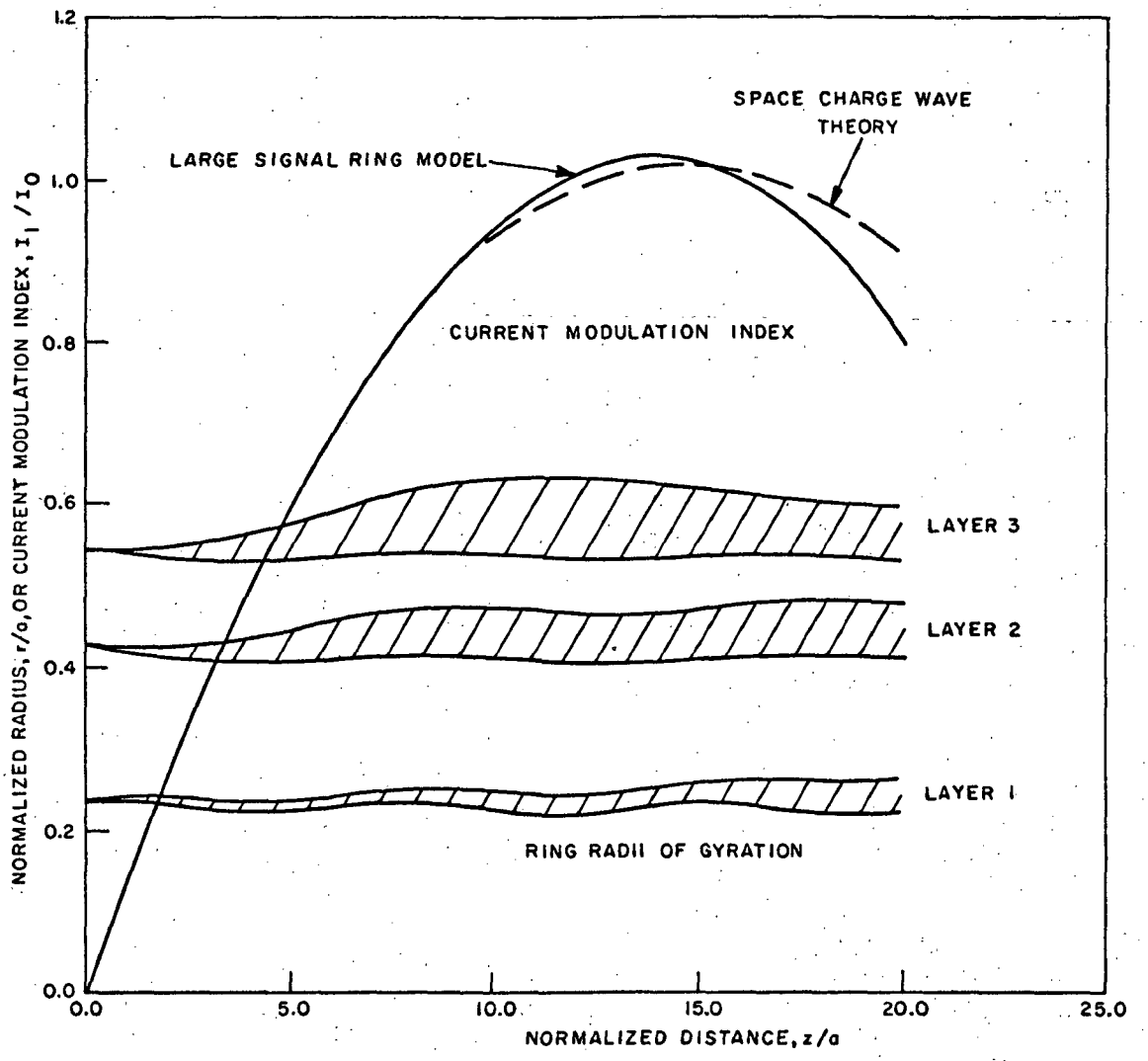

Figure 7 - Current Modulation Index and Range of Ring Radii of Gyration versus Drift Distance, as Computed in a Large-Signal Klystron Simulation Employing the Ring-Model Space-Charge Representation

$$\frac{\phi(r,z)}{\phi_{max}} = \frac{1}{2} + \frac{35}{32}\left\{\beta z - (\beta z)^3 + 0.6(\beta z)^5 - \frac{1}{7}(\beta z)^7 \right.$$

$$+ \frac{3}{2}\left[1 - (\beta z)^2\right]^2 (\beta z)(\beta r)^2 + \frac{3}{8}(\beta z)(\beta r)^4\left[3 - 5(\beta z)^2\right]$$

$$\left. + \frac{5}{16}(\beta z)(\beta r)^6 \right\} \qquad (16)$$

If the gap potential is normalized to the rf potential across the interaction gap, the normalized potential will be 0 at the left gap edge, $\frac{1}{2}$ at the gap center and 1 at the right gap edge for symmetrical fields. Inspection of the above equation shows that when z = 0 (at the gap center) the relative potential is equal to $\frac{1}{2}$. The potential will reduce to zero at some locus in r and z which may be determined by setting $\phi(r,z)$ equal to 0 and solving for r as a function of z. It proved convenient to normalize both r and z with respect to the effective width d', using a digital computer to generate a table of r/d' versus z/d' at this locus, and finally to fit a curve to the results. The resulting expression defines the locus of the edge of the gap fields within which the gradients of the potential must be computed and outside which the gap fields are zero:

$$r' = 0.970767 - z'(2.9868 - z'(4.93123 - z'(4.48976 - 1.57605\,z'))), \qquad (17)$$

where r' = r/d' and z' = z/d'. Since the fields are symmetric a corresponding limit at ϕ = 1 need not be computed.

DESCRIPTION OF FORTRAN PROGRAM FOR SPENT-BEAM TRAJECTORY COMPUTATIONS

The digital computer program was coded in Fortran IV. Since a large amount of trajectory coordinate information will be developed for each run with up to 100 rings, emphasis was placed on generating graphical output rather than pages of data. Consequently, an option for printing out either no trajectory data or data at only periodic intervals was programmed; however, a Calcomp plot can be made of all trajectories superimposed on a graph of the tunnel walls, cavity walls, the magnetic field, and potential profiles.

The program consists of the following subroutines: FOCUS, the main program for reading input and directing the sequence of events in the trajectory calculations; LOCUS, a fourth-order Runge-Kutta integration routine for the simultaneous integration of the velocity and acceleration differential equations; DERIV, computation of the derivatives at each time step; LOCATE, an interpolation routine to locate the position of each ring at each time step in the array of z planes at which the tunnel or wall radii, the on-axis potential, and the collimating magnetic field strengths are tabulated; LISTER, a subroutine for organizing the printed output; SPACHG, computation of space-charge forces between rings; EH, subroutine for elliptic functions required by SPACHG; GAPFLD, a subroutine for evaluating the axial and radial components of the microwave field in the klystron interaction gap; MAGFLD for evaluating the radial, axial, and theta components of the applied magnetic field at any ring location; and PLOTTR, a subroutine for organizing the trajectory information for plotting. In addition, many standard library subroutines are employed.

RING LOCATION AND TRAJECTORY PLOTTING PROGRAMS

The ring-model computer program FOCUS with its associated subroutines computes a table of successive coordinate pairs for a point lying on the radius of gyration of each electron ring and simultaneously generates a record on tape which may be subsequently used for making a plot of the trajectories, tunnel boundaries, and magnetic field and electric potential profiles. The program also has an option of punching trajectory information on data cards for the independent generation of a plot showing the ring cross-sections at selected time steps.

An example of a trajectory plot generated by FOCUS is given in Figure 8. The trajectories of the centroids of 60 electron rings traversing a klystron output interaction gap are shown. In this example, the klystron beam has a perveance of 0.5 microunits and the design frequency is 12 GHz. With a voltage modulation index of 1.0 at the output gap, the power conversion efficiency is computed to be 56.5 percent. Each wavelength of the beam is divided into 20 disks with each disk subdivided into three rings of equal volume and space charge.

It will be noted that as the faster electrons overtake the slower ones to develop the 1.69 current modulation index, space-charge concentrations increase and as a result the beam expands radially, as illustrated in the figure. Because of the violent interaction in the klystron gap, the spent-beam electrons have large radial accelerations as indicated by the scalloping

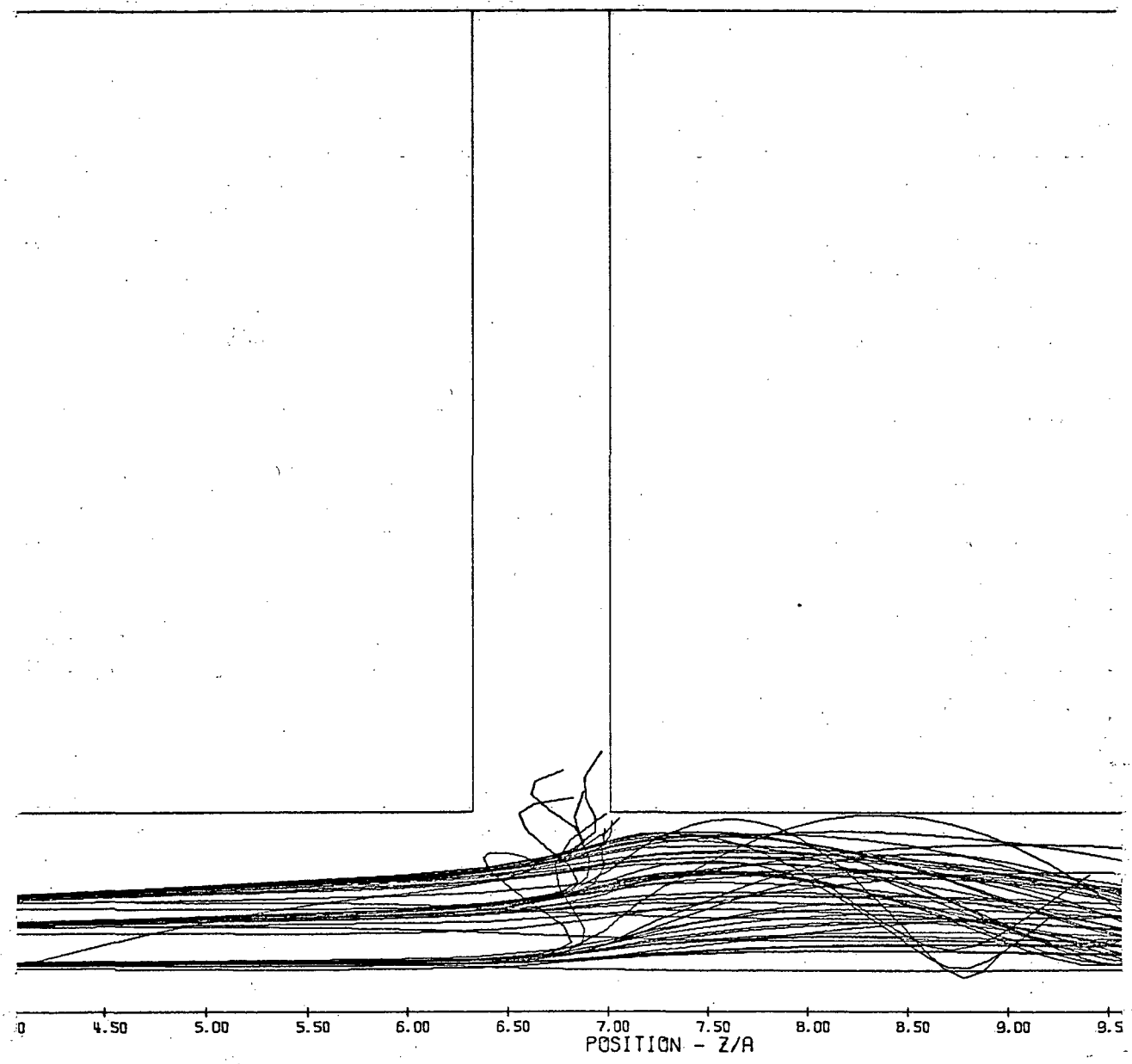

Figure 8 - Electron Ring Trajectories in the Vicinity of the Output Interaction Gap of a 12-GHz, 2-kW Klystron

of the trajectories. Very large radial deflections were experienced by a few rings which were retarded to low velocities in the gap. As a result, some rings were reflected and some were collected on the exit tunnel tip, a phenomenon which is often observed experimentally.

Two digital computer programs were written to provide an alternate way of portraying the refocusing characteristics of field distributions in the output and post-output regions of a klystron. The first program, PHOTO, was designed primarily to generate drawings at selected times of ring cross-sections in their passage through the klystron output gap. It has an option for making several diagrams on an $8\frac{1}{2}$ x 11 inch page, and for sketching schematically the location of the interaction gap. After reading punched card data generated by FOCUS, it calls on a subroutine DRAW to sketch an outline of each ring. An example of the plot generated by PHOTO is given in Figure 9, which corresponds to the same case portrayed in Figure 8. At the initial time step, as illustrated at the top of the figure, the leading electron is seen entering the fringing field of the interaction gap. The last diagram shows electron rings that have completely traversed the gap fields, with one ring having been reflected and hence moving to the left. Collected rings that have previously impinged on the tunnel wall are not shown in the diagram.

The program PHOTO was expanded into a new version PHOTON which has the capability of superimposing in one plot the instantaneous ring diagrams from many cycles, thus yielding an instantaneous distribution that approaches the steady-state distribution at any specified part of the rf cycle. The input distributions for PHOTON must be derived from a special run made with FOCUS in which card output has been punched at intervals of 2π radians. Normally, however, PHOTON would be used to generate at successive time steps the diagrams of all the rings in one rf cycle as is done by the program PHOTO. PHOTON has an additional capability of being able to sketch the outlines of the beam tunnel walls in the post-output region.

In Figure 10 is demonstrated a multiple-cycle diagram as drawn by PHOTON. In this plot nine sets of disks have preceded the tenth set that is poised to the left of the interaction gap schematically indicated near the left boundary. As indicated by this figure, the spent-beam electrons become uniformly spread out in position, following the output gap interaction, but with a spectrum of velocities. This observation lends support to the approximate model employed in the analog computer program described below. The analog computer model assumes that the spent beam has a uniform distribution of charge.

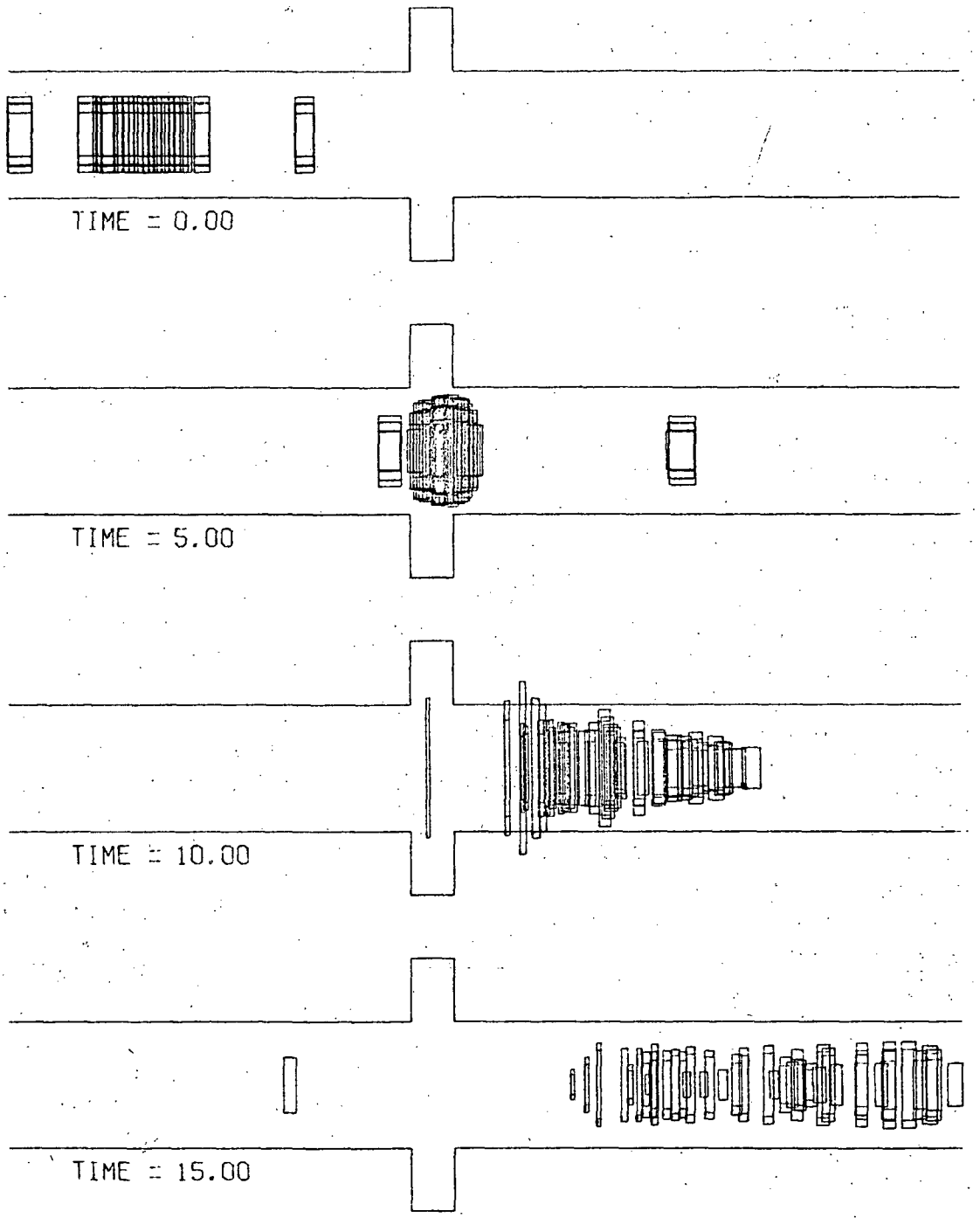

Figure 9 - Locations of Electron Rings at Successive Time Intervals in the Output Interaction Region of the 12-GHz Klystron

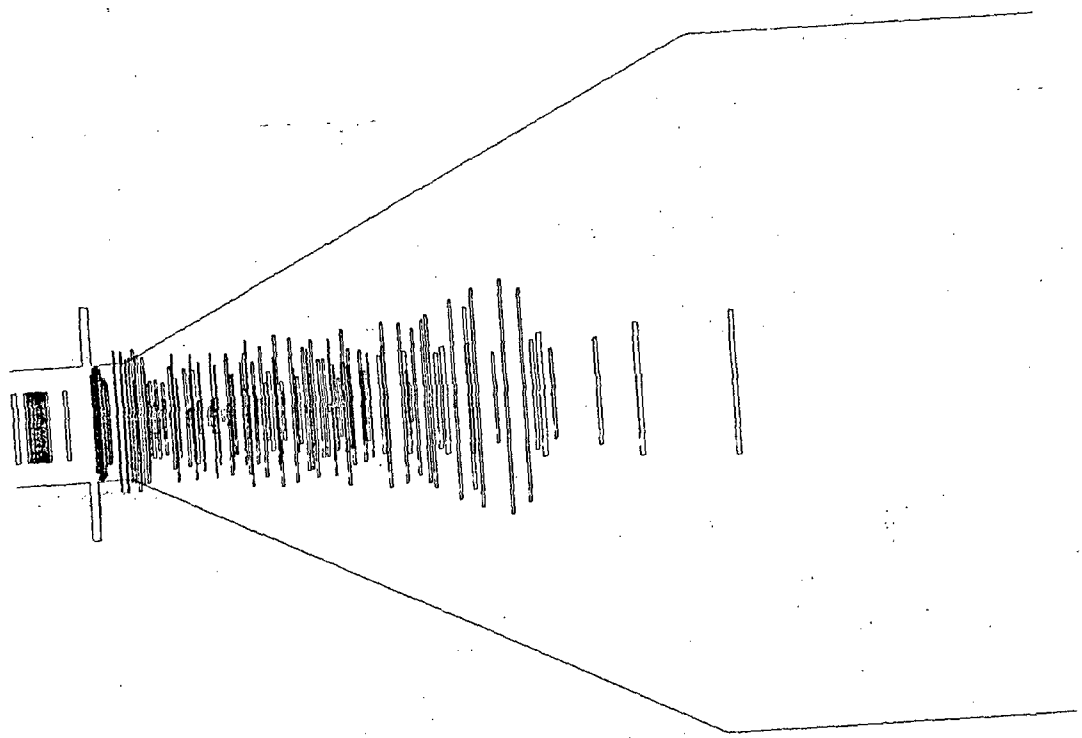

Figure 10 - Instantaneous Positions of 10 Cycles of Disks as Plotted by PHOTON

ANALOG COMPUTER PROGRAM FOR SPENT-BEAM ANALYSIS

To determine the effectiveness of any refocusing method, a large number of spent-beam trajectories must be analyzed in the fields presented by the refocusing structure. By means of analog computation a number of refocusing methods can be quickly evaluated. Since analog computers are generally limited in the number of variables, some approximations must be made in the calculation of electron trajectories. The computational model is described below.

MAGNETIC-FIELD MODEL

The magnetic-field pattern is introduced into the analog computer by means of an axial field profile from which the off-axis field components can be derived within certain limitations.

Consider the potential field

$$\Phi = A\,(r^2 - 2z^2) \tag{18}$$

which satisfies Laplace's equation and let $\bar{B}$ be the gradient of this potential function.

$$\bar{B} = \nabla\Phi = \bar{a}_r\,(2Ar) - \bar{a}_z\,(4Az) \tag{19}$$

Here A is an amplitude, r and z are radial and axial distances, respectively, and $\bar{a}_r$, $\bar{a}_z$ are unit vectors. This field is drawn in Figure 11 to show the nature of the field lines. The axial component varies linearly with z and is independent of r, while the radial magnetic field component is linear with r and independent of z. The pillbox region shown enclosed by the dashed lines in the figure is used as the model for an expanding magnetic field. The actual axial-magnetic field component as shown in Figure 12 is broken into linear segments (16 in a typical analog computer), and a pillbox region from Figure 11 is fitted to each of those linear segments by adjusting the amplitude A and the axial location. In this way a measured magnetic field distribution is introduced into the computer. The parameter A for each pillbox is found by differentiating the axial-magnetic field with respect to z. For each box

$$B_z = -4Az \tag{20}$$

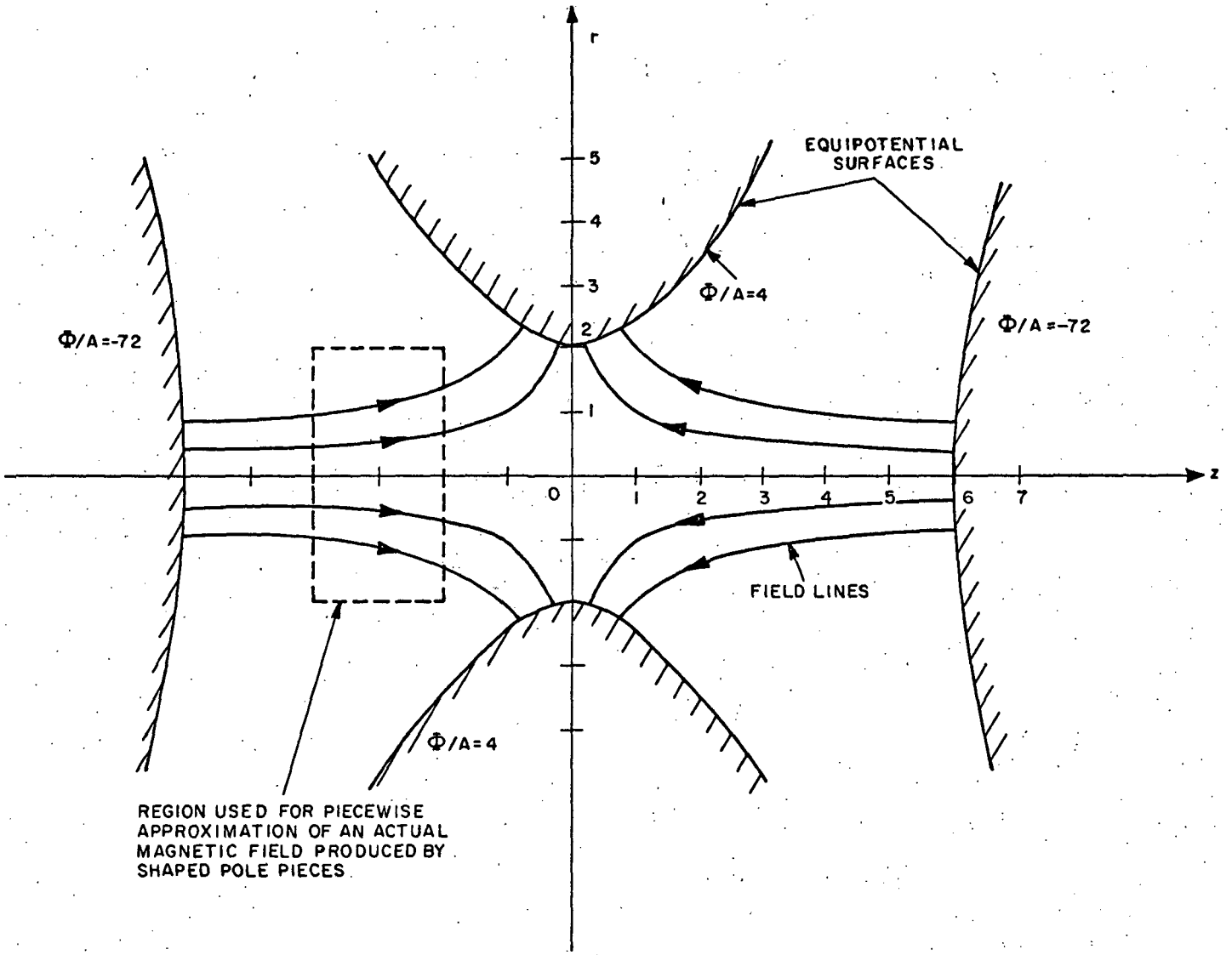

Figure 11 - Plot of the Field $\Phi = A(r^2 - 2z^2)$ and $\nabla\Phi$

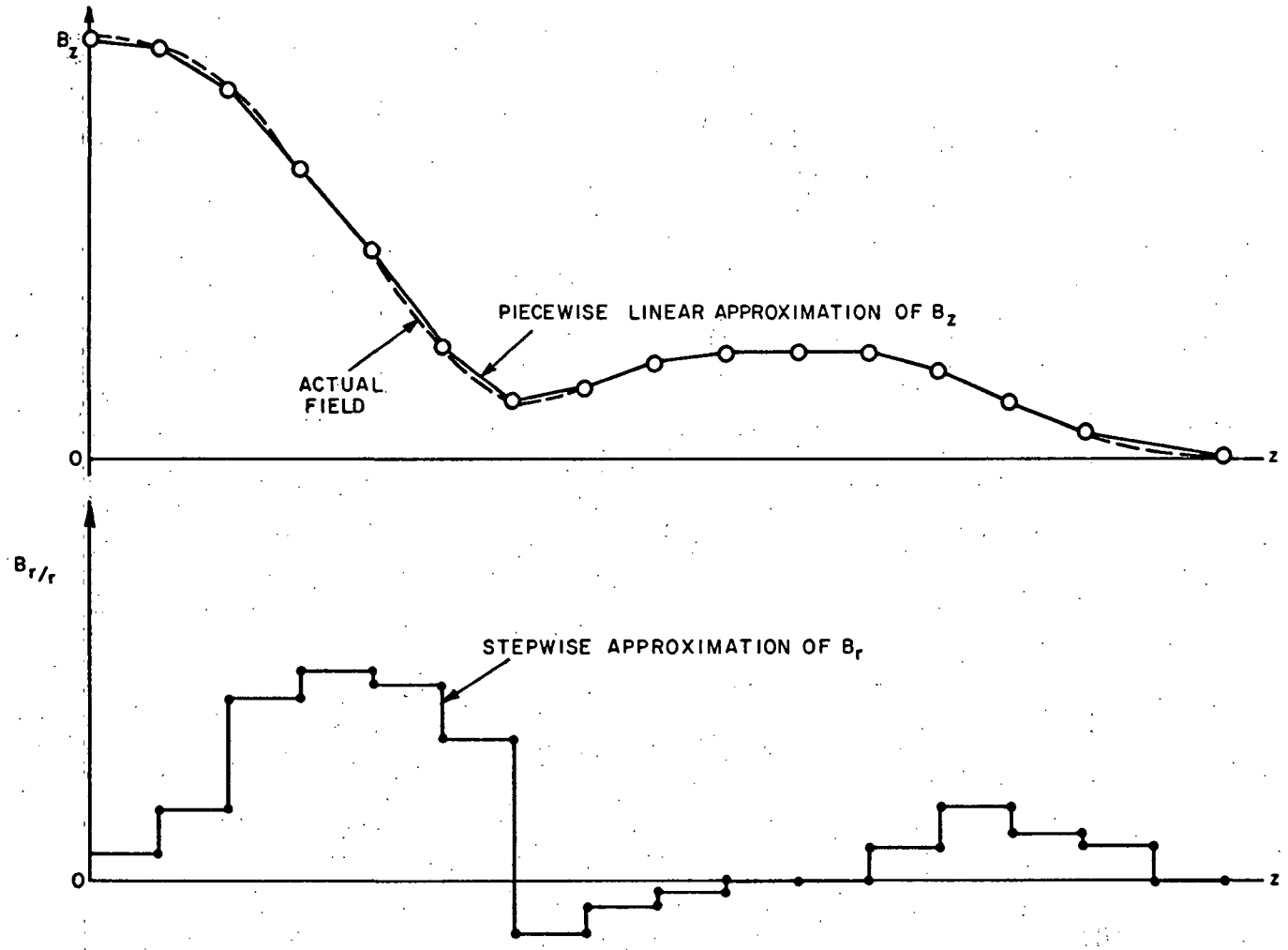

Figure 12 - Simulation of an Actual Field for Analog Computing Purposes

which upon differentiation yields

$$A = -\frac{1}{4}\frac{dB_z}{dz} \tag{21}$$

as the value for A. This can now be substituted into the equation for the radial component which can then be expressed in terms convenient for analog computation.

$$B_r = 2Ar = -\frac{r}{2}\frac{dB_z}{dz} = -\frac{r}{2\dot{z}}\frac{dB_z}{dt} \tag{22}$$

The radial magnetic field component used in the calculation is therefore a stepwise approximation as shown in Figure 12. It should be noted that this stepwise approximation is used only in computing the axial acceleration of electrons. It is not used for computing angular velocities which are obtained directly from the value of B_z by means of Busch's theorem. The approximation of B_r by a step function therefore appears mostly in the axial acceleration which in general has a small effect on the resulting electron trajectories. In the case of electrons having very low initial axial velocities this effect is more pronounced.

The piecewise linear approximation of the axial-magnetic field allows the rapid simulation of measured field profiles for the purposes of analog computation. The simulation consists of the first term in both B_z and B_r of the Taylor series expansion of the magnetic field in terms of the field on the axis of symmetry.[6] In measured magnetic field profiles, derivatives higher than the first are generally not available to the desired degree of accuracy. The simulation is quite accurate provided that the magnetic field can be represented by a series of pillboxes of the type shown in Figure 11. The fields may be represented by a series of pillboxes where the variation of the axial-magnetic field component with distance is slow enough to insure that B_z is uniform over the area occupied by the electron beam at any point along the axis. Even if B_z does not vary slowly, the above simulation may be very good if the pole piece geometry is such that B_z is not a function of radius. For example, a complete field reversal produced by the hyperbolic pole pieces shown in Figure 11 is simulated exactly by this model.

EQUATIONS OF MOTION

The non-relativistic particle acceleration is given by the equation

$$\bar{f} = m\bar{a} = m\bar{a}_r (\ddot{r} - r\dot{\theta}^2) + m\bar{a}_\theta (2\dot{r}\dot{\theta} + r\ddot{\theta}) + m\bar{a}_z (\ddot{z}) \tag{23}$$

where $\bar{a}_r$, $\bar{a}_z$, and $\bar{a}_\theta$ denote unit vectors, and the dots denote time differentiation. The force exerted by the electromagnetic fields on the particle is given by

$$\bar{f} = -e\left[\bar{E} + \bar{v} \times \bar{B}\right] \tag{24}$$

for electrons. Equation (24) is the Lorentz force. When (23) and (24) are equated, the theta part can be integrated directly (Busch's theorem):

$$m(2\dot{r}\dot{\theta} + r\ddot{\theta}) = -e(\dot{r} B_z - \dot{z} B_r) \tag{25}$$

to yield

$$\dot{\theta} = \frac{e}{2\pi m r^2} (\psi - \psi_c) \tag{26}$$

where ψ and ψ_c represent the final and initial flux linkages. Pierce has treated this problem in a left hand coordinate system rather than the right hand system used here.[7]

In the piecewise-linear magnetic-field model B_z is independent of radius and the flux linkages can be expressed very simply as

$$\psi = \pi r^2 B_z$$
$$\psi_c = \pi r_c^2 B_c \tag{27}$$

where the subscript c denotes the conditions at the cathode. Substitution of (27) into (26) and subsequently (26) into the radial force balance equation

$$m(\ddot{r} - r\dot{\theta}^2) = -e\left[E_r + r\dot{\theta}B_z\right] \tag{28}$$

yields after some rearrangement the paraxial ray equation

$$\ddot{r} = -\frac{e}{m}E_r - \frac{r}{4}\left(\frac{e}{m}\right)^2\left(B_z^2 - B_c^2\frac{r_c^4}{r^4}\right) \tag{29}$$

which includes the effects of cathode immersion. It is assumed that the angular field component B_θ is equal to zero. This equation is easily programmed on an analog computer once the radial electric field is evaluated.

EVALUATION OF THE ELECTRIC FIELD

Since the exact space-charge forces in the spent beam are rather complex, some simplifying assumptions are made: (See page 25 and Figure 10 for supporting information.)

1. All but the radial space-charge forces are neglected.
2. For computing electron trajectories within the beam a radially uniform charge distribution is assumed.
3. In computing the radial space-charge force it is assumed that the current within a trajectory remains constant if its radius is greater than its starting radius or the equilibrium beam radius, whichever is less. If a trajectory has a radius smaller than the lesser of either the starting radius or the equilibrium beam radius, the current within the trajectory is assumed to vary as the square of the radius.
4. The axial velocity used in computing charge density is taken to be the average axial velocity of the spent beam.

Under these assumptions Gauss's law leads to four expressions for the radial electric field, depending on the trajectory radius. If r_o is the initial radius and r_{bo} is the equilibrium beam radius, these equations are

$$E_r = -\frac{I}{2\pi\epsilon_o r \dot{z}_{avg.}} \qquad r_o > r_{bo} \text{ and } r > r_{bo} \tag{30a}$$

$$E_r = -\frac{rI}{2\pi\epsilon_o r_{bo}^2 \dot{z}_{avg.}} \qquad r_o > r_{bo} \text{ and } r < r_{bo} \tag{30b}$$

$$E_r = -\frac{r_o^2 I}{2\pi \epsilon_o r_{bo}^2 r \dot{z}_{avg.}} \qquad r_o < r_{bo} \text{ and } r > r_o \tag{30c}$$

$$E_r = -\frac{r I}{2\pi \epsilon_o r_{bo}^2 \dot{z}_{avg.}} \qquad r_o < r_{bo} \text{ and } r < r_o \tag{30d}$$

where I is the total spent beam current, ϵ_o is the permittivity of vacuum, and $\dot{z}_{avg}$ is the average axial velocity of the electrons. These equations specify that the electric field varies linearly with radius if an electron penetrates into the beam, while outside the beam this field varies as the reciprocal of radius. The radius at which this change occurs was chosen as the initial trajectory radius or the equilibrium radius, whichever is less. Other radii could have been chosen but this proved to be quite convenient and agreed well with digital results. The standard form of the equation of motion is obtained by letting $r_o = r_{bo}$ and assuming complete laminarity. Substitution of (30c) into (29) yields the equation

$$\ddot{r} = \frac{e r_o^2}{2 m \epsilon_o r \dot{z}_{avg}} \left(\frac{I}{\pi r_b^2}\right) - \frac{r}{4} \left(\frac{e}{m}\right)^2 \left(B_z^2 - B_c^2 \frac{r_c^4}{r^4}\right) \tag{31}$$

used by Rawls et al in analyzing PPM focused electron beams.[8]

AXIAL MOTION

The equation for axial motion is easily obtained from equations (23) and (24)

$$m\ddot{z} = e r \dot{\theta} B_r \tag{32}$$

which becomes

$$\ddot{z} = -\frac{1}{4} \left(\frac{e}{m}\right)^2 \frac{r^2}{\dot{z}} \left(B_z - \frac{B_c r_c^2}{r^2}\right) \frac{dB_z}{dt} \tag{33}$$

when equations (22), (26), and (27) are used to eliminate B_r and $\dot{\theta}$. In this equation $\dot{z}$ is the instantaneous axial velocity of the particle for which the trajectory is being computed. It is not the average velocity used in computing the radial space-charge force.

EVALUATION OF A SIMPLE MAGNETIC LENS FOR REFOCUSING

As the initial effort in testing the analog computer technique for developing a refocusing system, the refocusing capability of a magnetic lens was graphically investigated with the analog computer. A simple magnetic lens was studied with the analog computer to determine its usefulness for possible refocusing of the spent electron beam. For the purposes of computation it is assumed that the electrons originate from a point source and that electrons having 0.1 of the full energy are directed away from the axis of symmetry with an angle of 22 degrees. The initial radial velocity of all the other electrons is assumed to be the same as that of the 0.1 energy electron. For each lens investigated, ten electron paths are traced with initial energies equally spaced between 0.1 and full beam energy. By suitable scaling of the voltages, the results obtained can be applied to beams having a greater velocity distribution.

The refocusing characteristics of a magnetic lens for two different values of the magnetic field strength are shown in Figure 13. The shape of the field is held constant. In 13a the magnetic field amplitude is optimized for electrons having full energy. As may be seen, this field is much too strong and causes severe axis crossings for the lower energy electrons. For the trajectories of 13b the magnetic field strength is optimized for the 0.1 energy electrons. This field is obviously too weak to have much effect on the higher energy electrons. The magnetic field profile is given in 13c. Clearly, a single magnetic lens is not sufficient for refocusing a spent beam having a wide velocity distribution.

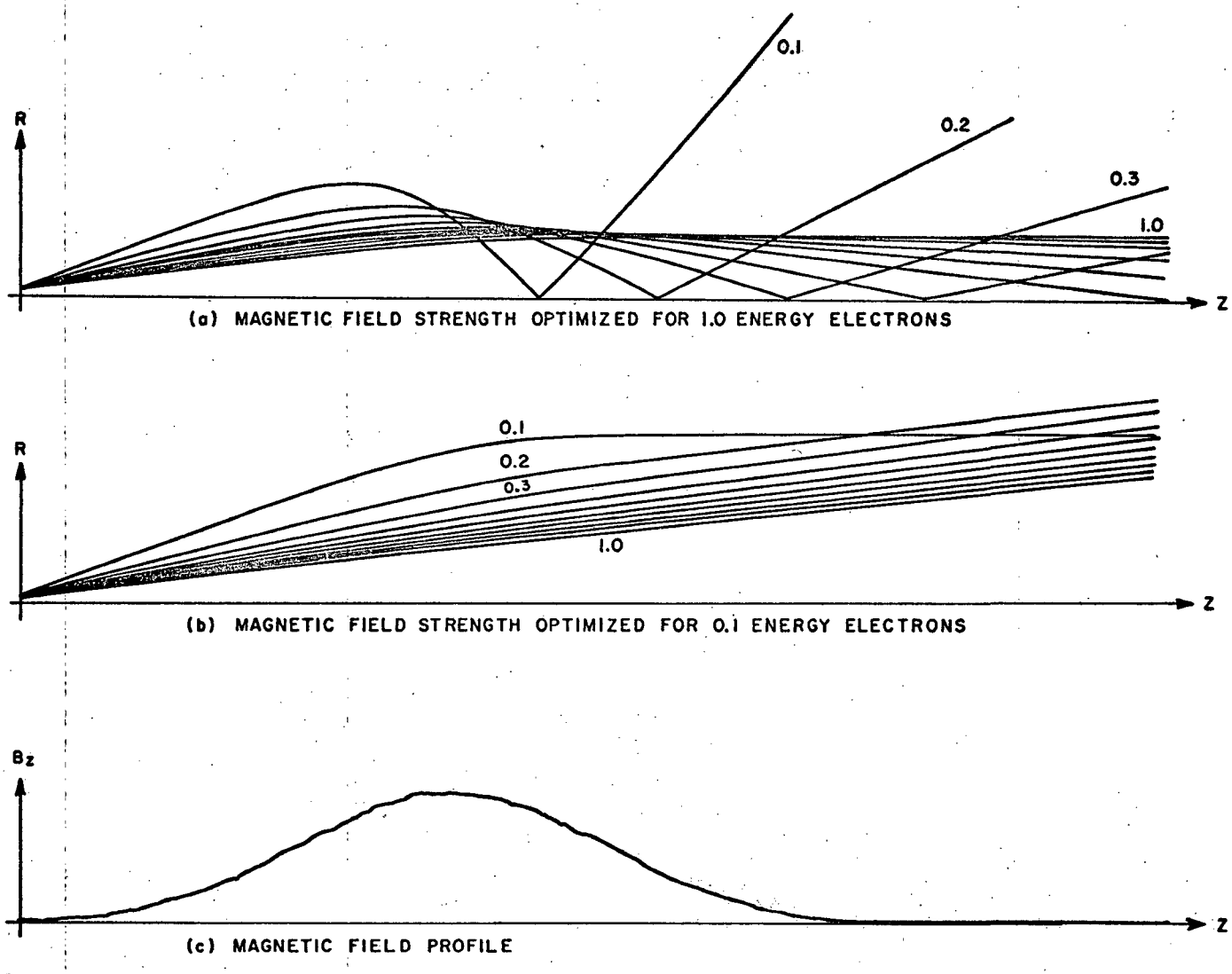

Figure 13 - Refocusing Characteristics of Simple Magnetic Lens

STUDY OF REFOCUSING METHODS

During previous studies of the properties of multistage depressed potential beam collectors for traveling wave tubes and klystrons, it was found that efficient spent-beam collection was hindered by the radial velocities of the spent electron beams.[1,2] These radial velocities are due to the combined effects of radial accelerations in the output interaction region of the linear-beam amplifier and of the radial acceleration caused by the beam space-charge forces. These forces are no longer balanced by the confining force of the main collimating magnetic field which is reduced to zero or to negligible magnitude before the beam enters the electrostatic collector. The general process of reducing the magnitude of the main collimating field to allow beam expansion with a consequent dilution of the beam space charge and reduction of space-charge forces combined with a recollimation of the electrons in the enlarged beam so that the beam enters the collector with trajectories parallel to the axis is called "refocusing the spent beam". The trajectories are not brought back to a point focus as is the case with a focused bundle of light rays.

Both the analog and digital computer methods were used to study the trajectories of electrons in a variety of refocusing field configurations. Because of the greater expense of making long computer runs with the digital programs and the greater convenience of the analog computer method, the ring-model digital computer program was used primarily for generating tables of radial and axial velocity spectra after passage through a typical klystron output interaction gap. The output of the digital computer program then was used as the input to the analog computer program which carried on the trajectory calculations through the relatively long refocusing region. Thus, the more accurate space-charge model of the digital program was used in the output gap interaction region where the electron rings are highly bunched and the space-charge forces are very critical. In the post-output region where there is little density modulation of the spent beam (as illustrated in Figure 10), the approximate model used in the analog computer program is sufficiently accurate and yields plots of the trajectories much more conveniently and economically.

DEVELOPMENT OF TABLES OF INITIAL DISK VELOCITIES AND LOCATIONS

For the first computation task in this study the GE Large-Signal Disk-Model Klystron Simulation Program was utilized to compute velocity spectra

for a high-efficiency klystron with parameters similar to those expected to be of interest in the future development of spaceborne television transmitters. It was assumed that the klystron would have a 40-MHz bandwidth at a center frequency of 12.0 GHz. The beam perveance of 0.5 microunits was chosen with the value of γ_a approximately equal to 1.0 radian. The normalized velocities (relative to the dc-beam velocity) and the positions of the 60 electron rings at the instant when the leading electron is entering the rf field of the output interaction gap are listed in Table III-A, B, and C. These tables are reproductions of pages printed out by the program FOCUS at the beginning of the trajectory computation (TIME = 0). The initial ring positions and velocities for the 11.98-, 12.00-, and 12.02-GHz frequencies are given. Note that Rings 1, 21, and 41 have the same axial position and velocity and were formed from the subdivision of Disk 1.

RING-MODEL STUDY OF OUTPUT GAP INTERACTION

As part of the task to delineate the refocusing problem, the ring-model output gap interaction program was used to study the electron trajectories in the output gap region of the 2-kW, 12-GHz klystron, both at band center and at band edges. The results indicate that not only is the energy extraction in the output gap a strong function of the output gap voltage phase (previously demonstrated with the rigid-disk model), but beam defocusing is also strongly dependent on this phase.

Efficiencies computed with both the disk and ring models are listed in Table IV for the three frequencies of 11.98, 12.00 and 12.02 GHs. For these computations the phase and amplitude of the output gap voltage correspond to the values yielding the proper gap impedance when the disk model is employed. At the lowest frequency the radial defocusing of the electrons in the gap was qualitatively similar to that computed at midband as illustrated in Figure 8. At the highest frequency, however, the interaction in the gap appears to be more violent, causing many rings to reflect after receiving large radial accelerations, resulting in a lower computed efficiency.

Ring-model computations show the refocusing problem to be more severe than the disk-model computations have indicated and that a satisfactory refocusing scheme must be capable of coping with the vector velocity distributions encountered at the band edges as well as in the more well-behaved center region.

TABLE III-A - INITIAL POSITIONS AND VELOCITIES OF RINGS

NASA 12 GHZ, 2 KW KLYSTRON AT 11.98 GHZ (ALPHA = 1.0, 2X BRILLOUIN) CALCULATION DATE 2/24/71

TIME = 0.

RING	Z	Z DOT	R	R DOT	RING	Z	Z DOT	R	R DOT
1	3.520	0.978	0.245	0.	31	4.452	0.937	0.424	0.
2	3.454	1.010	0.245	0.	32	4.351	0.934	0.424	0.
3	2.832	1.017	0.245	0.	33	4.201	0.931	0.424	0.
4	2.515	0.978	0.245	0.	34	4.105	0.939	0.424	0.
5	3.057	1.044	0.245	0.	35	4.016	0.951	0.424	0.
6	3.330	1.059	0.245	0.	36	3.937	0.961	0.424	0.
7	2.896	1.105	0.245	0.	37	3.846	0.964	0.424	0.
8	0.785	0.998	0.245	0.	38	3.716	0.962	0.424	0.
9	4.649	0.900	0.245	0.	39	3.651	0.963	0.424	0.
10	4.594	0.940	0.245	0.	40	3.583	0.966	0.424	0.
11	4.452	0.937	0.245	0.	41	3.520	0.978	0.548	0.
12	4.351	0.934	0.245	0.	42	3.454	1.010	0.548	0.
13	4.201	0.931	0.245	0.	43	2.832	1.017	0.548	0.
14	4.105	0.939	0.245	0.	44	2.515	0.978	0.548	0.
15	4.016	0.951	0.245	0.	45	3.057	1.044	0.548	0.
16	3.937	0.961	0.245	0.	46	3.330	1.059	0.548	0.
17	3.846	0.964	0.245	0.	47	2.896	1.105	0.548	0.
18	3.716	0.962	0.245	0.	48	0.785	0.998	0.548	0.
19	3.651	0.963	0.245	0.	49	4.649	0.900	0.548	0.
20	3.583	0.966	0.245	0.	50	4.594	0.940	0.548	0.
21	3.520	0.978	0.424	0.	51	4.452	0.937	0.548	0.
22	3.454	1.010	0.424	0.	52	4.351	0.934	0.548	0.
23	2.832	1.017	0.424	0.	53	4.201	0.931	0.548	0.
24	2.515	0.978	0.424	0.	54	4.105	0.939	0.548	0.
25	3.057	1.044	0.424	0.	55	4.016	0.951	0.548	0.
26	3.330	1.059	0.424	0.	56	3.937	0.961	0.548	0.
27	2.896	1.105	0.424	0.	57	3.846	0.964	0.548	0.
28	0.785	0.998	0.424	0.	58	3.716	0.962	0.548	0.
29	4.649	0.900	0.424	0.	59	3.651	0.963	0.548	0.
30	4.594	0.940	0.424	0.	60	3.583	0.966	0.548	0.

TABLE III-B - INITIAL POSITIONS AND VELOCITIES OF RINGS

NASA 12 GHZ, 2 KW KLYSTRON WITH UNIFORM MAGNETIC FIELD (ALPHA = 0.9, 2X BRILLOUIN) CALCULATION DATE 2/22/71

TIME = 0.

RING	Z	Z DOT	R	R DOT	RING	Z	Z DOT	R	R DOT
1	2.179	0.951	0.245	0.	31	0.167	1.174	0.424	0.
2	2.109	0.966	0.245	0.	32	4.649	0.947	0.424	0.
3	2.028	0.983	0.245	0.	33	3.019	0.807	0.424	0.
4	1.937	1.007	0.245	0.	34	2.734	0.851	0.424	0.
5	1.800	1.033	0.245	0.	35	2.661	0.887	0.424	0.
6	1.628	1.032	0.245	0.	36	2.584	0.905	0.424	0.
7	1.536	1.027	0.245	0.	37	2.529	0.913	0.424	0.
8	1.531	1.036	0.245	0.	38	2.428	0.917	0.424	0.
9	1.492	1.058	0.245	0.	39	2.346	0.925	0.424	0.
10	1.264	1.140	0.245	0.	40	2.248	0.938	0.424	0.
11	0.167	1.174	0.245	0.	41	2.179	0.951	0.548	0.
12	4.649	0.947	0.245	0.	42	2.109	0.966	0.548	0.
13	3.019	0.807	0.245	0.	43	2.028	0.983	0.548	0.
14	2.734	0.851	0.245	0.	44	1.937	1.007	0.548	0.
15	2.661	0.887	0.245	0.	45	1.800	1.033	0.548	0.
16	2.584	0.905	0.245	0.	46	1.628	1.032	0.548	0.
17	2.529	0.913	0.245	0.	47	1.536	1.027	0.548	0.
18	2.428	0.917	0.245	0.	48	1.531	1.036	0.548	0.
19	2.346	0.925	0.245	0.	49	1.492	1.058	0.548	0.
20	2.248	0.938	0.245	0.	50	1.264	1.140	0.548	0.
21	2.179	0.951	0.424	0.	51	0.167	1.174	0.548	0.
22	2.109	0.966	0.424	0.	52	4.649	0.947	0.548	0.
23	2.028	0.983	0.424	0.	53	3.019	0.807	0.548	0.
24	1.937	1.007	0.424	0.	54	2.734	0.851	0.548	0.
25	1.800	1.033	0.424	0.	55	2.661	0.887	0.548	0.
26	1.628	1.032	0.424	0.	56	2.584	0.905	0.548	0.
27	1.536	1.027	0.424	0.	57	2.529	0.913	0.548	0.
28	1.531	1.036	0.424	0.	58	2.428	0.917	0.548	0.
29	1.492	1.058	0.424	0.	59	2.346	0.925	0.548	0.
30	1.264	1.140	0.424	0.	60	2.248	0.938	0.548	0.

TABLE III-C - INITIAL POSITIONS AND VELOCITIES OF RINGS

NASA 12 GHZ, 2 KW KLYSTRON AT 12.02 GHZ (ALPHA = 1.12, 2X BRILLOUIN) CALCULATION DATE 2/25/71

TIME = 0.

RING	Z	Z DOT	R	R DOT	RING	Z	Z DOT	R	R DOT
1	2.613	0.880	0.245	0.	31	1.944	1.053	0.424	0.
2	2.572	0.899	0.245	0.	32	1.828	1.103	0.424	0.
3	2.512	0.913	0.245	0.	33	1.530	1.185	0.424	0.
4	2.451	0.928	0.245	0.	34	0.820	1.222	0.424	0.
5	2.383	0.947	0.245	0.	35	-0.162	1.123	0.424	0.
6	2.311	0.967	0.245	0.	36	4.649	0.920	0.424	0.
7	2.234	0.983	0.245	0.	37	3.276	0.777	0.424	0.
8	2.156	0.997	0.245	0.	38	2.806	0.777	0.424	0.
9	2.077	1.010	0.245	0.	39	2.701	0.815	0.424	0.
10	2.015	1.026	0.245	0.	40	2.646	0.851	0.424	0.
11	1.944	1.053	0.245	0.	41	2.613	0.880	0.548	0.
12	1.828	1.103	0.245	0.	42	2.572	0.899	0.548	0.
13	1.530	1.185	0.245	0.	43	2.512	0.913	0.548	0.
14	0.820	1.222	0.245	0.	44	2.451	0.928	0.548	0.
15	-0.162	1.123	0.245	0.	45	2.383	0.947	0.548	0.
16	4.649	0.920	0.245	0.	46	2.311	0.967	0.548	0.
17	3.276	0.777	0.245	0.	47	2.234	0.983	0.548	0.
18	2.806	0.777	0.245	0.	48	2.156	0.997	0.548	0.
19	2.701	0.815	0.245	0.	49	2.077	1.010	0.548	0.
20	2.646	0.851	0.245	0.	50	2.015	1.026	0.548	0.
21	2.613	0.880	0.424	0.	51	1.944	1.053	0.548	0.
22	2.572	0.899	0.424	0.	52	1.828	1.103	0.548	0.
23	2.512	0.913	0.424	0.	53	1.530	1.185	0.548	0.
24	2.451	0.928	0.424	0.	54	0.820	1.222	0.548	0.
25	2.383	0.947	0.424	0.	55	-0.162	1.123	0.548	0.
26	2.311	0.967	0.424	0.	56	4.649	0.920	0.548	0.
27	2.234	0.983	0.424	0.	57	3.276	0.777	0.548	0.
28	2.156	0.997	0.424	0.	58	2.806	0.777	0.548	0.
29	2.077	1.010	0.424	0.	59	2.701	0.815	0.548	0.
30	2.015	1.026	0.424	0.	60	2.646	0.851	0.548	0.

TABLE IV - RING AND DISK-MODEL COMPUTED EFFICIENCIES

Frequency GHz	Normalized Gap Impedance		Current Mod. Index	Gap Voltage Mod. Index	Efficiency (Percent)	
	Magnitude	Phase			Disk	Ring
11.98	0.9301	0.4683	1.5238	0.9424	42.2	57.8
12.00	0.9068	0.0	1.6920	1.0032	55.5	58.0
12.02	0.9302	-0.4853	1.6902	1.1176	59.4	40.7

The analog computer program requires as inputs the velocity spectra and location of electron rings after they have traversed the output interaction gap. The required data are obtained by calculating for trajectories of the rings listed in Tables III-A, III-B, and III-C, using the digital computer program FOCUS. The resulting lists of ring radii, axial locations and axial and radial velocities are given in Tables V-A, V-B, and V-C, for the three frequencies 11.98-, 12.00-, and12.02-GHz, respectively.

QUADRUPOLE-DOUBLET REFOCUSING LENS

As discussed previously,a simple magnetic lens will refocus electrons only over a very narrow range of energies. The subsequent search for an achromatic-refocusing lens led to the concepts of a magnetic-quadupole-doublet, the conical-grid lens, and the permanent-magnet-wedge lens. The quadrupole-doublet lens as a natural sequel to the simple magnetic lens is discussed first.

The magnetic field components associated with a quadrupole are simply expressed by a proportionality constant G:

$$B_x = Gy \tag{34a}$$

$$B_y = Gx \tag{34b}$$

As illustrated in Figure 14, the magnetic field coefficient G is first zero, then positive, zero, negative, and finally zero after the beam has been refocused. An interesting phenomenon was discovered and is demonstrated in the trajectories of this figure. When a point source beam having constant axial but variable radial velocities is considered, the resulting trajectories are almost perfectly refocused. When a more realistic model with variable axial velocities is considered, however, the magnetic-

TABLE V-A - POST-OUTPUT GAP POSITIONS AND VELOCITIES OF RINGS

NASA 12 GHZ, 2 KW KLYSTRON AT 11.98 GHZ (ALPHA = 1.0, 2X BRILLOUIN) CALCULATION DATE 2/24/71

TIME = 7.5

RING	Z	Z DOT	R	R DOT	RING	Z	Z DOT	R	R DOT
1	-1.000	0.278	0.	0.395	31	10.322	0.689	0.378	-0.041
2	8.417	0.424	0.714	0.044	32	9.903	0.627	0.413	-0.049
3	8.351	0.504	0.770	0.103	33	9.668	0.598	0.483	-0.065
4	8.805	0.723	0.558	0.072	34	9.374	0.548	0.492	-0.068
5	7.994	0.382	0.917	0.124	35	9.319	0.547	0.586	-0.062
6	8.941	0.530	0.531	-0.008	36	9.121	0.504	0.600	-0.071
7	8.647	0.505	0.632	0.038	37	8.980	0.484	0.671	-0.066
8	8.788	1.281	0.259	0.045	38	8.945	0.500	0.759	-0.044
9	10.907	0.784	0.205	-0.014	39	8.687	0.447	0.810	-0.039
10	11.303	0.865	0.211	-0.017	40	8.245	0.355	0.904	-0.010
11	10.520	0.726	0.245	-0.039	41	-1.000	0.205	0.	0.191
12	10.084	0.659	0.260	-0.042	42	-1.000	0.363	0.	0.051
13	9.873	0.641	0.334	-0.046	43	-1.000	0.457	0.	0.123
14	9.663	0.607	0.348	-0.046	44	8.814	0.682	0.893	0.054
15	9.538	0.590	0.405	-0.036	45	-1.000	0.283	0.	0.183
16	9.359	0.557	0.431	-0.039	46	8.865	0.499	0.904	-0.049
17	9.189	0.533	0.493	-0.032	47	8.521	0.443	0.963	-0.017
18	9.124	0.545	0.545	-0.014	48	8.808	1.290	0.541	0.055
19	8.870	0.502	0.593	0.005	49	10.454	0.700	0.466	-0.001
20	8.312	0.398	0.735	0.052	50	10.914	0.789	0.481	-0.013
21	-1.000	0.291	0.	0.190	51	10.185	0.666	0.516	-0.048
22	8.345	0.382	0.876	-0.016	52	9.741	0.596	0.534	-0.055
23	8.376	0.491	0.989	0.079	53	9.566	0.581	0.653	-0.077
24	8.791	0.695	0.807	0.070	54	9.192	0.511	0.624	-0.075
25	-1.000	0.358	0.	0.132	55	9.072	0.491	0.701	-0.078
26	8.863	0.499	0.737	-0.043	56	8.959	0.470	0.747	-0.075
27	8.578	0.466	0.830	0.001	57	8.773	0.437	0.820	-0.079
28	8.801	1.287	0.424	0.054	58	8.757	0.452	0.898	-0.058
29	10.697	0.746	0.360	-0.004	59	8.574	0.420	0.946	-0.054
30	11.115	0.828	0.365	-0.007	60	-1.000	0.292	0.	0.091

TABLE V-B - POST-OUTPUT GAP POSITIONS AND VELOCITIES OF RINGS

NASA 12 GHZ, 2 KW KLYSTRON WITH UNIFORM MAGNETIC FIELD (ALPHA = 0.9, 2X BRILLOUIN) CALCULATION DATE 2/22/71

TIME = 7.5

RING	Z	Z DOT	R	R DOT	RING	Z	Z DOT	R	R DOT
1	8.365	0.588	0.202	0.024	31	7.895	0.638	0.000	-0.001
2	8.158	0.524	0.191	0.027	32	13.750	1.300	0.011	-0.125
3	7.930	0.431	0.210	0.035	33	9.638	0.918	0.136	-0.057
4	8.042	0.482	0.211	0.029	34	9.065	0.738	0.228	-0.053
5	8.010	0.470	0.243	0.033	35	9.460	0.868	0.204	-0.057
6	7.516	0.336	0.295	0.096	36	9.402	0.857	0.259	-0.041
7	6.762	-0.131	0.260	0.164	37	9.193	0.789	0.294	-0.036
8	7.185	0.222	0.221	0.112	38	8.827	0.698	0.404	-0.016
9	7.324	0.282	0.245	0.108	39	8.625	0.649	0.407	-0.017
10	7.823	0.427	0.208	0.061	40	8.472	0.616	0.451	-0.001
11	7.886	0.633	0.146	0.090	41	8.222	0.524	0.598	-0.017
12	13.736	1.296	0.166	0.053	42	8.092	0.469	0.593	-0.015
13	9.799	0.961	0.155	-0.003	43	7.981	0.420	0.601	-0.011
14	9.313	0.821	0.099	-0.009	44	8.147	0.499	0.562	-0.020
15	9.670	0.935	0.079	-0.012	45	8.111	0.486	0.553	-0.013
16	9.540	0.898	0.076	-0.012	46	7.585	0.324	0.651	0.059
17	9.387	0.853	0.109	-0.009	47	7.070	0.165	0.701	0.151
18	8.929	0.723	0.215	0.012	48	7.395	0.310	0.646	0.098
19	8.724	0.680	0.198	0.012	49	7.630	0.360	0.592	0.047
20	8.534	0.637	0.199	0.018	50	8.131	0.525	0.445	-0.005
21	8.291	0.557	0.447	-0.001	51	7.932	0.660	0.005	-0.033
22	8.105	0.486	0.448	0.005	52	13.725	1.296	0.006	-0.151
23	7.909	0.399	0.472	0.029	53	9.164	0.758	0.176	-0.080
24	8.047	0.462	0.450	0.012	54	8.878	0.694	0.416	-0.045
25	8.023	0.453	0.456	0.017	55	9.229	0.797	0.367	-0.051
26	7.566	0.343	0.510	0.092	56	9.129	0.768	0.405	-0.052
27	6.813	-0.103	0.466	0.149	57	8.988	0.728	0.442	-0.049
28	6.945	0.000	0.510	0.172	58	8.702	0.651	0.521	-0.038
29	7.472	0.330	0.443	0.091	59	8.505	0.610	0.537	-0.035
30	7.893	0.439	0.343	0.044	60	8.373	0.580	0.592	-0.017

TABLE V-C - POST-OUTPUT GAP POSITIONS AND VELOCITIES OF RINGS

NASA 12 GHZ, 2 KW KLYSTRON AT 12.02 GHZ (ALPHA = 1.12, 2X BRILLOUIN) CALCULATION DATE 2/25/71

TIME = 7.5

RING	Z	Z DOT	R	R DOT	RING	Z	Z DOT	R	R DOT
1	9.696	0.936	0.302	-0.009	31	6.673	-0.129	0.846	0.098
2	9.775	0.961	0.304	-0.008	32	8.281	0.487	0.490	-0.075
3	9.595	0.915	0.310	-0.008	33	9.294	0.849	0.499	-0.043
4	9.120	0.768	0.266	-0.018	34	7.925	0.393	0.531	-0.018
5	8.937	0.708	0.306	-0.013	35	-1.000	1.123	0.	0.
6	8.553	0.573	0.307	-0.023	36	14.049	1.368	0.446	0.013
7	7.970	0.370	0.314	-0.021	37	9.488	0.816	0.414	-0.020
8	7.101	0.087	0.502	0.063	38	6.282	-0.336	0.852	0.058
9	6.110	-0.433	0.643	0.123	39	6.820	-0.050	0.819	0.106
10	5.865	-0.537	0.637	0.099	40	8.596	0.596	0.505	-0.072
11	6.445	-0.219	0.665	0.162	41	8.912	0.713	0.743	-0.079
12	8.003	0.390	0.341	-0.006	42	9.204	0.804	0.803	-0.062
13	8.953	0.725	0.320	-0.013	43	8.827	0.685	0.789	-0.075
14	7.891	0.382	0.378	0.026	44	8.594	0.610	0.829	-0.068
15	-1.000	1.123	0.	0.	45	8.469	0.561	0.783	-0.088
16	14.018	1.361	0.248	0.004	46	8.420	0.546	0.782	-0.086
17	9.791	0.905	0.290	-0.012	47	8.003	0.393	0.756	-0.102
18	7.814	0.292	0.364	0.007	48	7.319	0.127	0.658	-0.142
19	7.944	0.352	0.327	-0.008	49	6.489	-0.160	0.981	-0.012
20	9.061	0.743	0.269	-0.016	50	6.270	-0.349	0.980	-0.036
21	9.479	0.882	0.558	-0.046	51	7.370	0.152	0.636	-0.129
22	9.581	0.913	0.558	-0.048	52	8.746	0.666	0.706	-0.068
23	9.136	0.775	0.541	-0.053	53	9.475	0.899	0.660	-0.048
24	8.904	0.706	0.547	-0.065	54	7.962	0.409	0.624	-0.037
25	8.676	0.630	0.566	-0.064	55	-1.000	1.123	0.	0.
26	8.433	0.542	0.562	-0.071	56	14.062	1.372	0.575	0.019
27	7.846	0.305	0.531	-0.106	57	9.569	0.865	0.601	-0.018
28	7.270	0.127	0.625	-0.049	58	-1.000	-0.690	0.	0.251
29	6.107	-0.449	0.920	0.046	59	-1.000	-0.735	0.	0.238
30	5.841	-0.604	0.940	0.084	60	7.211	0.084	0.654	-0.146

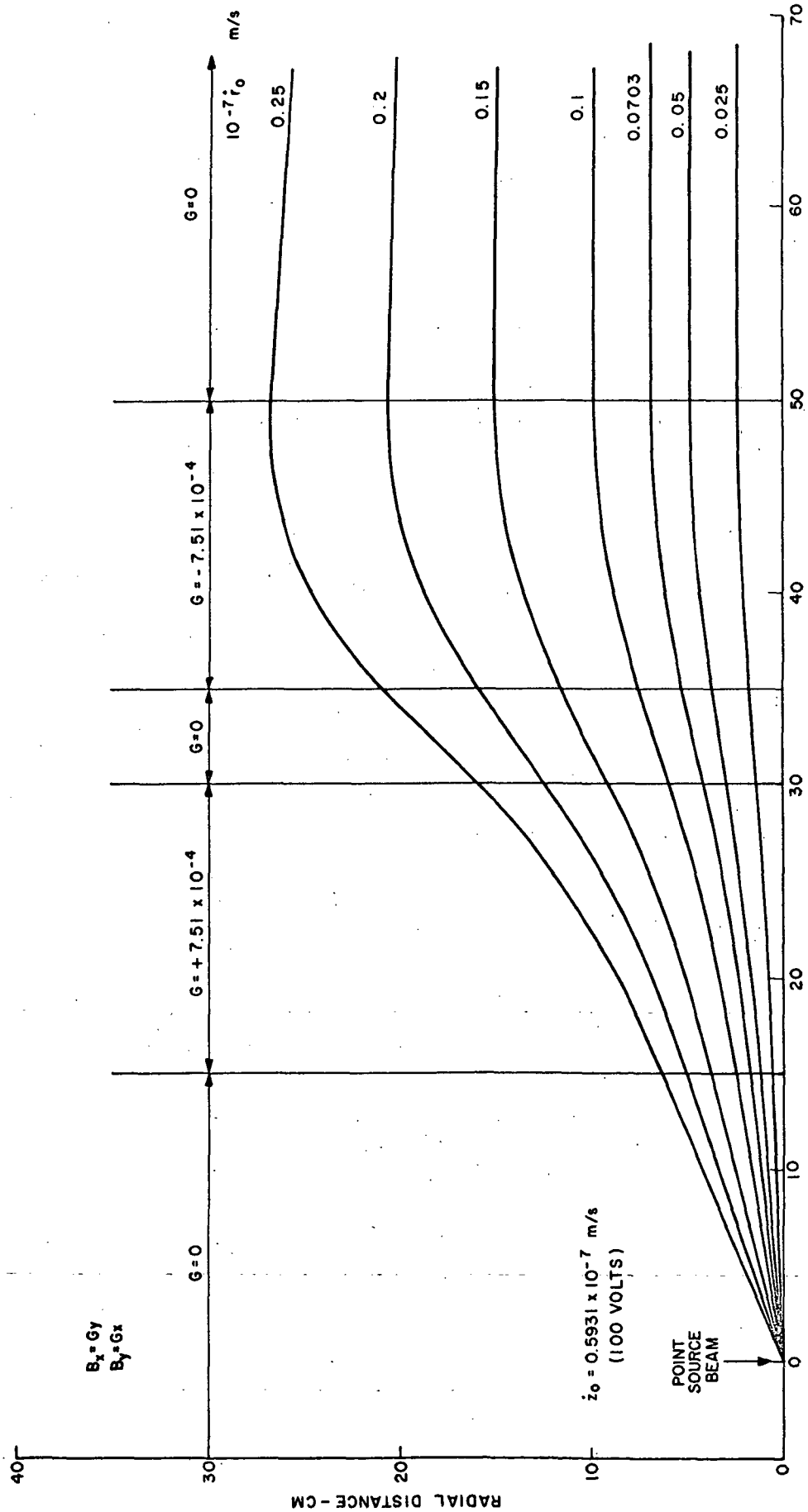

Figure 14 - Analysis of Magnetic Quadrupole Doublet

quadrupole doublet is revealed to be very deficient as a refocusing lens. Low energy electrons may be completely reflected and refocusing action is found to occur only over a narrow range of initial axial velocities.

CONICAL-GRID REFOCUSING LENS

A promising refocusing magnetic field is a θ-directed field which can perfectly refocus an electron beam originating from a point source with a wide spectrum of velocities. It was demonstrated by analog computation that a beam of this nature can be perfectly refocused with a magnetic field produced by currents flowing in a conical grid. This grid consists of straight wires forming a conical surface stretched between two support rings. The apex of the cones is made to lie on the beam axis as shown in Figure 15. The current producing the angular magnetic field flows through the grid wires in a direction opposing the motion of electrons in the beam. The refocusing field is zero except in the region exterior to the cones as indicated in the figure. Trajectories emanating from the point source with different axial velocities are all focused into a parallel beam by the action of this field. As indicated, a 100-volt beam requires approximately 10.8 amperes of grid current for good refocusing. In general, the required grid current varies as the square root of the beam voltage. A 10 kV beam, therefore, would be refocused with grid current near 100 amperes. It should be noted that the required grid current and the focusing action are completely independent of the size of the structure. This means that the grid can be made large and rugged enough to withstand the heating caused by ohmic losses and the interception of electrons from the spent beam. The distance of the grid from the point source determines the diameter of the refocused beam. The refocusing action of this magnetic field is extremely broad, as is shown by the range of energies from 0.05 to twice the dc beam voltage of the electrons studied in Figure 15.

One disadvantage of the conical grid is that a separate power supply is necessary to produce the current. The grid will also suffer from current interception, although this can be reduced by the proper design of a high-transparency grid. Because of the limitations imposed by the conical grid, a method of generating θ-magnetic fields with a permanent magnet was considered.

PERMANENT-MAGNET-WEDGE REFOCUSING SYSTEM

As described previously, the flow of current in the conical-grid refocusing lens produces a magnetic field which can, independent of the total particle energy, remove a fixed radial velocity from every electron passing

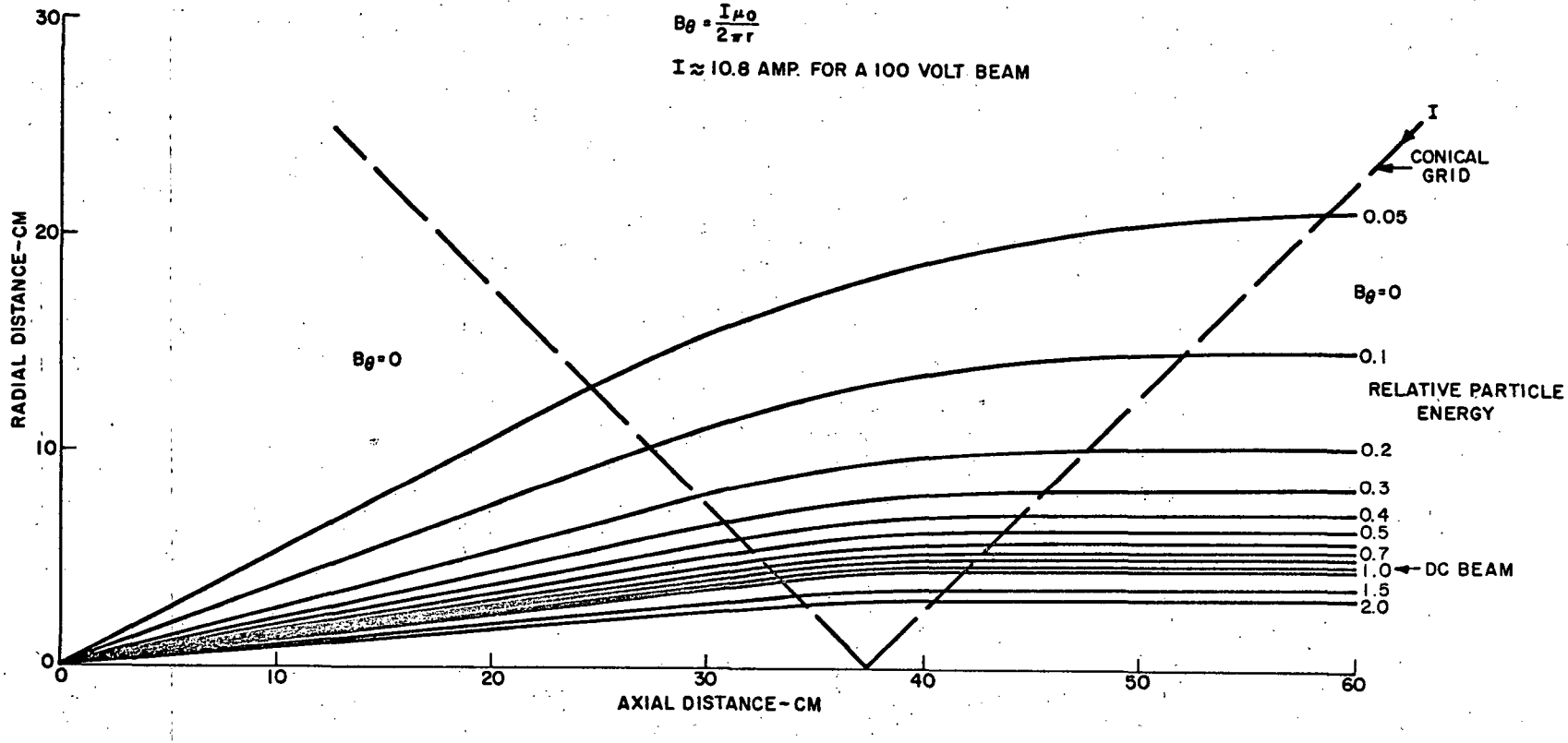

Figure 15 - Analysis of Angular Field (B_θ) Refocusing Lens

through it. The main disadvantage of this lens is the necessity of a separate power supply to produce the flow of grid current. It now will be shown that the same angular refocusing fields can be established by various permanent-magnet structures or by a combination of magnetic materials and permanent magnets.

The basic concept of the permanent-magnet-wedge lens is depicted in Figure 16 where rectangular wedges of the magnetic materials are shown oriented around the axis of the spent electron beam. The material is magnetized in a direction perpendicular to the large surfaces. This magnetization produces the angular magnetic field as indicated. The field strength is given by the approximate formula

$$B_\theta \approx \mu_o H_c \left(\frac{\theta}{2\pi}\right) \tag{35}$$

where μ_o is the permeability of free space, H_c is the coercive force of the material, and θ is the total angle occupied by this material. If high coercive force material like samarium-cobalt ($H_c \approx 8000$ oersteds) is used, the total angle required for a 10 kV electron beam is less than one degree of arc. Because of the focusing action of the magnetic field, electrons from the point source (shown in Figure 16) entering the lens will emerge with a smaller radial velocity distribution. Some current will be intercepted on the lens elements, but this can be minimized by the use of a highly transparent structure. Adequate cooling will have to be provided to preserve the integrity of the lens system.

Another version of the lens is shown in Figure 17 where flat pieces of magnetic material are used instead of wedges. The magnetic field strength for this structure is now inversely proportional to radius as indicated by the formula

$$B_\theta = \mu_o H_c \left(\frac{t}{2\pi r}\right) \tag{36}$$

where t is the thickness of the plates. Again the material is magnetized in a direction perpendicular to the large surface. Since B_θ varies with radius it is necessary to shape the lens elements when viewed transverse to the axis. Analog computation has previously shown that a triangular shape is optimum when the radial velocity of all the electrons is the same. This shape may be different depending on the exact conditions prevailing in a spent beam. The focusing action of this lens was shown in Figure 15,

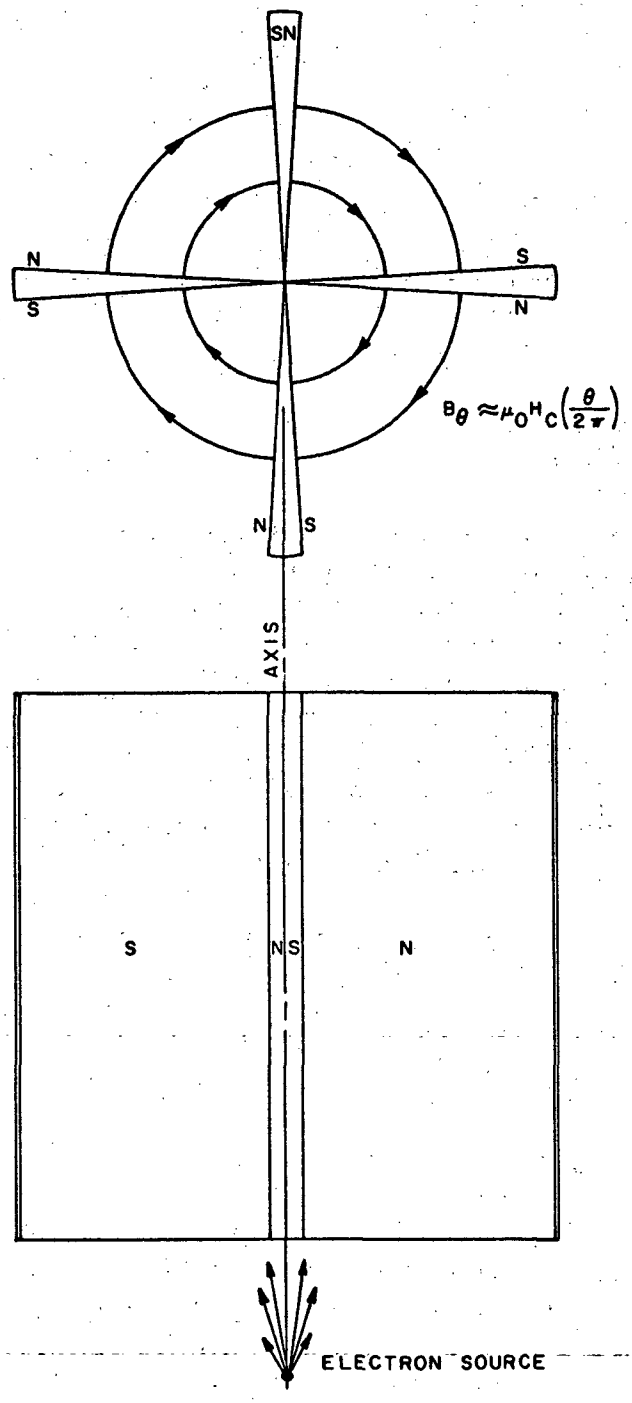

Figure 16 - Permanent-Magnet-Wedge Lens

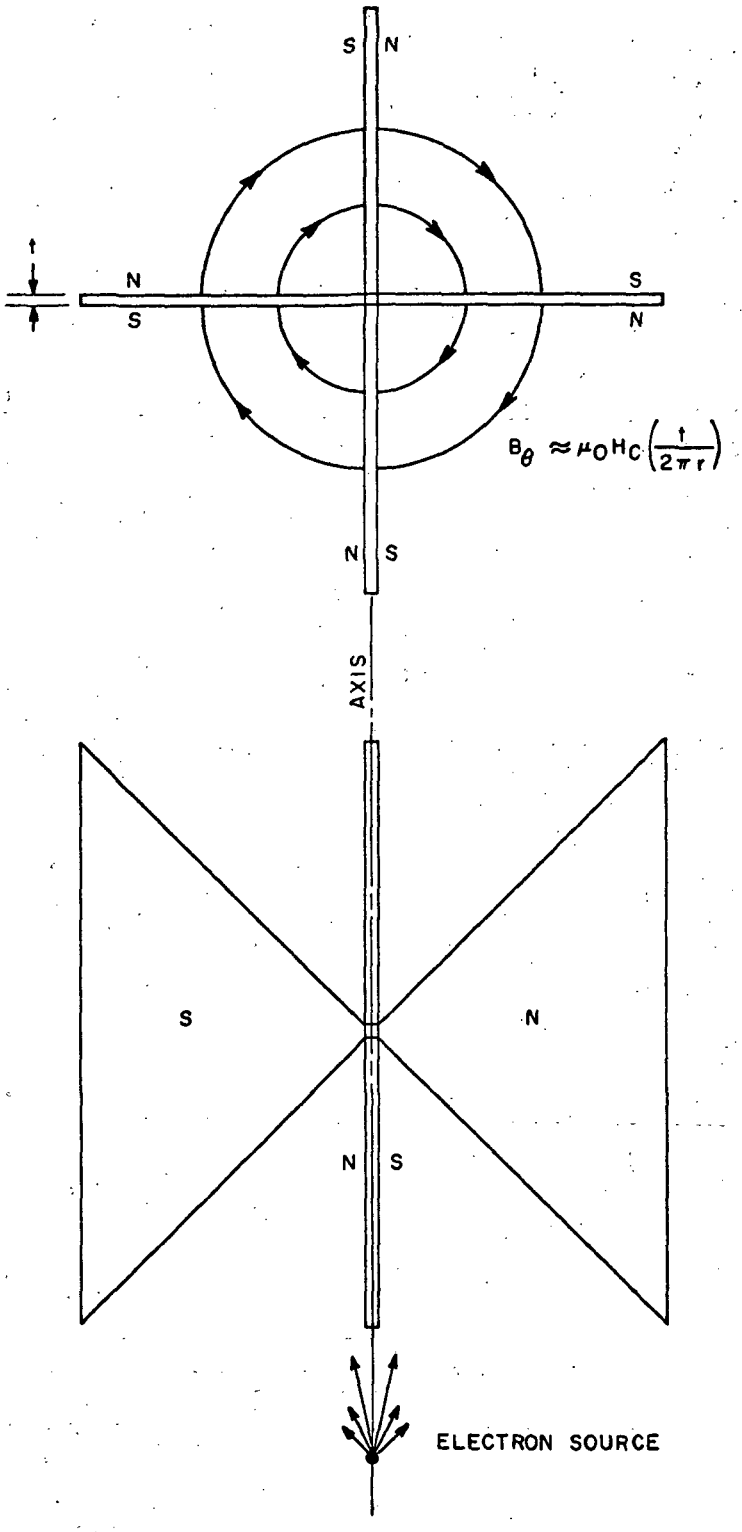

Figure 17 - Permanent-Magnet Flat-Plate Lens

where electrons having widely varying axial velocities but constant radial velocities were injected into the angular magnetic field. All the electrons emerged from the lens in a direction parallel to the original beam axis. This focusing action is completely independent of the initial axial velocities of the electrons, and is identical to the focusing associated with the conical-grid lens. The wedge lens has similar focusing properties.

If it should prove undesirable to expose the permanent magnet material to the electron beam, the lens elements shown in Figure 18 may be used. In these structures the magnetic flux from the permanent magnets is directed into the refocusing region by a high permeability material such as iron. To establish the proper fields a "sandwich" arrangement must be used as shown. A layer of non-magnetic material must separate the two iron layers of each lens element. The "sandwich" elements may be used in either the wedge- or flat-type of refocusing structure. The number of elements may be more or less than those shown in the illustrations.

The feasibility of a permanent-magnet-lens structure was checked by a simple experiment. Two disks of Alnico 9, 2 inches in diameter and 5/32-inch thick, were magnetized normal to the large surface. These disks

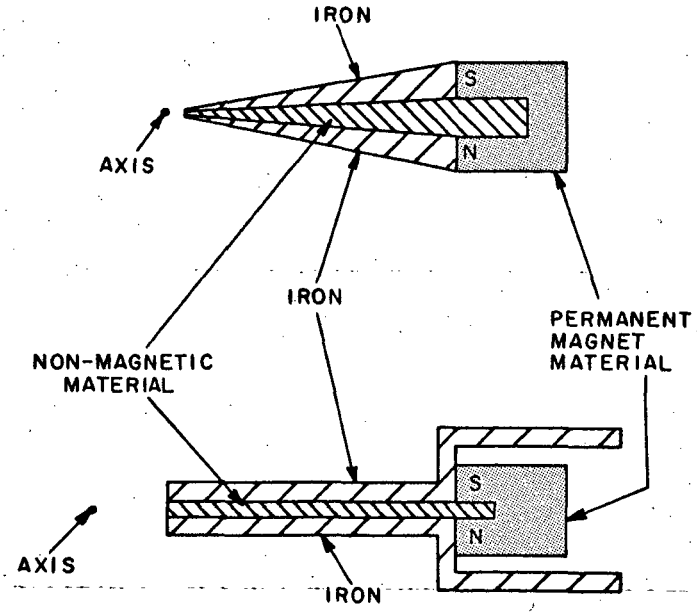

Figure 18 - Sandwich-type Lens Elements
(Not drawn to scale)

were then oriented at 90 degrees with respect to one another and the angular field B_θ was measured as a function of radius. At 2 cm radius the field produced by these disks was over 100 gauss, which is more than ten times that required to refocus a 10 kV electron beam. The variation of field strength with radius closely approximated the theoretical reciprocal radius function.

BEAM EXPANSION IN A SHAPED-AXIAL MAGNETIC FIELD

Initial studies of the expansion of spent electron beams in a variable axial-magnetic field were implemented with an idealized model of the electron beam. The electrons are assumed to originate at a shielded cathode (Brillouin flow) and pass through a 50 percent efficient klystron so the average velocity beyond the output gap is $1/\sqrt{2}$ times the initial dc velocity. It is further assumed that the bunches are sufficiently dispersed in the refocusing field region to allow computation of the radial space-charge forces from the average velocity. The axial acceleration terms are assumed to be small and are neglected in this calculation.

The computed dispersion of the spent beam is depicted in Figure 19 for the magnetic field profile indicated in the figure. The illustrated axial-field distribution is similar to that used for good beam dispersion in a conventional collector.

As may be seen in Figure 19, the optimum magnetic field for this case allows beam expansion and refocusing in order to produce a larger beam having virtually no radial velocities at the collector entrance plane. This would also be true in practice if all the electrons in the spent beam were to behave as the "average electron". Unfortunately, real tubes do not produce such an electron beam. In Figure 20 a beam from a 69 percent efficient tube was investigated in the same optimum magnetic field associated with the average electron. Initial axial velocities were obtained from a digital disk model calculation.

The magnetic field was first optimized for the average electron which lies between trajectory 15 and 16. The great effect that initial axial velocities had on the refocusing action is apparent. No initial radial velocities were used in this initial test and parallel entry was assumed.

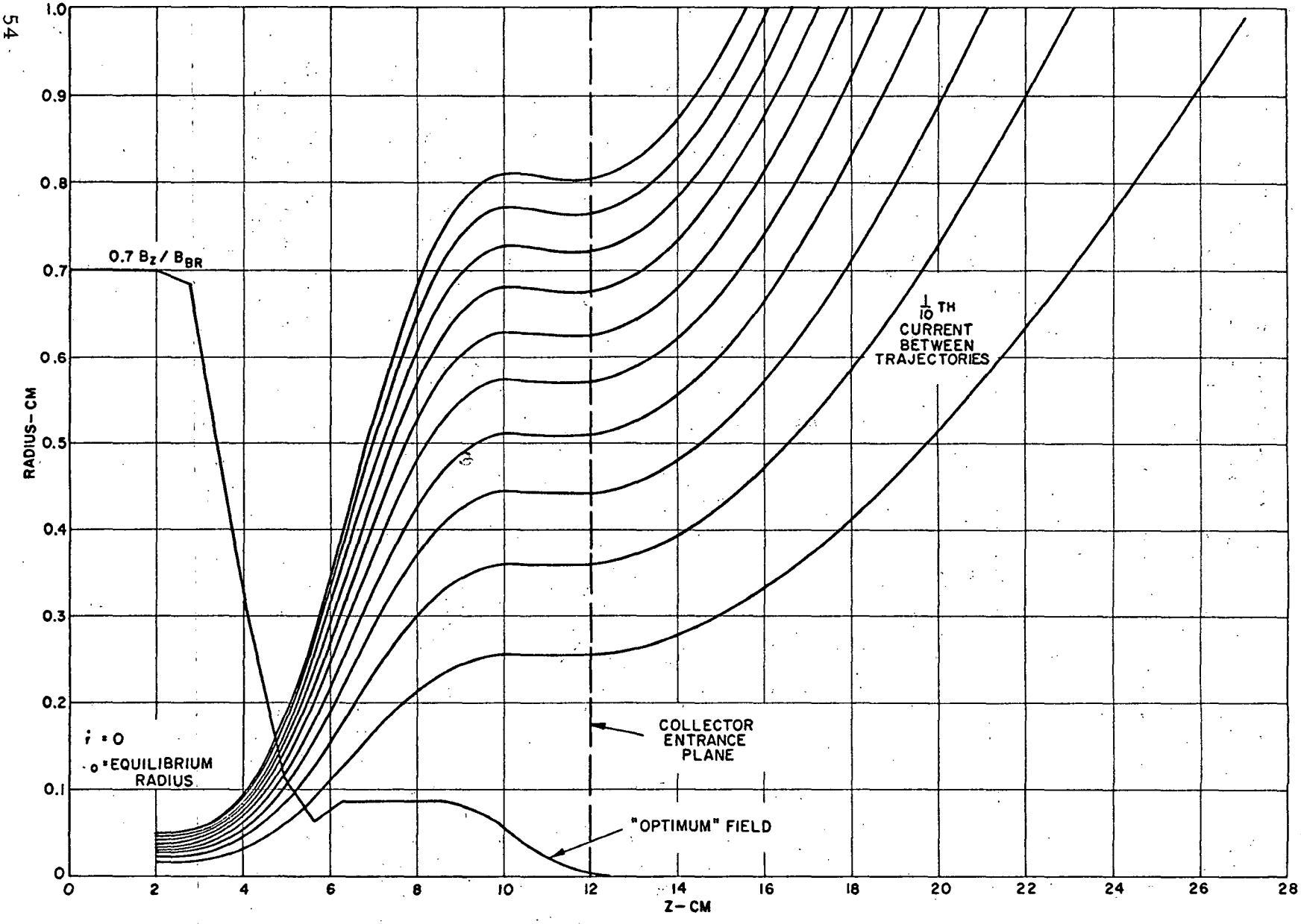

Figure 19 - Dispersion of a Uniformly-Retarded Electron Beam in a Given Magnetic-Field Distribution

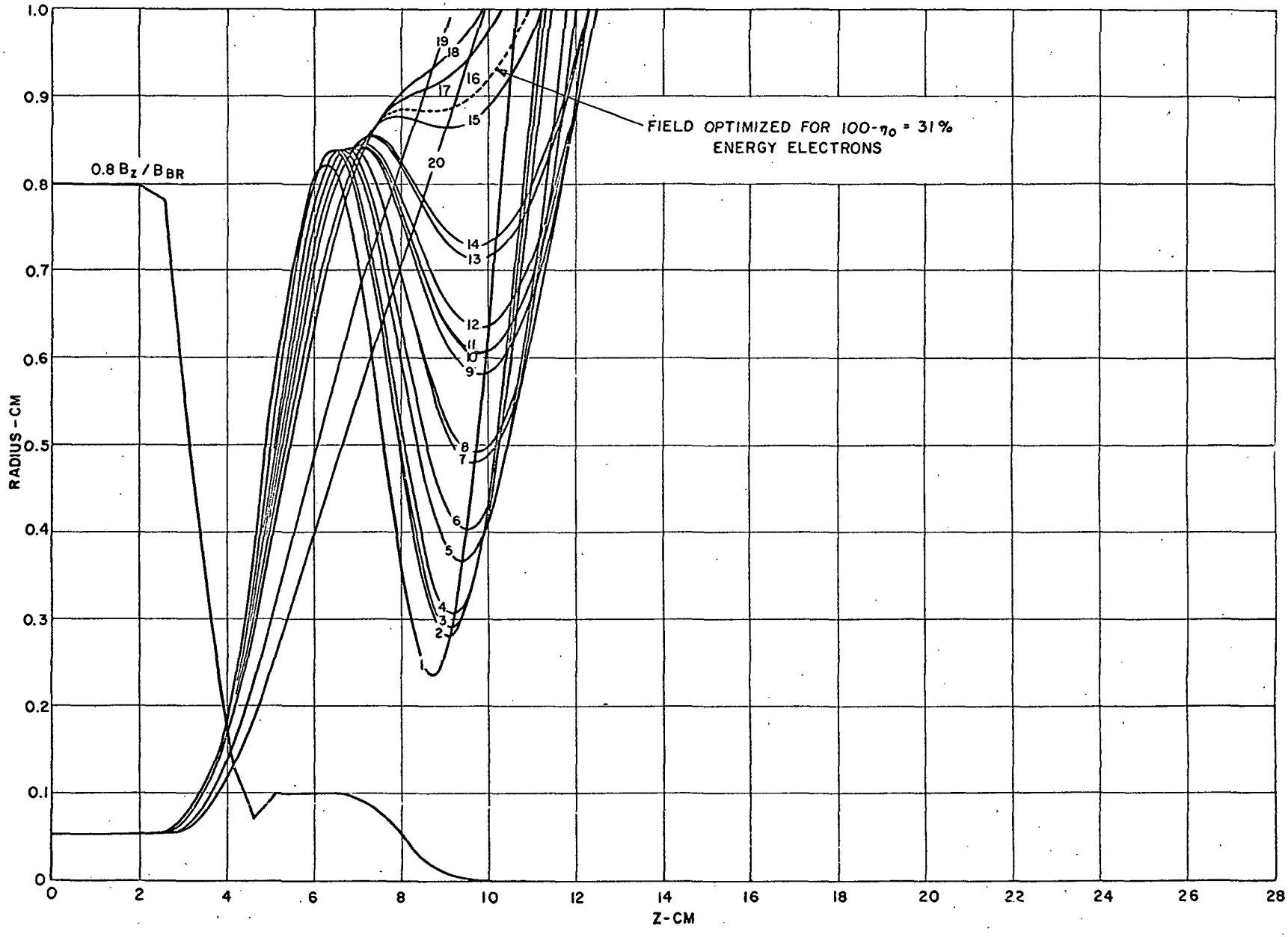

Figure 20 - Dispersion of an Electron Beam With a Velocity Distribution Derived From a Large-Signal Disk-Model Digital Computer Simulation of a Klystron

REFOCUSING IN TAPERED-AXIAL MAGNETIC FIELDS

The next refocusing-field distribution to be investigated was a tapered magnetic field distribution suggested by Dr. H. G. Kosmahl.[4] This field distribution consists of a gradual decrease of the main collimating field to an intermediate field level to allow for beam expansion, followed by a short plateau at the reduced field level to induce the conversion of radial velocities of the expanding beam electrons into axial velocities, thus recollimating the beam for entry into the collector. The length of the beam expansion region in this case was chosen to be two cyclotron wavelengths, the amplitude of the plateau was one-third the initial collimating field strength, and the plateau length was one-half the beam expansion length.

The trajectories of the 20 electron rings were calculated on a digital computer for a total of 15 rf cycles with space charge introduced for only the first cycle. (Because of the high degree of bunching existing in the output gap region, consideration of only one cycle of charge is usually necessary since successive bunches do not overlap.) Figure 21 illustrates the trajectories computed for the 20 rings. It should be noted that the vertical scale is five times the horizontal scale so the apparent angles of the trajectories with respect to the axis are exaggerated by a factor of five.

Figure 10 shows the positions of the rings for ten of these 15 cycles at the instant the tenth cycle is ready to enter the output gap interaction region. This plot was obtained by recording the ring positions at intervals of 2π radians after the initial injection of the first cycle and superimposing the individual sketches of each group of rings. This figure illustrates graphically that distribution of electron velocities in the spent beam after interaction in the output gap causes a smearing of the individual bunches yielding a beam with a reduction in average velocity and rf density modulation. The relatively even distribution of charge lends support to the reduced-velocity dc space-charge model used in the analog computer simulation program.

Trajectories computed with the digital computer program in which three cycles of charge were injected into the output gap are shown in Figure 22. Only the middle cycle of trajectories was recorded and plotted, with space-charge forces being summed over all three groups of rings. The first cycle injected left a distribution of slowly moving rings while fast-moving rings from the last cycle overtook the middle rings, showing the effect of space-charge forces for adjacent cycles. A comparison of Figure 22 with Figure 21 shows that extra space charge from the preceding and following cycles causes greater beam divergence. The greater accuracy, however, is achieved at a cost of increasing the computation time by a factor

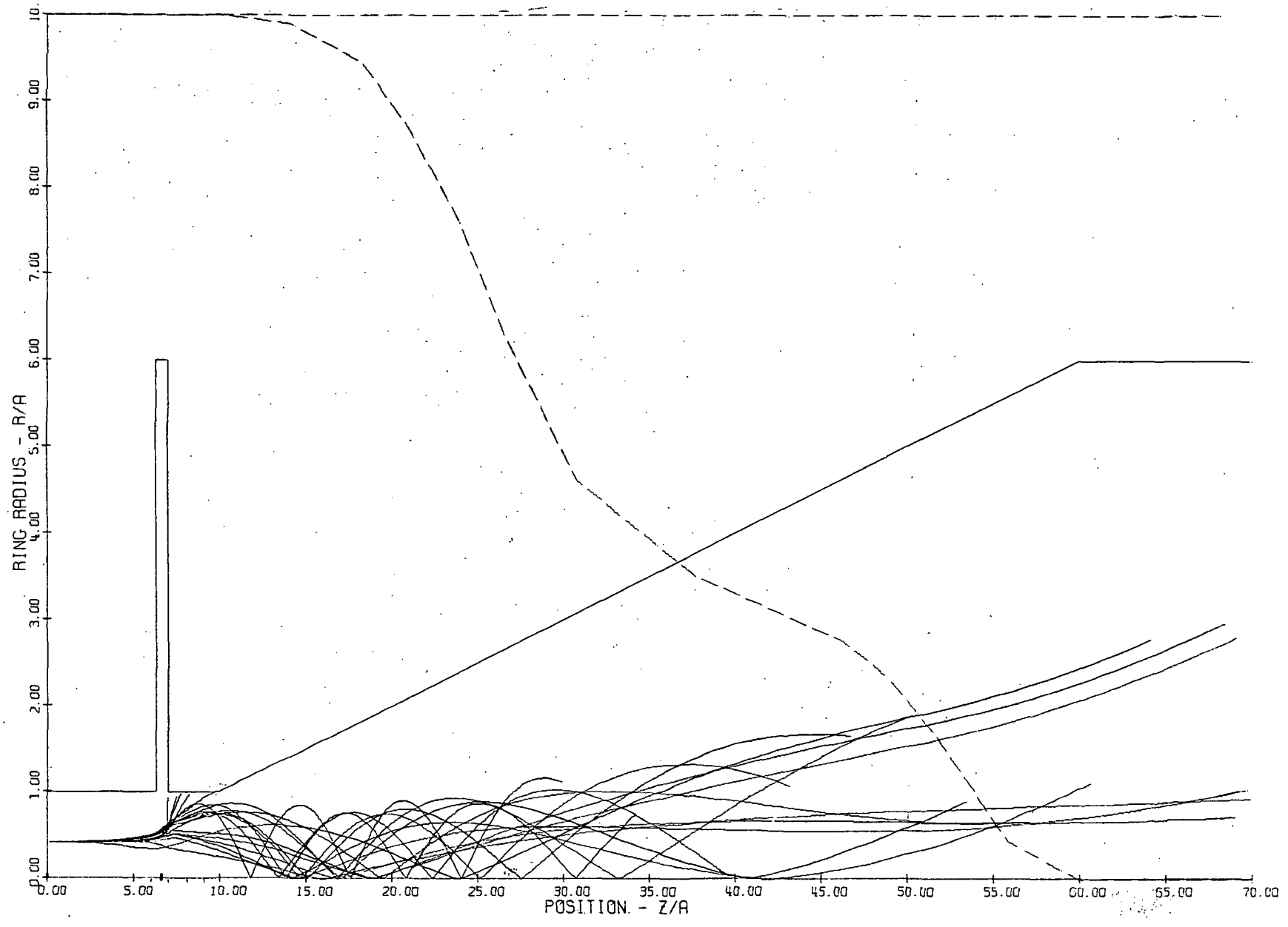

Figure 21 - Digitally Computed Trajectories in Klystron Output Gap Region. Dashed Line Represents the Magnetic Field Profile

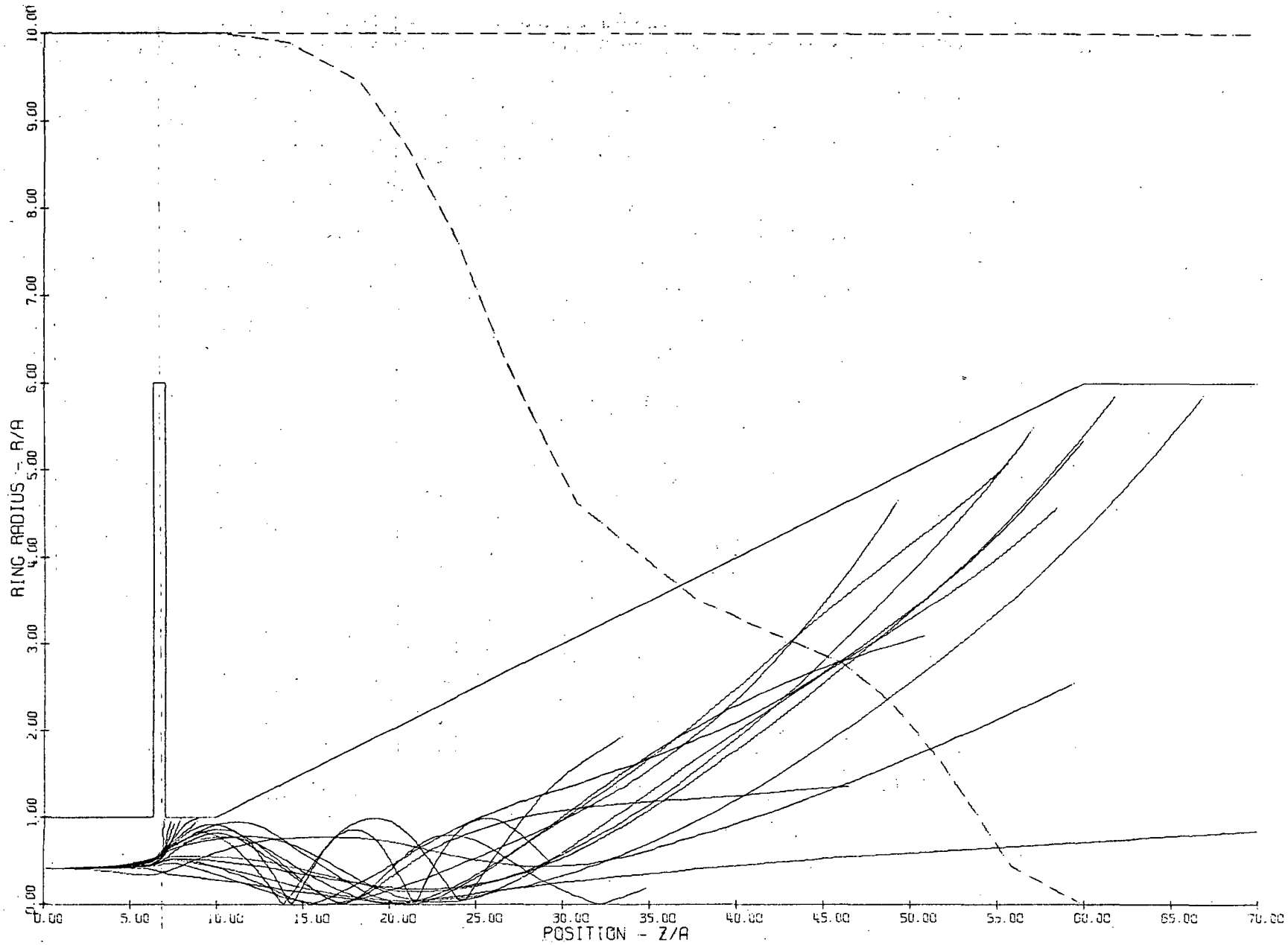

Figure 22 - Digitally Computed Trajectories in Klystron Output Gap Region With One Klystron Bunch Preceding and One Following the Plotted Bunch

of five. A subdivision of each of the 60 disks into three rings would increase this factor to about 45.

The trajectories computed by the analog computer for the same set of input vector velocities used above are plotted in Figure 23. The analog-computed trajectories exhibit more divergence than the one-cycle digital computation, but less than the three-cycle case. In the latter case, the trajectories in the weak magnetic-field region may be in error because a long time step of 0.2π radians was used in the Runge-Kutta integration in order to reduce computation time. Thus the analog computation is in good agreement with either the one cycle or three-cycle disk calculation.

The maximum trajectory angle computed with the analog simulation is 22 degrees, whereas the maximum final angle for the digital computation as illustrated in Figure 22 is 18 degrees.

REFOCUSING IN TAPERED-AXIAL-MAGNETIC FIELDS COMBINED WITH THETA FIELDS

The capability of a theta-magnetic-field region to reduce the residual radial velocities of klystron spent-beam electrons after the beam has been allowed to expand and refocus in a tapered-axial-magnetic field was studied on the analog computer. Trajectories of electrons in an idealized electron beam in which all electrons have been reduced to an average velocity corresponding to a conversion efficiency of 55 percent are illustrated in Figure 24. (The axial-field distribution is the same as that shown in Figure 21.) The "Theta-Field Region" in Figure 24 extends over an axial distance of about nine times the tunnel radius in length. The circumferential field strength is 50 gauss for an initial beam voltage of 9.2 kV.

When the axial-magnetic field is made to drop to zero in a much shorter distance, as in Figure 25, a more compact refocusing region results; however, the theta-field region must be increased in length in order to obtain a sufficient reduction in the radial velocities. A typical plot of the trajectories in the idealized spent beam with uniform velocities is given in Figure 25.

A more detailed analysis with the computed distribution of spent-beam velocities in a 2-kW klystron with an internal conversion efficiency of 55 percent is illustrated in Figure 26. A rapidly decreasing axial-magnetic field distribution is followed by a shaped region in which the circumferential magnetic field has a uniform magnitude of 55 gauss for a 9.2 kV beam. Because electrons moving near the axis require less correction than those further from the axis, it was found desirable to increase the width of the theta-field magnets from about 6.5 tunnel radii on axis to an approximate width of 21 radii at a radius of 12 tunnel radii.

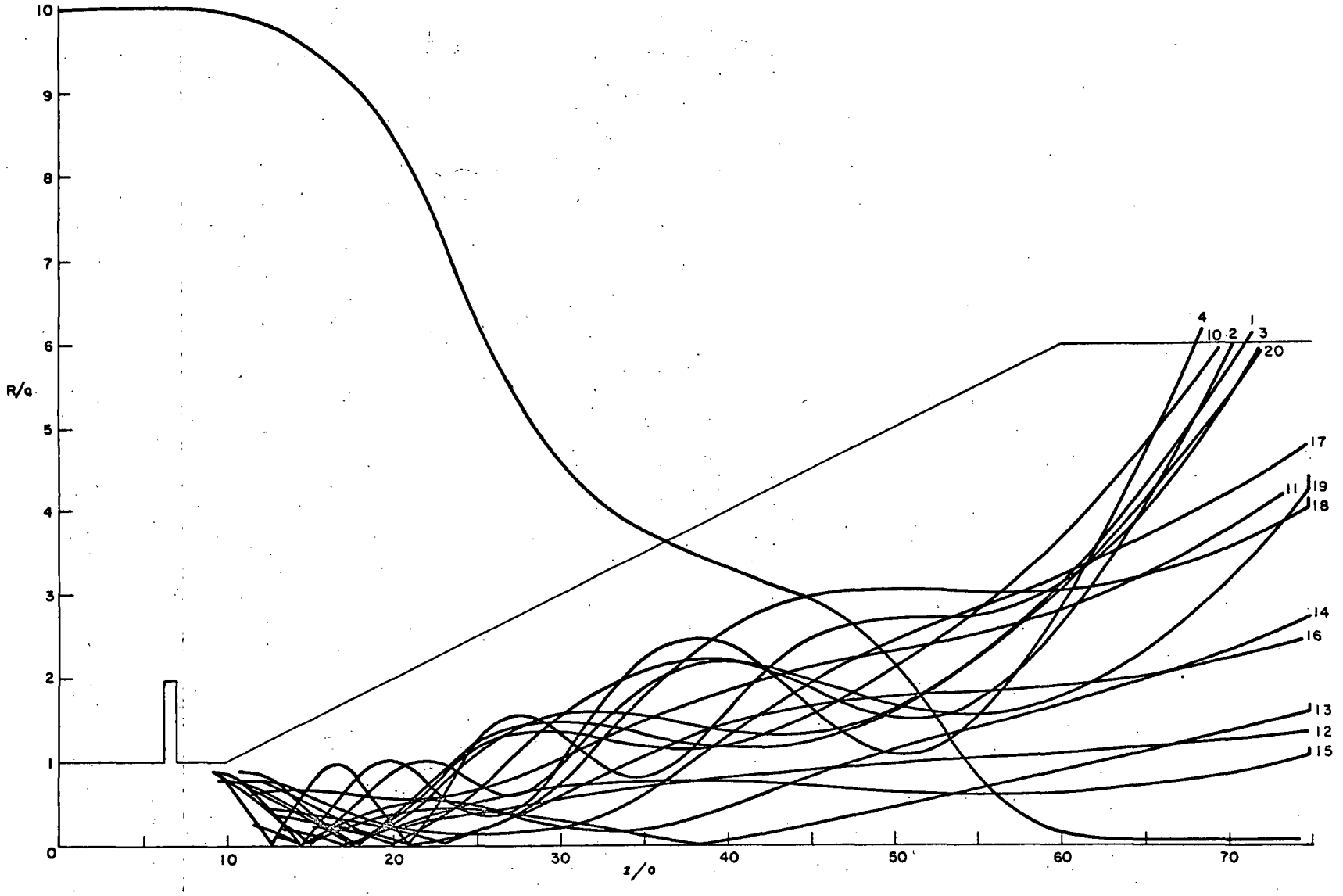

Figure 23 - Analog Computed Trajectories in Klystron Output Gap Region

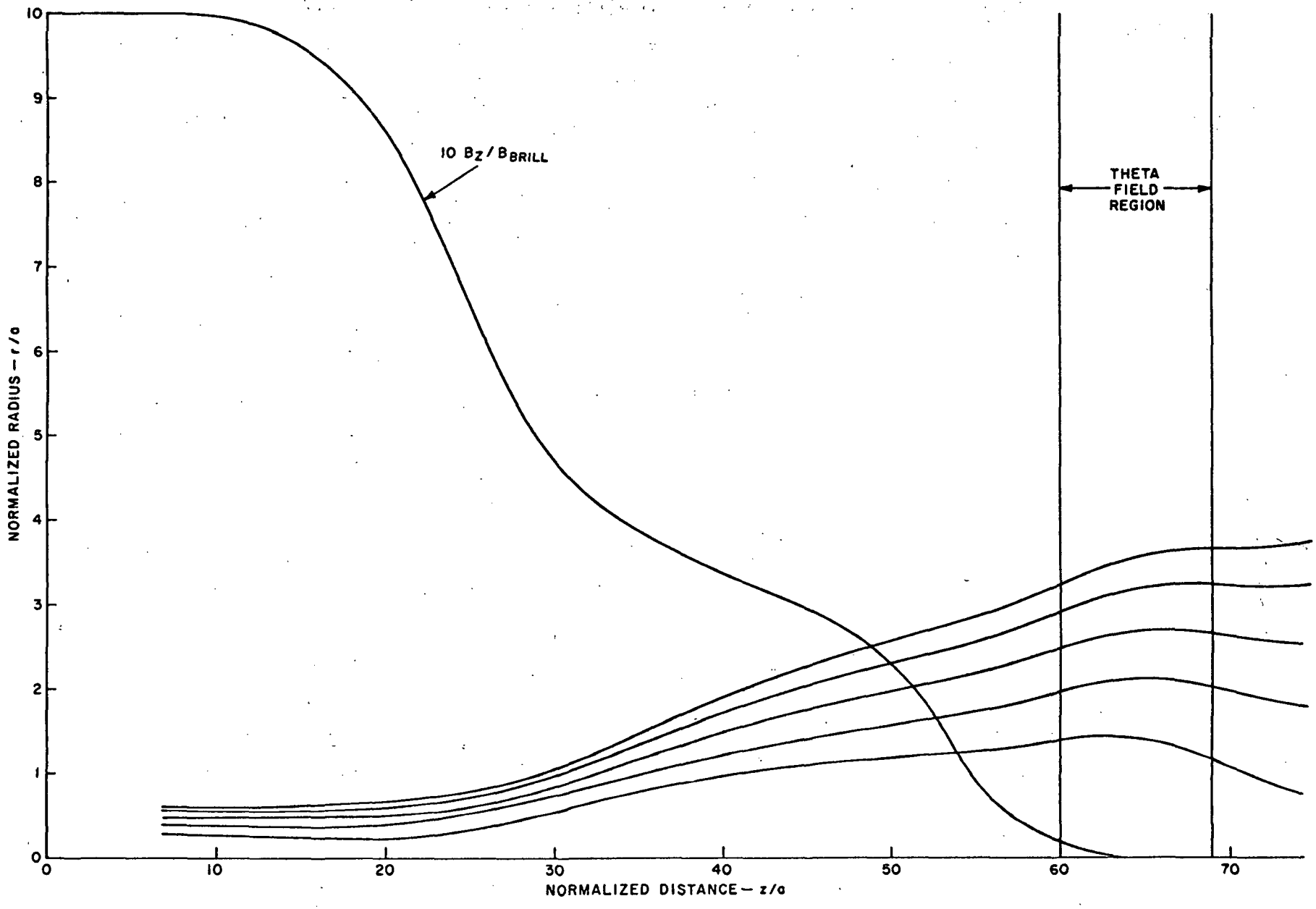

Figure 24 - Trajectories of Idealized Spent-Beam Electrons in a Slowly Decaying Axial-Magnetic-Field Distribution Followed by a Theta-Field Region (All electrons are assumed to have the average velocity corresponding to 45 percent of the beam energy)

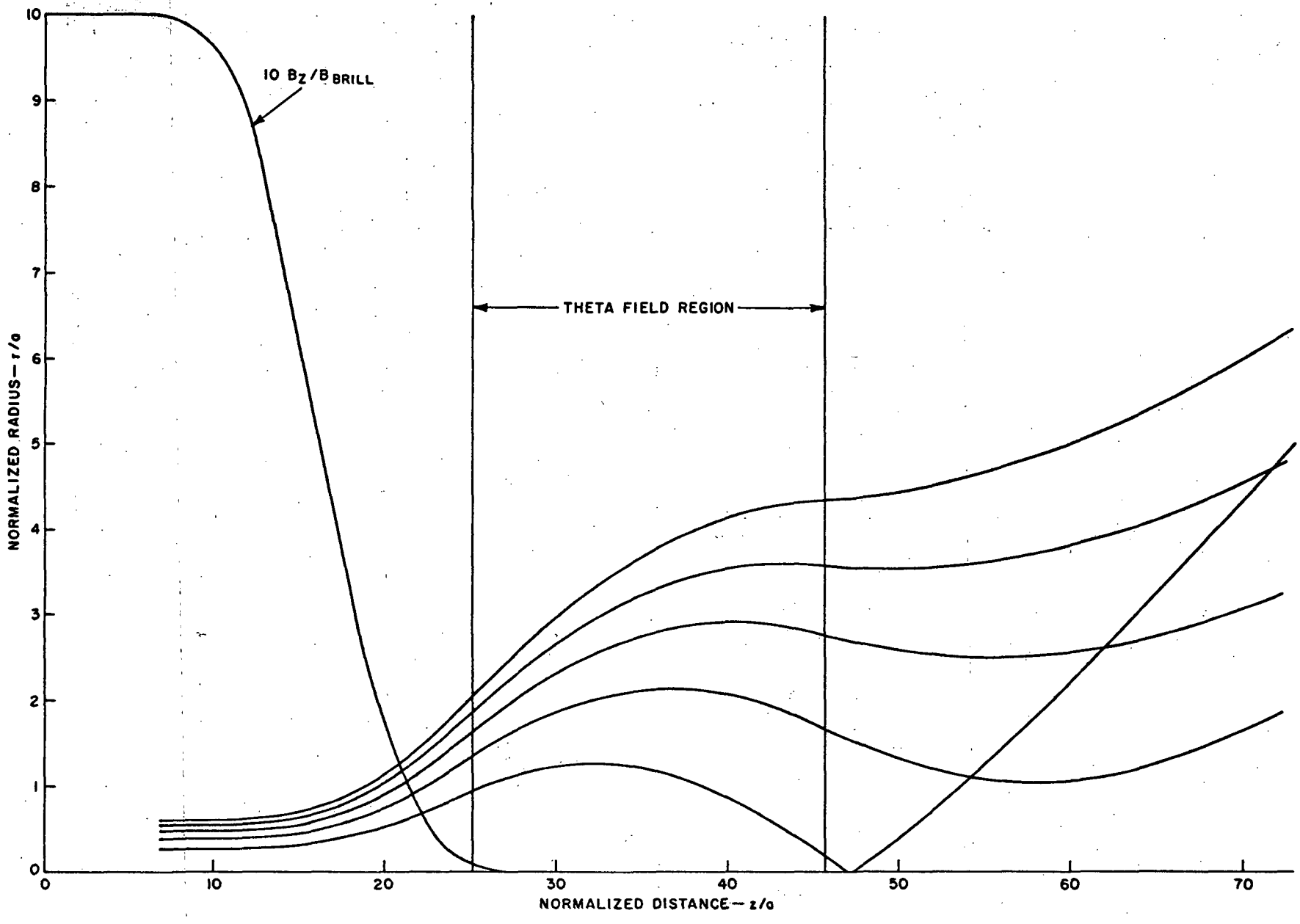

Figure 25 - Trajectories of the Same Spent-Beam Electrons as in Figure 24 In a Rapidly Decaying Axial Magnetic-Field Distribution Followed by a Theta-Field Region

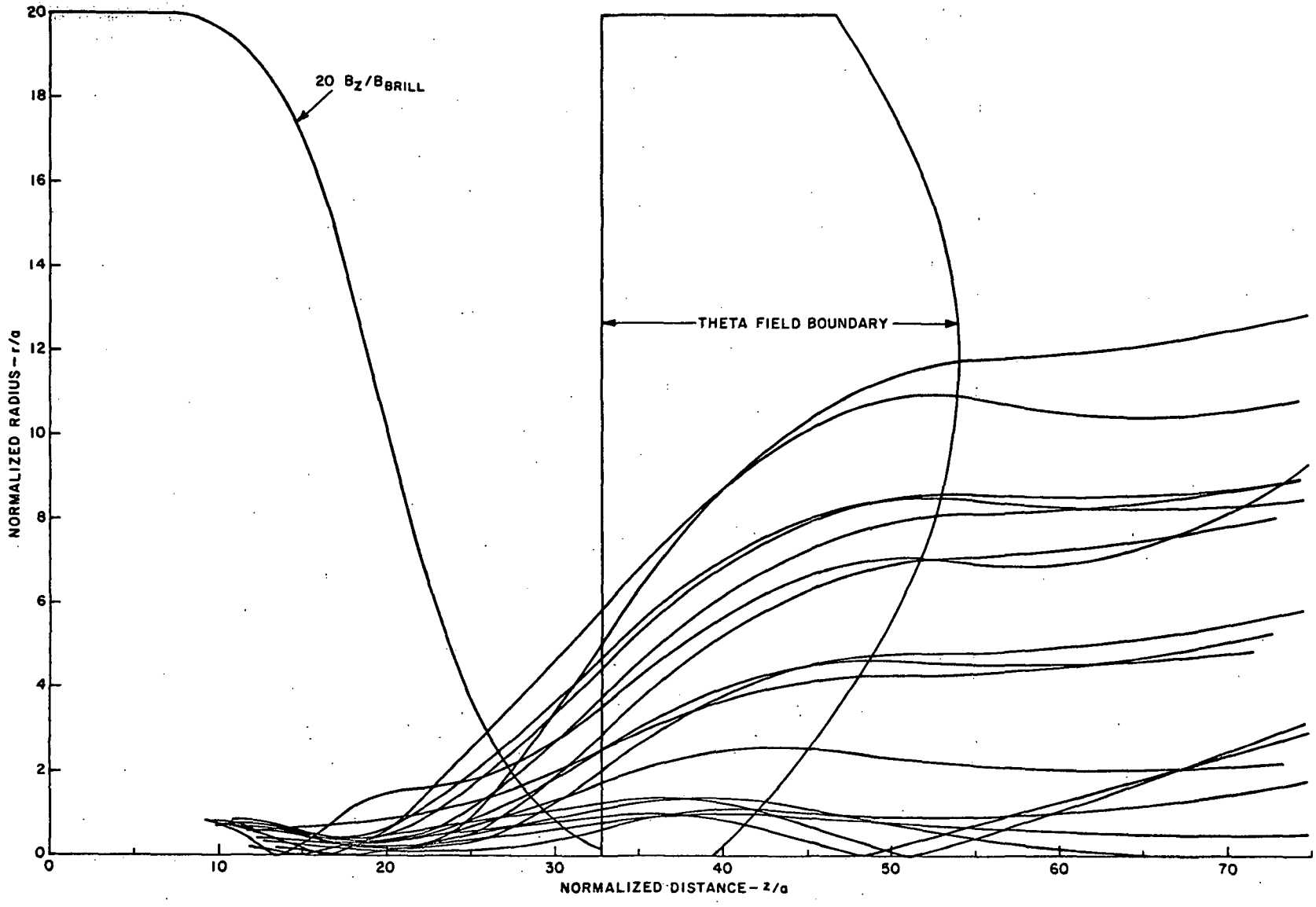

Figure 26 - Trajectories of Spent-Beam Electrons in a Klystron with a Conversion Efficiency of 55 Percent. Rapidly Decaying Axial-Field Distribution is Followed by a Shaped-Theta-Field Region

STATISTICAL EVALUATION AND DISCUSSION OF RESULTS

SELECTION OF REFOCUSING METHODS

The survey of the characteristics of various refocusing methods conducted in the "Study of Refocusing Methods" reported in the preceding section disclosed two types of field distribution that warrant a full statistical evaluation: 1) the Tapered-Axial-Field Distribution, and 2) the Hybrid-Refocusing Field.

The Tapered-Field Distribution consists of an axial-magnetic field that begins with the amplitude of the main beam collimating field, reduces an intermediate value over a linear distance of a cyclotron wavelength more or less, and continues with a short plateau before finally reducing to zero amplitude. The Hybrid-Refocusing-Field Distribution consists of a rapidly decreasing axial-magnetic field from the full amplitude of the main collimating field to a negligible-field amplitude in the shortest possible distance with an apertured magnetic pole piece, followed by a region containing a theta-directed magnetic field component. The theta-directed fields are of uniform amplitude in a region bounded either by parallel planes normal to the axis or by a plane and a curved boundary as illustrated in Figure 26. In both types of refocusing field distributions, the initial field-decay region allows the beam to expand in order to reduce its space charge density to an acceptable level for injection into a subsequent depressed-potential collector. The second field region serves as a beam stabilization region in which the electrons are recollimated to yield reduced injection angles.

Both types of refocusing fields were studied with the analog computer method. Trajectories for the electron rings with the velocity spectra derived by the digital ring-model program at both band edges and at band center of the hypothetical 2-kW, 12-GHz satellite-borne klystron power amplifier were traced and the refocused ring radii and velocity components were recorded. This preliminary study was followed by an extensive study of 40 different cases involving 6 basic high-efficiency klystrons and one low-efficiency klystron designed for 12-GHz operation.

STATISTICAL COMPARISONS OF HYBRID AND TAPERED-FIELD REFOCUSING SYSTEMS

In order to provide a basis for judging the effectiveness of the refocusing methods, a statistical analysis was made of the ring radii and

trajectory angles after the traversal of the output interaction gap as given in Table V. The statistical properties of the emerging beam including the standard deviation σ_θ of the electron trajectory angles are given in Table VI.

In addition to the case of focusing of the main beam with the Brillouin magnetic field, the case of strong focusing with a collimating field equal to twice the Brillouin field with the cathode both shielded and unshielded was also considered. In all cases, the spectra as developed for Table V were used. Although these spectra were derived for the particular case of twice-Brillouin collimation of the main electron beam emitted from an unshielded partially-immersed cathode, there would be little difference in the post-output gap spectra for the other types of focusing. By using the same spectra at a given frequency for all the types of refocusing fields considered, a more direct comparison of their properties may be made.

Eleven sets of trajectories in various refocusing fields were computed with the analog computer program and the final ring radii and velocity components were recorded. The results of a statistical analysis of these trajectories is given in Table VII. A complete tabulation of the final radii, velocities and angles for all the rings for each case is given in Appendix B.

An inspection of the results tabulated in Table VII shows that, in general, both the Kosmahl field distribution and the Hybrid distribution perform better at midband than at either band edge in the hypothetical 40-MHz bandwidth klystron. Defining the beam expansion ratio as the square of the

- - - - - - -

TABLE VI - STATISTICAL PROPERTIES OF BEAM AFTER TRAVERSING OUTPUT INTERACTION GAP

Frequency (GHz)	$(r/a)_{max}$	$(r/a)_{rms}$	θ_{avg} (deg)	σ_θ (deg)	θ_{max} (deg)
11.98	0.99	0.64	-1.7	5.6	18.0
12.00	0.70	0.38	2.6	8.7	42.5
12.02	0.83	0.54	-6.3	14.0	60.1

TABLE VII - COMPUTED STATISTICAL PARAMETERS OF REFOCUSED BEAMS

Case	Frequency (GHz)	Field Distribution Type	Main Beam Collimation	Area Expansion Ratio	$(r/a)_{max}$	$(r/a)_{rms}$	θ_{avg} (Degree)	$\theta_{std.dev.}$ (Degree)	θ_{max} (Degree)
1	11.98	Tapered	Brillouin Field	67	5.6	3.5	5.5	3.2	11.6
2	12.00	Tapered	Brillouin Field	50	5.2	3.0	3.8	3.0	12.2
3	12.02	Tapered	Brillouin Field	85	7.5	3.9	7.1	7.2	31.9
4	11.98	Hybrid	Brill, Shaped θ Field	174	9.5	5.6	0.8	1.7	7.7
5	12.00	Hybrid	Brill, Shaped θ Field	94	14.2	4.1	2.0	4.1	21.3
6	12.02	Hybrid	Brill, Shaped θ Field	200	13.0	6.0	0.9	3.0	11.2
7	12.00	Tapered	2xBrill, Shielded Cath.	24	5.0	2.1	6.2	5.5	19.6
8	12.00	Tapered	2xBrill, Immersed Cath.	56	5.3	3.2	10.0	4.7	18.0
9	12.00	Hybrid	Brill, Straight θ Field	123	16.0	4.7	5.5	6.1	32.6
10	12.00	Hybrid	2xBrill, Shielded Cath.	112	10.5	4.5	3.2	4.2	19.0
11	12.00	Hybrid	2xBrill, Immersed Cath.	230	11.0	6.4	6.0	6.1	34.8

final rms beam radius divided by the initial rms beam radius preceding the output gap, one observes that across the band the Kosmahl tapered distribution allows a beam expansion ratio of about 6 whereas the Hybrid distribution allows an expansion of about 100. At both band edges the Hybrid distribution performs better than the Kosmahl tapered distribution in limiting the maximum trajectory angle, but conversely, the Kosmahl distribution is superior at midband.

The field amplitudes for both the Kosmahl tapered-field distribution and the Hybrid distribution were modified successively to correspond to three types of beam collimation:

1) Brillouin focusing of the beam emitted from a shielded cathode;

2) Strong focusing of the beam emitted from a partially immersed cathode, with the collimating field amplitude equal to twice the Brillouin amplitude; and

3) Augmented field focusing at the output interaction gap, of a beam emitted from a shielded cathode, the augmented field at the output gap having an amplitude equal to twice the Brillouin value.

The first two types of beam collimation represent classical, ideal methods of focusing. The third type is representative of actual practice; wherein it is often found necessary to increase the magnitude of the collimating field in the output interaction region of klystrons in order to counteract excessive beam expansion caused by increased space-charge forces in the highly bunched beam and radial accelerations encountered in the output gap. Brillouin focusing was employed in cases using both the tapered distribution and the Hybrid-field distribution at both band edges and at band center of the 12-GHz klystron with a 40-MHz bandwidth. The strong focused and augmented field-focused beam cases were computed only for the center frequency. In all Hybrid-field cases except one, the theta-field region was assumed to have an optimally curved boundary as illustrated in Figure 26. The slight compromise in performance that results from having a simpler planar boundary to the theta-field region is demonstrated in one case of Brillouin collimation.

An examination of Table VII shows the refocusing properties of either the tapered distribution or the Hybrid-field distribution to be about equal for both Brillouin and strong focusing of electron beam. In the case of enhanced field collimation of the beam emitted from an unshielded cathode, expansion is less than that for the Brillouin beam in both types of refocusing field distributions.

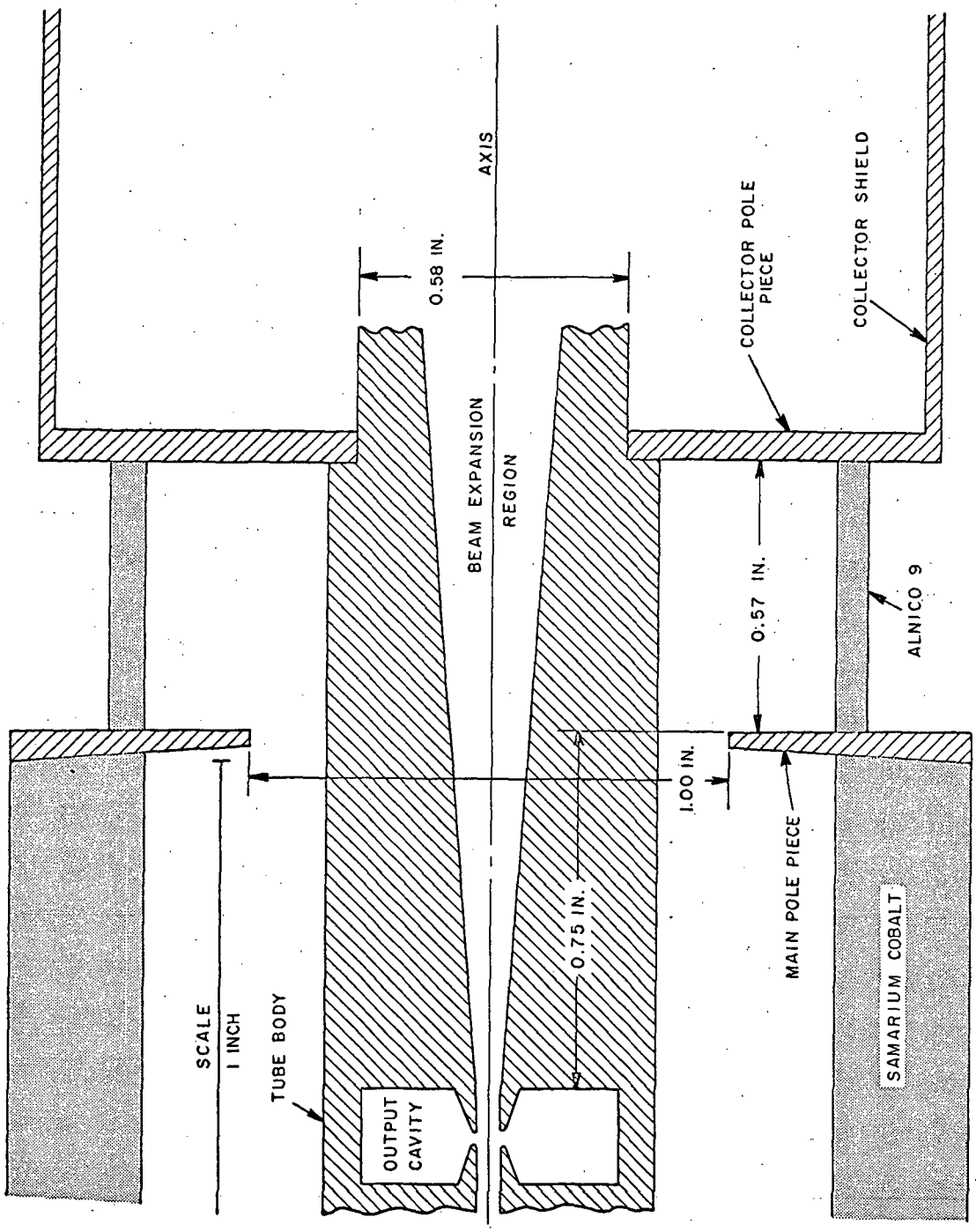

Figure 27 - Permanent Magnet and Pole Piece Geometry for Tapered-Refocusing Fields

PHYSICAL DESIGN OF REFOCUSING SYSTEM

The physical implementation of the tapered-axial magnetic field requires a slight departure from conventional methods of terminating the field between the output interaction region and the collector. By a proper choice of pole-piece geometry (eg. multiple apertures or auxiliary permanent magnets) the desired axial-field distribution can be achieved for either electromagnetic or permanent magnetic-focused beams. In Figure 27 is sketched a typical pole piece and magnet configuration that will yield the taper-field configuration required for the hypothetical 2-kW, 12-GHz klystron considered in this study.

The Hybrid-Field Refocusing system requires a conventional pole piece for the rapid reduction of the main collimating magnetic field followed by a set of wedge-shaped permanent magnets for generating the theta field. Since the axial component of the magnetic field has been reduced to zero in the theta-field region, there is no transverse motion of the spent beam from a shielded cathode, hence no beam interception will occur on the faces of the wedge magnets. Beams from unshielded cathodes will contain some residual angular velocities in the magnetic field free region which may lead to interception on the wedge faces. The leading edge of the wedge magnets may be shielded by a heavy copper grid.

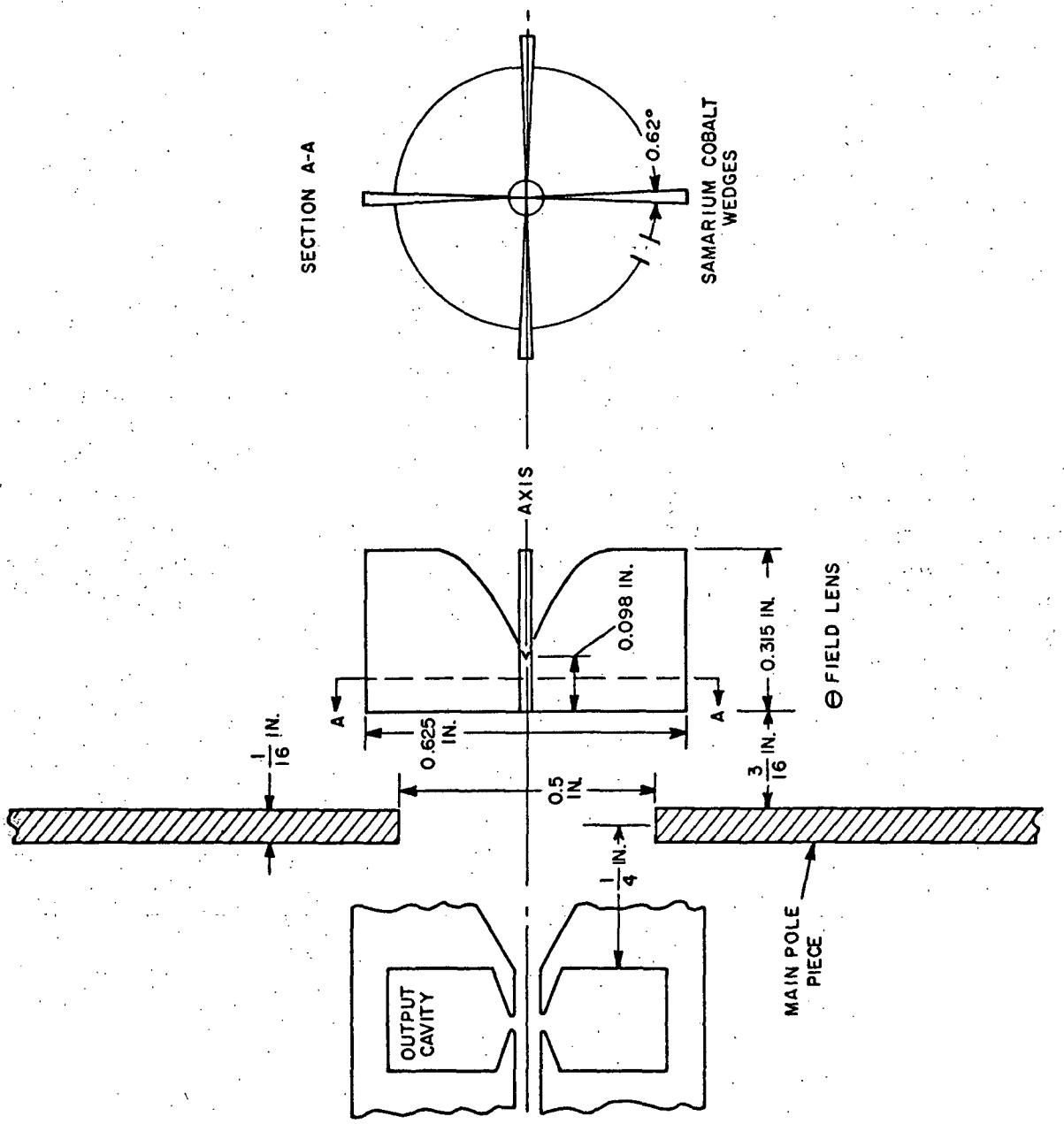

Figure 28 - Hybrid-Type Refocusing System

GENERAL PARAMETRIC SURVEY OF REFOCUSING CHARACTERISTICS

DEVELOPMENT OF BASIC SATELLITE-BORNE KLYSTRON DESIGNS OF 12 GHz

In order to provide a larger base for evaluating the characteristics of tapered magnetic field beam refocusing methods, a set of 12 basic klystron designs for application as power amplifiers at 12 GHz in satellite-borne broadcast systems was developed with the use of the GE Small-Signal Klystron Simulation Computer Program. For reasons discussed below, only six of the 12 designs were considered feasible. The six acceptable designs, designated by the letters A through F were subsequently simulated with the GE Large-Signal Klystron Simulation Program to yield tables of disk position just prior to entry into the output gap. The digital program FOCUS previously described, was then used to extend the trajectories of the 20 disks (now subdivided into 3 rings each) through the output gap of each klystron. Finally, the analog computer was used to generate the complete electron trajectories through the beam expansion and beam recollimation regions following the output gap before injection into the entrance aperture of a depressed-potential collector. After the computation of the trajectories a complete statistical analysis of the spent-beam electrons with respect to velocity classes was made both before and after traversing the refocusing region.

The basic parameters of the 12 designs developed are given in Table VIII. Beam power levels of 2, 4, and 8 kW were selected to give a range of output power levels of approximately 1, 2, and 4 kW, respectively -- a range considered to be of interest for satellite-based broadcast systems within the next decade. Microperveance levels of 0.5 and 0.75 were chosen as being in the range of interest for klystrons with the high efficiencies required for space applications. Also, values of the tunnel size parameter γa equal to 0.75 and 1.00 were selected as being realistic values for good klystron design. With these parameters considered as fixed, the dependent parameters such as beam voltage, beam current, beam current density, beam plasma frequency, plasma wavelength, tunnel i.d., cavity R/Q and output cavity bandwidth can be computed, as shown in the Table. For the computations leading to the parameters listed in the table, the largest possible transit angle between 0.5 and 1.0 radian was selected in order to provide the highest possible value of R/Q and the maximum bandwidth. (Selection of output gap transit angle can not be independent of other parameters, since the length of the interaction gap determines the physical height of the cavity,

TABLE VIII - 12-GHz KLYSTRON DESIGN PARAMETERS

Design	No.	Beam Power (kW)	γa	$\mu perv$	V_o (kV)	I_o (A)	J_o (A/cm^2)	ω_q/ω	$\lambda_q/4$ (in.)	Tunnel I.D. (in.)	Min Final Drift (in.)	Output Cavity θ (rad)	Output Cavity R/Q (ohms)	Bandwidth (MHz)
A	1	2	0.75	0.50	6.94	.289	104	7.35	.541	.039	.277	.75	190	96
B	2	4	0.75	0.50	9.15	.438	119	7.31	.623	.045	.306	1.0	200	115
C	3	8	0.75	0.50	12.10	.666	140	7.26	.718	.051	.306	1.0	195	128
	4	2	0.75	0.75	5.89	.339	143	9.08	.403	.036	.244	.5	175	122
	5	4	0.75	0.75	7.78	.515	168	9.04	.464	.041	.243	.5	165	130
	6	8	0.75	0.75	10.30	.784	195	8.99	.535	.047	.244	.5	150	139
	7	2	1.00	0.50	6.94	.289	59	7.11	.560	.052	.279	1.0	170	85
	8	4	1.00	0.50	9.15	.438	69	7.09	.643	.059	.279	1.0	165	95
	9	8	1.00	0.50	12.10	.666	79	7.03	.742	.068	.278	1.0	155	104
D	10	2	1.00	0.75	5.89	.339	81	8.78	.417	.048	.222	.5	135	93
E	11	4	1.00	0.75	7.79	.515	93	8.74	.479	.055	.253	1.0	170	134
F	12	8	1.00	0.75	10.30	.784	108	8.70	.553	.063	.279	1.0	160	148

which may be limited by the close spacing between the penultimate cavity and the final output cavity as required for efficient broadband design.) The cathodes of these klystrons were considered to be partially immersed in the main collimating field, which was 2.5 times the Brillouin value in magnitude.

Of the twelve designs considered, six were found to incorporate parameters that were not mutually compatible, the lower perveance requiring the lower value of γa, and the higher perveance the higher values of γa. Design 4 was eliminated because its plasma wavelength was too short for good cavity spacing. In Designs 5 and 6, the beam density is greater than 150 A/cm^2, which value is taken as a limit in the state-of-art of beam formation for long-lived, high beam transmission klystrons. Designs 7, 8, and 9 were eliminated because they exhibited insufficient bandwidth for a multi-channel transmitter.

In addition to the six acceptable designs (letters A through F) a seventh design (G) was considered. This design, a 4-kW, 12-GHz klystron, was operated under low-efficiency conditions and was analyzed with an independent large-signal ring-model output gap simulation program at NASA-LeRC. The computed velocity spectra after the beam had traversed the output gap were supplied by NASA-LeRC for this study.

The essential computed features of the seven electron beams used for evaluating refocusing fields are listed in Table IX. Two perveance values are listed with tube efficiencies ranging from a high of 65 percent to a low of 23 percent. The lowest efficiency among the six high-efficiency designs is 57 percent. For each perveance three different power levels were studied. The cyclotron wavelength λ_{c1} listed in the table was computed in terms of the main collimating field and the average electron velocity of the spent beam after traversing the output gap. It was found that the beam from Design D with a large velocity spread was the most difficult to refocus properly, while beams having a small axial velocity spread could be easily refocused with practically any reasonable field. The standard deviation of the normalized axial velocities varied from 0.19 to 0.25. While these numbers appear to be quite close together, the ease of refocusing is quite different. The velocity spectra of all seven beams are given in Appendix C together with a statistical analysis of the axial velocities and exit angles. No clear-cut relationship between the angular dispersion before and after refocusing was observed indicating that the refocused beam spectrum is not strongly influenced by radial velocities.

TABLE IX - KLYSTRON SPENT-BEAM PARAMETERS

Design	Efficiency (%)	Beam Power (kW)	μperv	$\overline{r/a}$	r/a_{rms}	$\overline{\theta}$ (Deg)	θ_{rms} (Deg)	θ_{max} (Deg)	$\overline{\dot{z}/u_o}$	$\sigma_{\dot{z}/u_o}$	λ_{cl}/a	Collimating Field* (Tesla)
A	65	2	.50	.460	.488	1.03	7.14	21.2	.533	.241	4.60	0.4122
B	61	4	.50	.450	.472	0.76	6.92	14.2	.575	.224	4.96	0.4103
C	65	8	.50	.385	.406	0.36	10.04	23.7	.530	.240	4.59	0.4161
D	62	2	.75	.452	.472	-0.92	8.61	20.1	.552	.252	3.89	0.3789
E	57	4	.75	.447	.467	0.03	5.15	10.8	.618	.203	4.36	0.3800
F	57	8	.75	.423	.445	0.96	5.82	11.3	.616	.208	4.34	0.3813
G	23	8	.50	.420	.440	-1.82	4.70	30.8	.874	.191	7.36	0.4165

*2.5 x Brillouin Field

STATISTICAL ANALYSIS OF THE REFOCUSED TRAJECTORIES

In order to establish design specifications for refocusing field distributions, a statistical analysis was made of the trajectory angles and radii of the spent beam electrons after passing through various field configurations. Twenty different field shapes were investigated and a total of 40 sets of 60 trajectories were computed through the refocusing region. Each of the seven beam spectra previously described were used. After tracing the trajectory of each electron through the desired refocusing field distribution, the final vector velocity components and radius were recorded on punched tape. Each punched tape containing a set of data was given a serial tape number which subsequently was used to identify the trajectory set, and the resulting data were statistically analyzed with a time-sharing digital computer.

As above, the rms radius of the beam, the average angle, rms angle and standard deviation of the angles of the beam electrons after traversing the refocusing fields to reach the aperture of the collector were computed. In addition, the 60 electrons in each set were arranged monotonically with respect to their energy and divided into four subsets with approximately equal total energy content, and an independent analysis was made of each subset. The number of electrons falling in each energy class is inversely proportional to the average energy of the class, with the number in the low, second, third and high energy groups usually being about 30, 15, 10, and 5, respectively, for a total of 60 electrons.

Representative examples of plots of electron trajectories for each of the seven klystrons are given in Figures 29 through 35. Also sketched in Figure 29 is the refocusing magnetic field distribution denoting the lengths L_1 and L_2 and the field amplitudes B_o (alternatively given as B_1 below) and B_2. The B_2 to B_1 ratio is chosen so the beam current density is reduced from its initial value in the beam before refocusing to a final value of less than 4 amperes/cm^2. The length L_1 defining the beam expansion region is the length over which the axial component of the magnetic field is caused to fall from its initial amplitude B_o or B_1 to the plateau magnitude B_2. L_2 spans the beam stabilization region over which the magnetic field remains at approximately plateau amplitude B_2 before falling rapidly to zero amplitude. The plane at which the axial component of the magnetic field falls to zero is taken to be the entrance plane to a multistage depressed-potential collector.

Two sets of criteria were used in evaluating the characteristics of a field configuration of expanding and refocusing the spent electron beams. The basis for the first standard was the initial assumption that a slightly

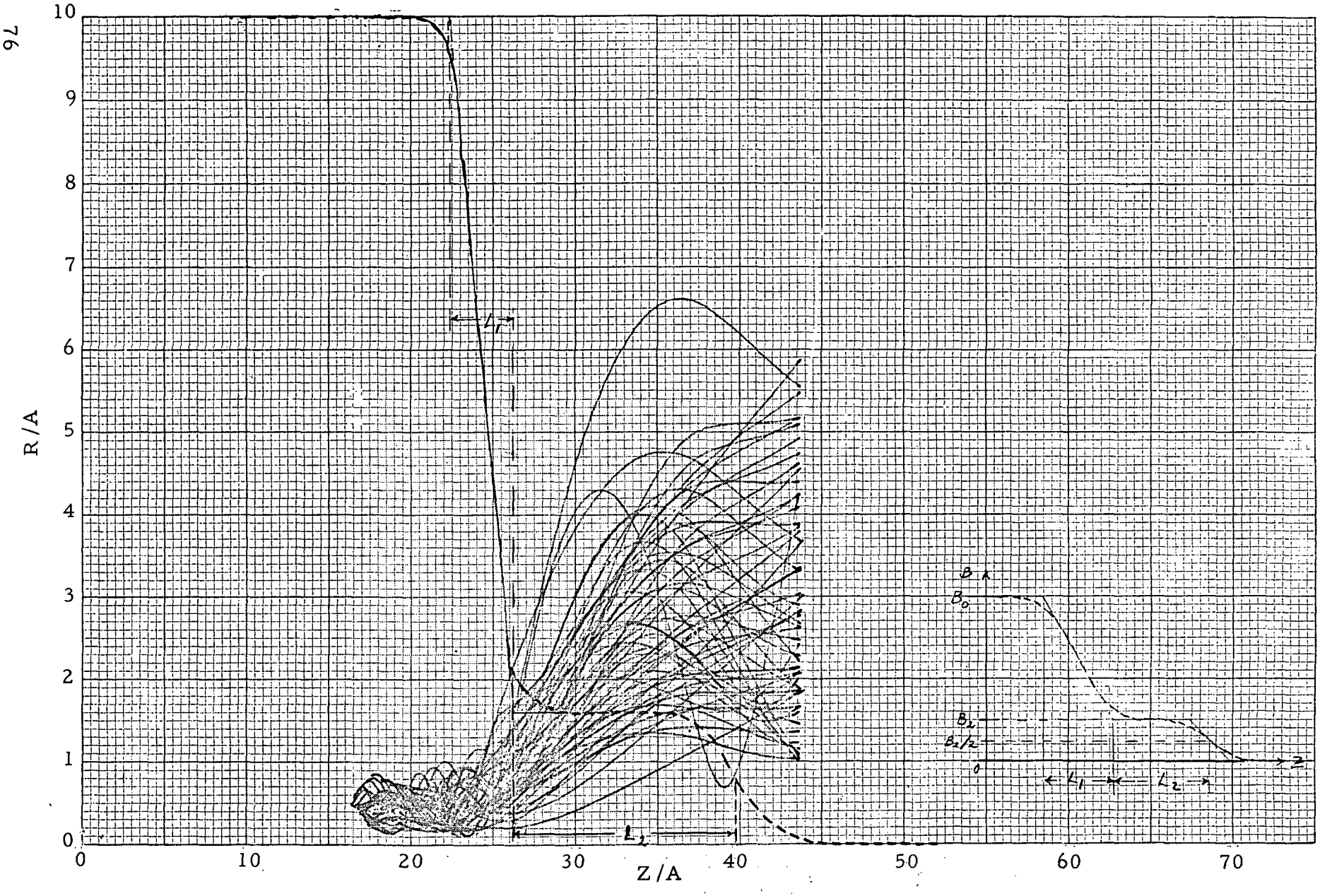

Figure 29 - Design A, Field G - Tape 7

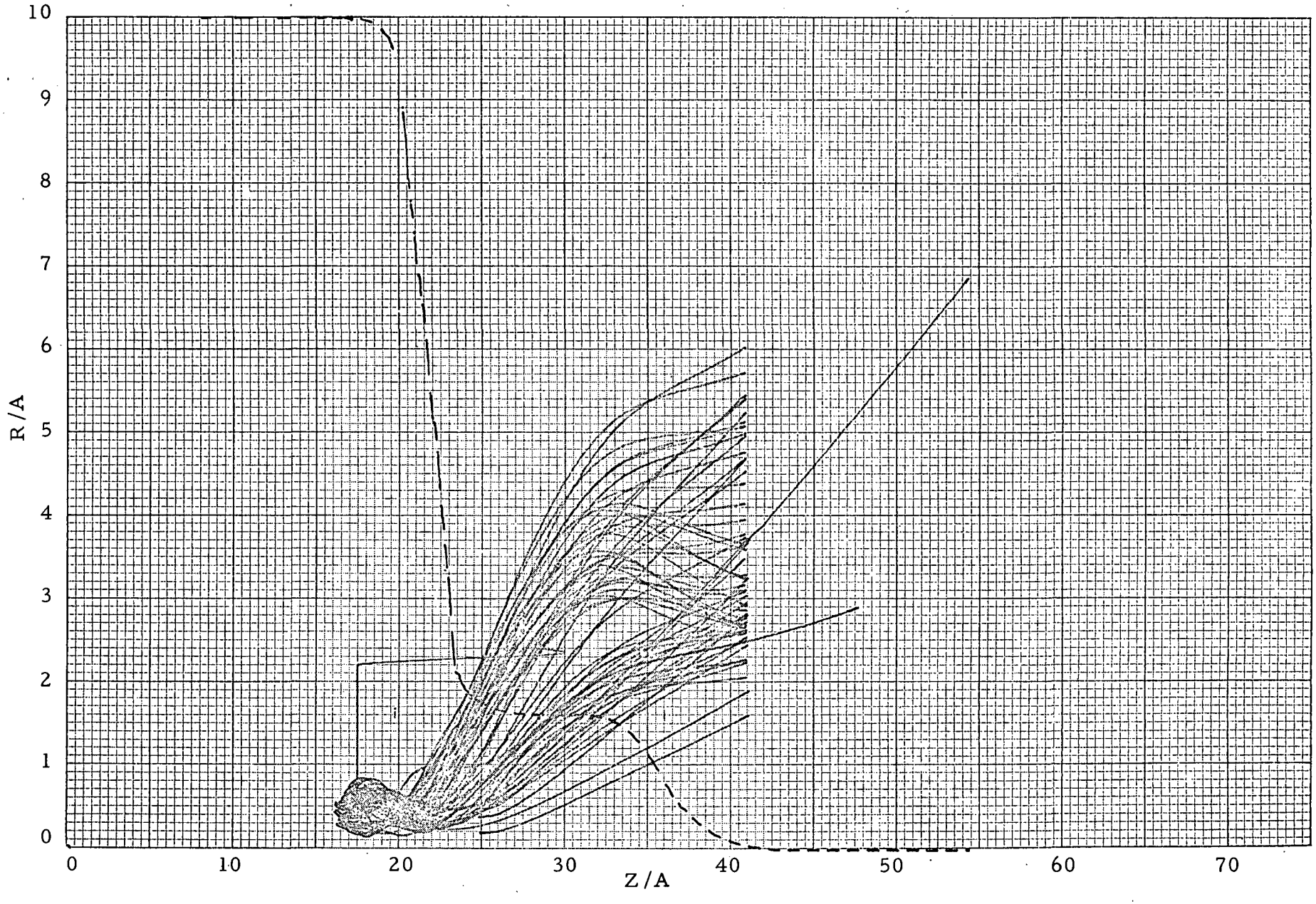

Figure 30 - Design B, Field N - Tape 14

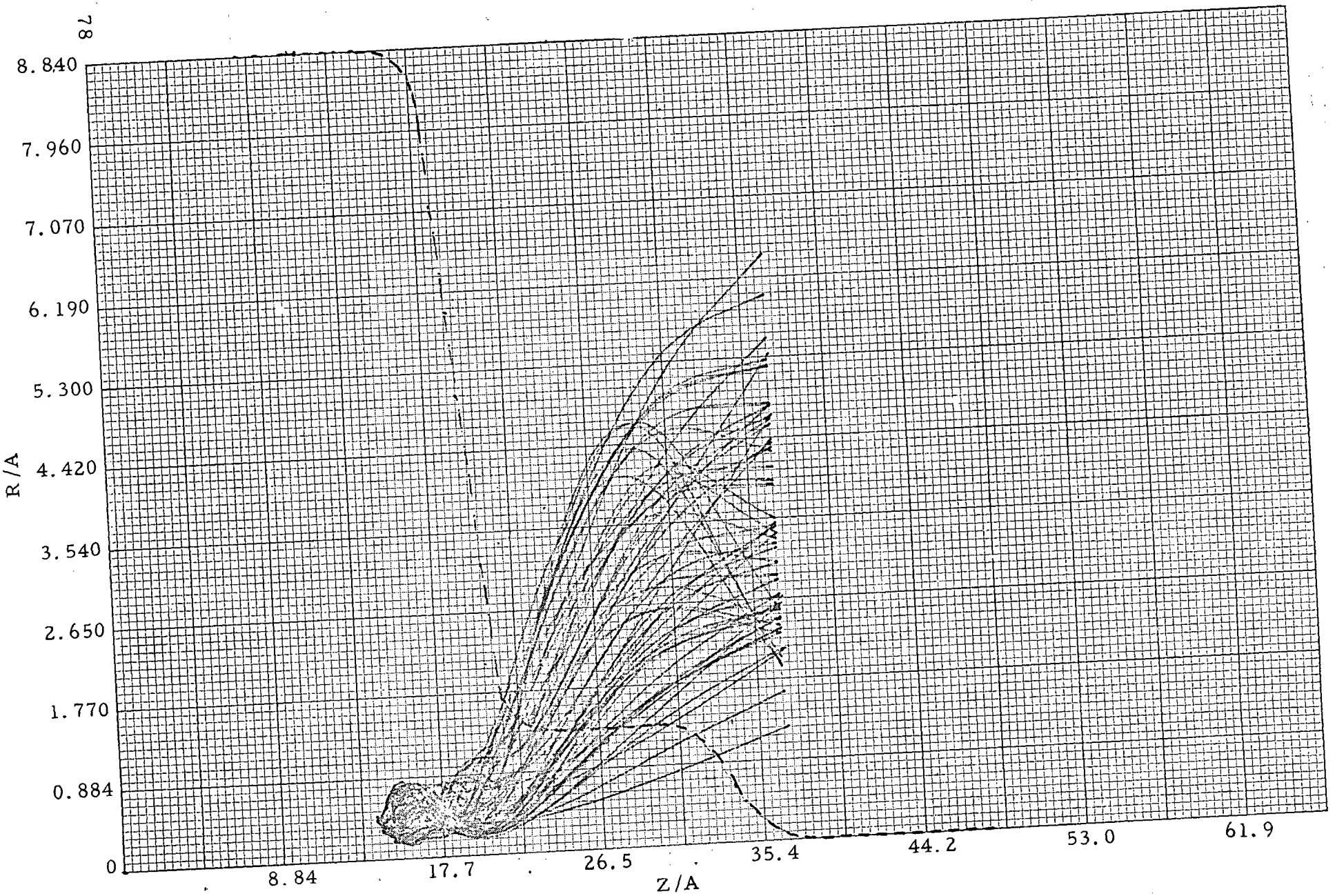

Figure 31 - Design C, Field P - Tape 15

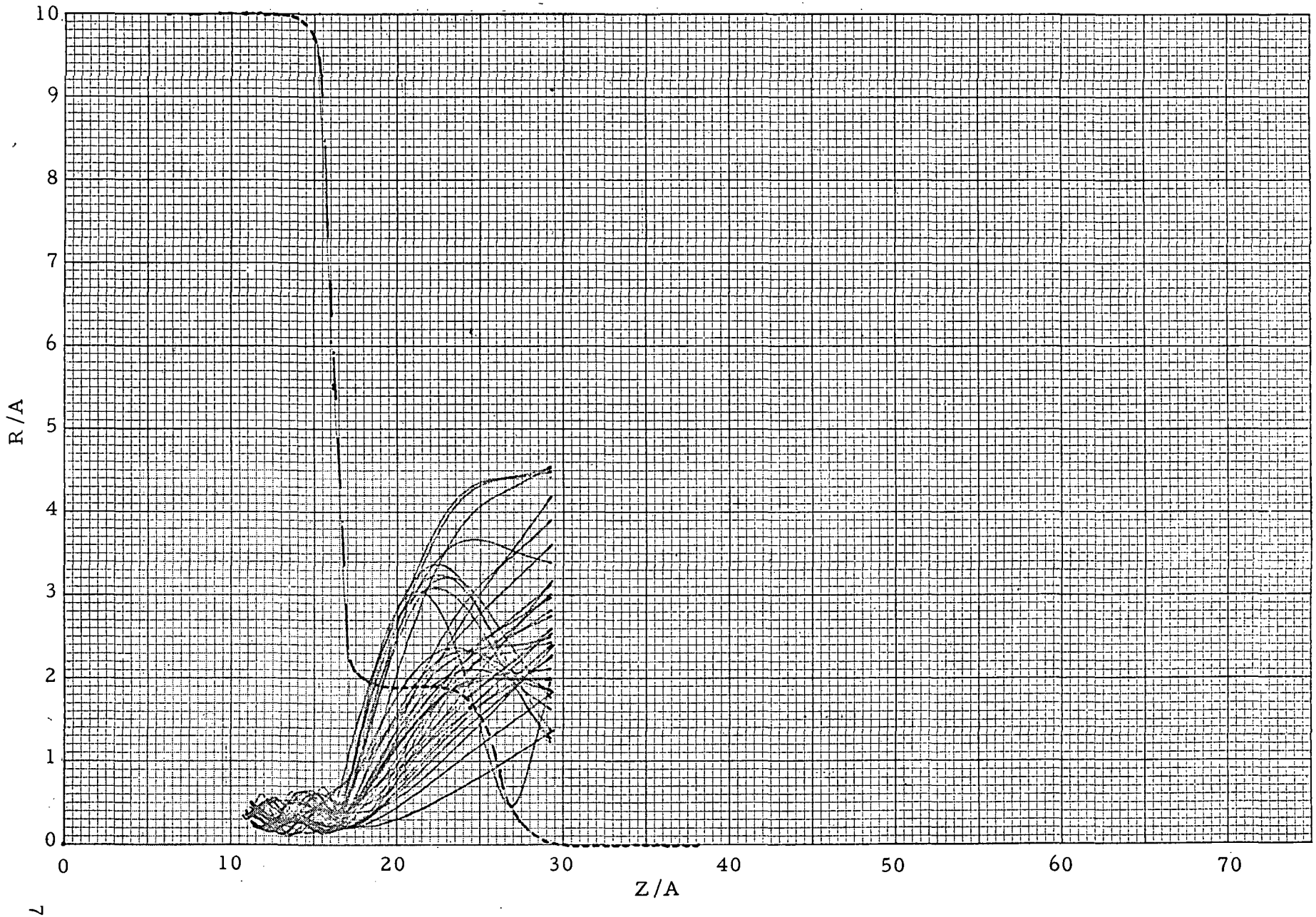

Figure 32 - Design D, Field Q - Tape 16

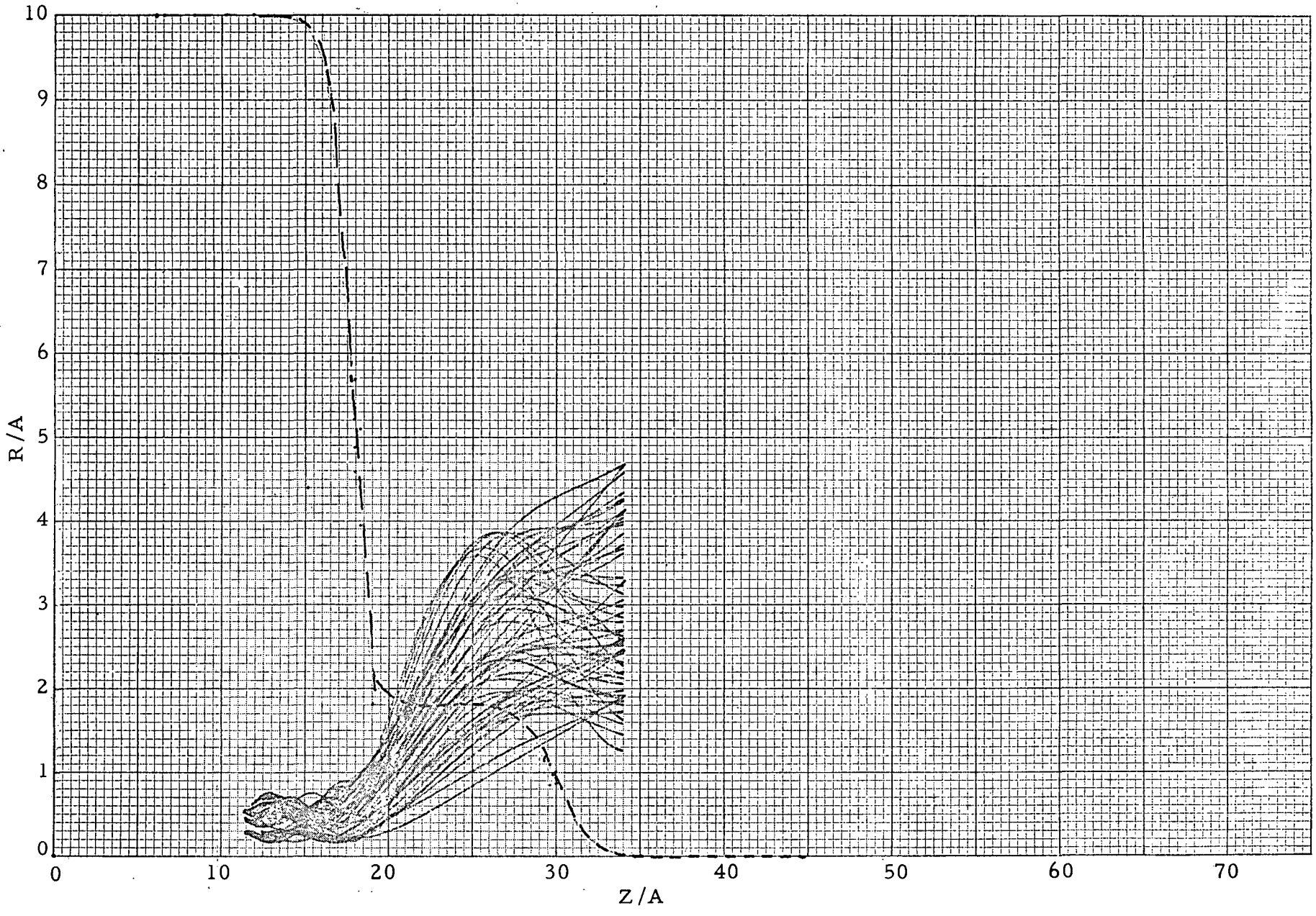

Figure 33 - Design E, Field R - Tape 18

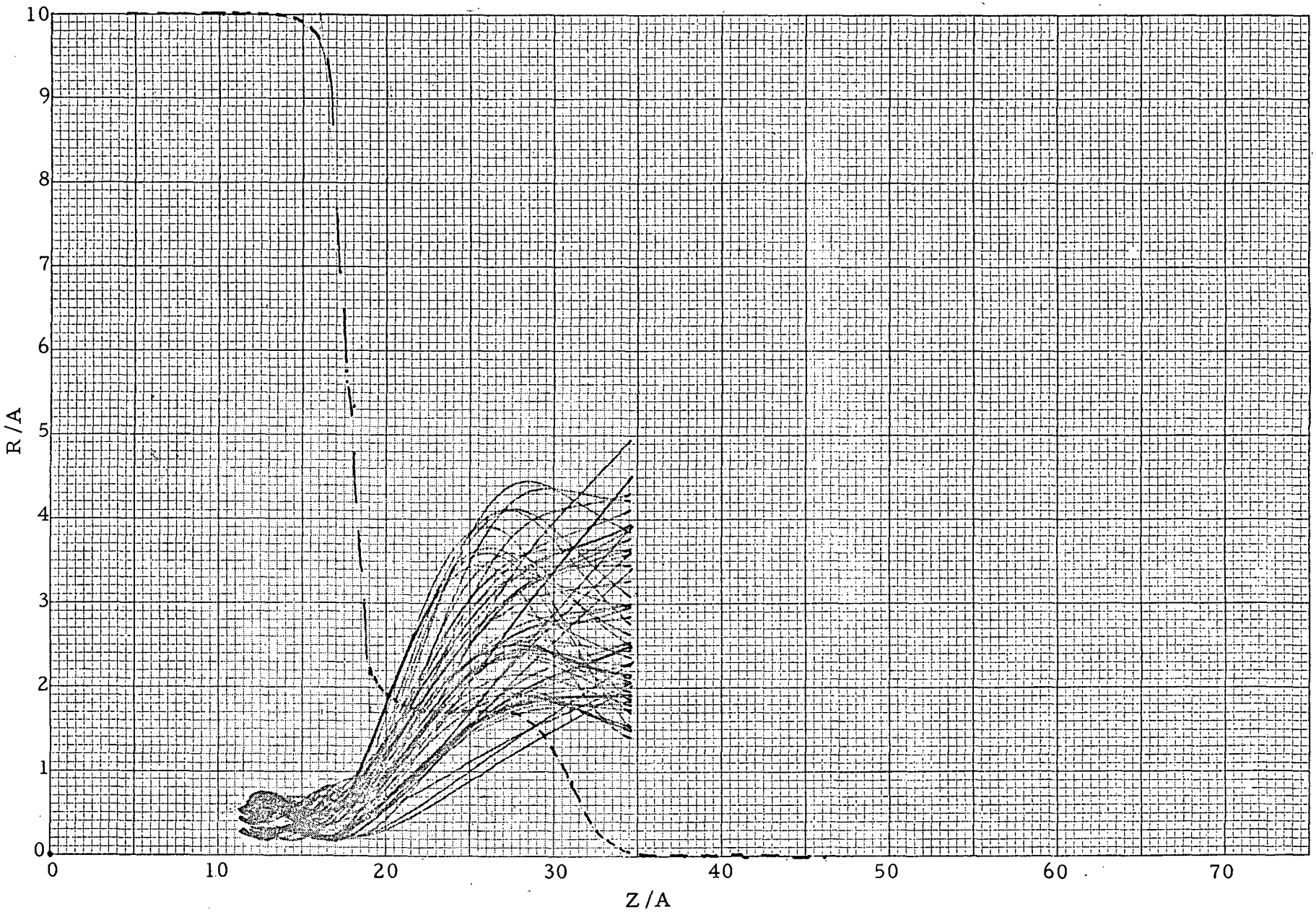

Figure 34 - Design F, Field S - Tape 18

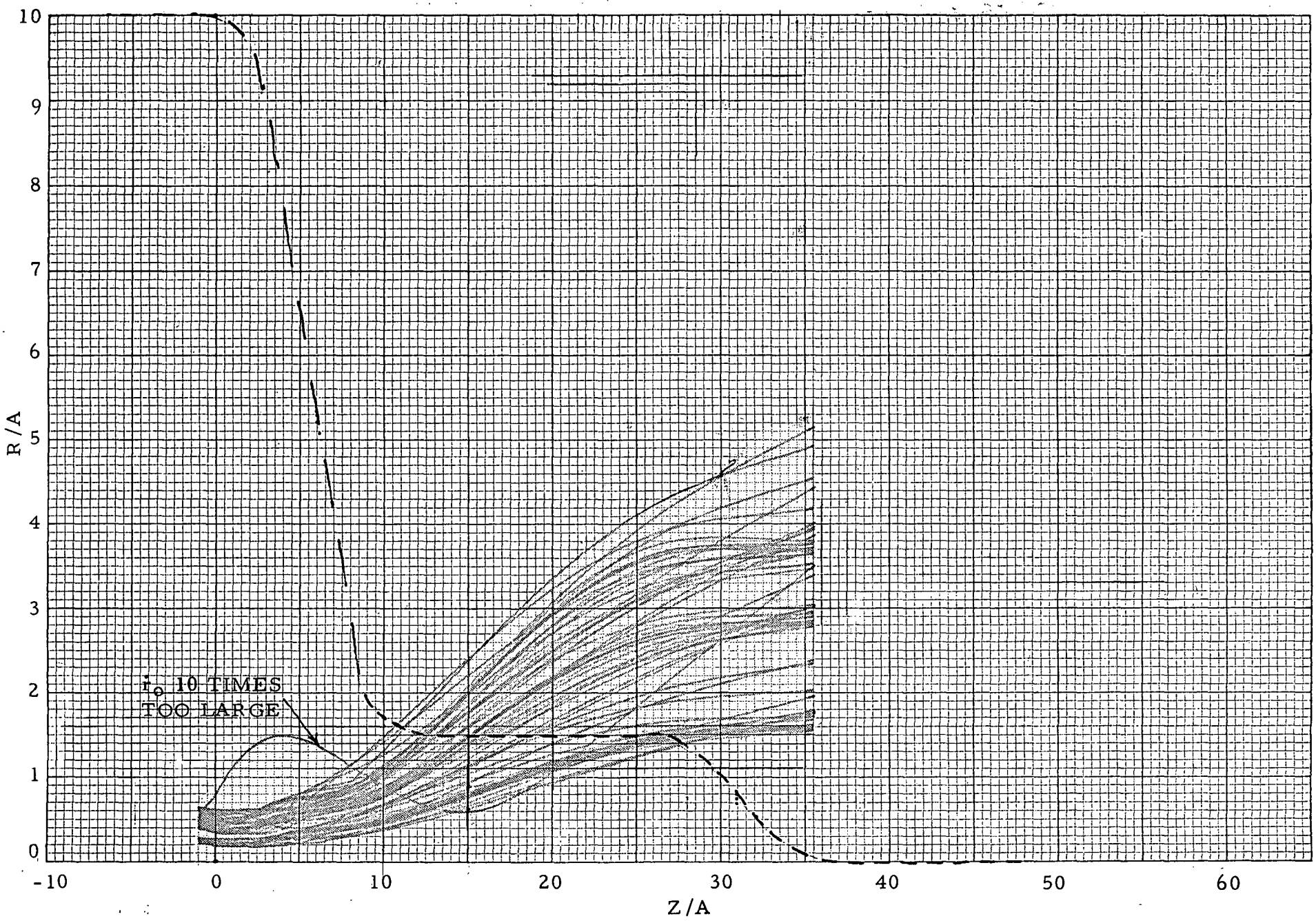

Figure 35 - NASA Low Efficiency Klystron, Field T - Tape 22

expanding beam would be desirable for entrance into the multistage depressed-potential collector, it having been observed that an average entrance angle of between 2 and 5 degrees would minimize the incidence of electrons on the central spike of the collector. Minimum Average Angle Refocusing Standard for a successful refocusing field configuration requires the following criteria to be met: the average trajectory angle in the refocused beam must be less than 8 degrees; and no more than 10 percent of the trajectories may have an angle above 15 degrees with reference to the axis. Of the 40 complete cases studied, 24 passed this test and 16 failed. The trajectory plots shown in Figures 29 through 35 meet this standard for an overall slightly diverging beam. The output angles of all trajectories of the seven best designs meeting this standard are given in Appendix C. A second set of criteria leading to better energy recovery is discussed below.

The dependence of refocusing system performance on the lengths L_1 and L_2 is graphically shown in Figure 36 where the symbol o denotes passing performance and the symbol x denotes failure according to the Minimum Average Angle Refocusing Standard. While some beams can be refocused with practically any reasonable field, a region around $0.5 < L_1/\lambda_{c1} < 1$ and $L_2/\lambda_{c2} = 0.45$ assures a passing performance for all seven klystron beams. In particular, designs A and D, which have the greatest axial velocity dispersion (and, incidentally, the lowest beam power of 2 kW) could not be acceptably refocused with any other combination of L_1 and L_2 under consideration. Design A was extensively studied with L_1 as long as 7.54 cyclotron wavelengths and L_2 as long as 1.03 cyclotron wavelengths in the local field. It was therefore concluded that the best refocusing systems meeting the Minimum Average Angle Refocusing criteria has a rapid field drop-off over a distance somewhat less than one cyclotron wavelength, followed by a plateau having a length of slightly less than one-half a local cyclotron wavelength.

Subsequent to the calculation of the preceding 40 sets of electron trajectories in various field configurations and their rating based on average angle criteria for the complete set of trajectories, a more detailed analysis was made with respect to velocity classes in the spent beam spectrum. This study revealed that optimum average angle focusing based on computations of all 60 trajectories in a set was obtained at the expense of a relatively large angle for the fast electrons. Since the fast electrons penetrate the deepest into the multistage collector before being retarded to a low collection velocity, large apertures would be required in the collector plates with a consequent reduction in collection efficiency and increase in back streaming. A new standard was developed for rating the refocusing effectiveness of a given field configuration for a given spent beam velocity spectrum primarily requiring better recollimation of the fastest group of electrons. The Maximum Energy Recovery Refocusing Standard requires that the fastest group of electrons have an rms angle of 5 degrees or less, the slowest group-

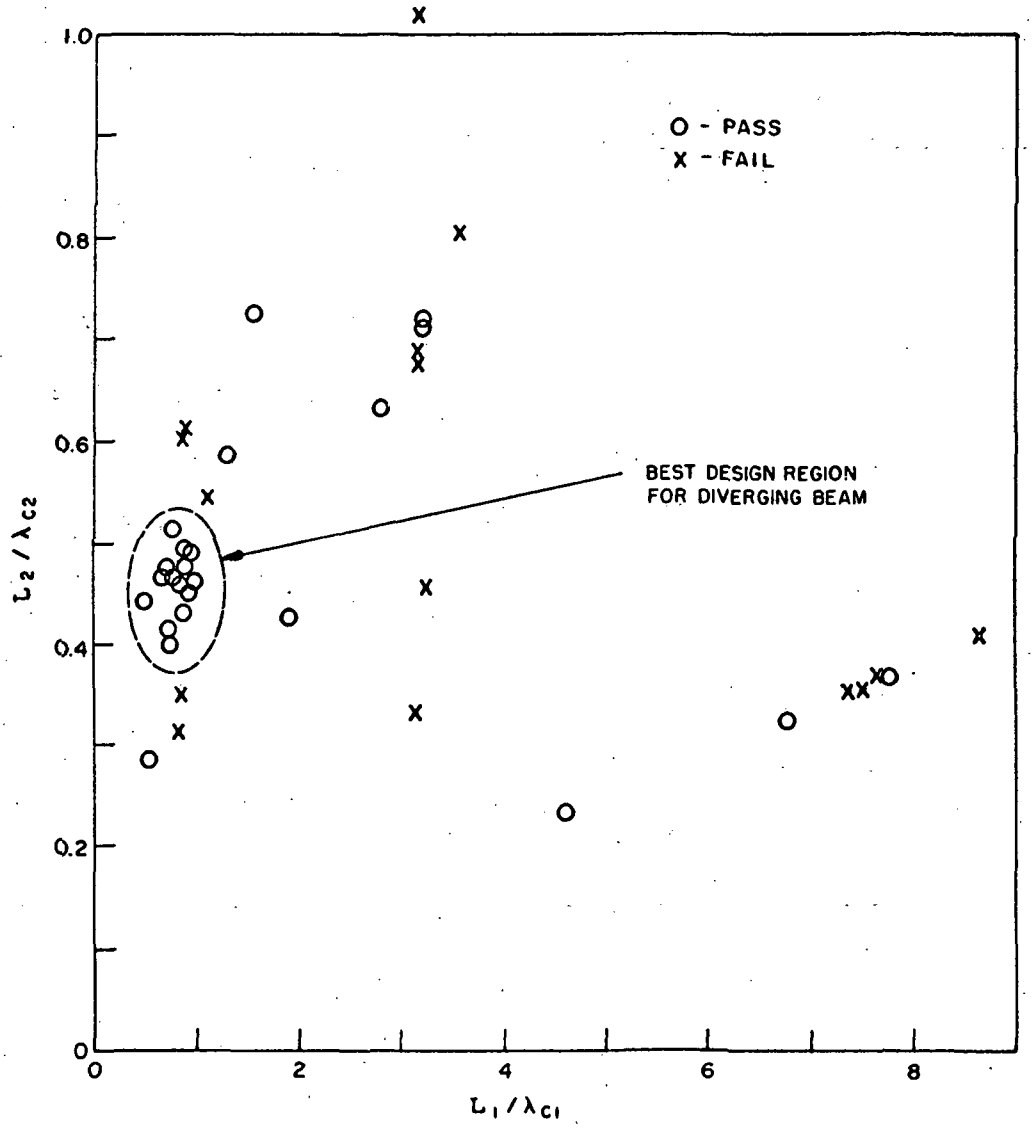

Figure 36 - Combinations of Normalized Beam Expansion Lengths, L_1/λ_{c1}, at Beam Stabilization Lengths, L_2/λ_{c2} Considered. Dashed Oval Indicates Region of Universal Good Refocusing as Rated by the Average Electron Focusing Criteria. For Some of the Near Passing Cases the Fast Electrons Have Excessively Large Angles.

an rms angle of 10 degrees or less, with electrons in the intermediate velocity groups having intermediate rms angles.

The rating of the various combinations of L_1 and L_2 lengths according to the Maximum Energy Recovery Refocusing Standard is shown in Figure 37, where again the symbol o denotes a passing case and x a failing case. The dashed circle indicates a region where most of the cases studied pass these criteria. Only one x appears in this circle, but this one case failed only because the slowest group of electrons had an rms angle of 12 degrees instead of the arbitrary maximum of 10 degrees, the rms angles of the remaining groups being satisfactory. It thus appears that for good refocusing with minimum angles for the fast electrons, the length L_1 should be between 2 and 3 cyclotron wavelengths and the length L_2 should be between 0.6 and 0.8 cyclotron wavelength in the reduced magnetic field amplitude. A statistical summary of the 40 cases studied is given in Table X. The best designs according to the Minimum Average Angle and Maximum Energy Recovery Standards are indicated by the symbols $<$ and = in Column 1. Average, rms, and maximum angles together with the standard deviation of the angles are listed for the 60 electrons grouped together. In addition, the average and rms angles for the electrons divided into four equal energy-content groups are shown. Other items listed include the final beam current density after beam expansion and the average and rms radii of the electron trajectories after refocusing.

The principle behind the success of the fast drop-off field is that practically independent of initial velocity, all electron trajectories expand rapidly in radial position immediately after the drop in the field. This rapid expansion is independent of initial velocities only if the drop-off is short compared with a cyclotron wavelength. Once all electrons have gained a significant radial velocity they are turned in an axial direction by the plateau field. Since scalloping trajectories follow an approximately sinusoidal motion, a plateau field length of approximately one-half scallop wavelength will cause an electron having an initial small radius with both axial and radial velocity components to expand radially and then be turned so its motion is parallel to the axis. If the plateau field is cut off at this point, optimum refocusing will have been achieved. In short, the fast magnetic field drop-off causes the space charge forces to impart large radial velocities to all electrons which are then turned to axial velocities by means of a plateau field of specified length.

The quality of the refocused beam is predominantly influenced by the axial velocity spread of the spent beam after the output gap. Figure 38 shows the standard deviation of the trajectory angles after refocusing as a function

TABLE X - STATISTICAL PROPERTIES OF KLYSTRON SPENT BEAMS AFTER REFOCUSING

Best Design	Tape No.	Design	Field Shape	L_1/a	L_2/a	L_1/λ_{c1}	L_2/λ_{c2}	B_2/B_o	Avg. Angle	Rms Angle	Max. Angle	Std. Dev.	Avg. R/a	Fraction $> 15^o$	Avg. Angle vs. Energy Class				λ_{co}/a	$J \approx J_o \left(\frac{R_o\ avg}{R\ avg}\right)^2$	RMS Angle vs. Energy Class			
															Low	2	3	High			Low	2	3	High
									Deg.	Deg.	Deg.	Deg.			Deg.	Deg.	Deg.	Deg.		A/cm^2	Deg.	Deg.	Deg.	Deg.
<	1	A	A	14.3	18.3	3.11	.676	.17	5.77	9.18	24.2	7.13	2.74	.15	6.13	5.97	5.38	4.28	4.604	2.93	9.72	9.65	8.76	4.42
	2	A	B	14.7	12.4	3.19	.458	.17	6.16	9.19	19.5	6.82	3.06	.117	4.76	6.78	8.49	5.35	4.604	2.35	8.27	10.85	9.50	5.54
	3	A	C	14.2	27.8	3.08	1.03	.17	10.0	15.0	33.7	11.2	2.58	.35	14.9	12.2	1.43	.875	4.604	3.31	18.36	14.51	11.06	2.55
	4	A	D	14.2	8.5	3.08	.332	.18	10.5	13.5	34.5	8.47	3.46	.267	8.25	14.3	10.9	6.88	4.604	1.84	11.42	16.60	14.35	7.25
	5	A	E	34.7	9.7	7.54	.358	.17	9.83	13.3	32.8	8.88	3.57	.283	9.89	10.7	7.66	11.3	4.604	1.73	12.87	14.38	11.21	14.91
	6	A	F	5.8	15.8	1.26	.583	.17	5.26	8.06	19.3	6.11	2.97	.10	5.20	3.60	6.75	9.04	4.604	2.50	9.23	5.84	7.09	9.30
=	7	A	G	4.0	13.6	.869	.473	.16	3.20	9.61	46.2	9.06	2.94	.033	1.20	3.15	8.16	9.81	4.604	2.55	11.22	5.80	8.63	10.13
	8	A	H	3.8	10.1	.825	.351	.16	7.63	9.88	18.0	6.27	3.50	.15	4.50	10.5	11.1	11.3	4.604	1.80	8.08	11.19	11.65	11.66
	9	A	I	3.8	17.5	.825	.608	.16	5.83	14.5	39.3	13.3	2.50	.267	11.0	-3.10	3.91	8.93	4.604	3.52	19.19	6.79	4.51	9.23
	10	A	J	3.75	13.2	.815	.602	.21	7.70	11.3	42.1	8.31	2.57	.15	11.0	2.61	5.87	9.90	4.604	3.33	14.81	5.69	6.10	10.14
	11	A	K	4.0	13.0	.869	.311	.11	10.0	12.2	21.0	7.06	5.40	.267	6.35	14.0	13.2	13.2	4.604	.755	9.90	14.52	13.73	13.94
	12	B	L	3.8	15.7	.765	.506	.16	-1.57	6.26	12.6	6.06	2.69	0	-4.58	-2.67	5.75	9.19	4.968	3.34	6.13	5.44	6.14	9.80
	13	B	M	3.8	14.4	.765	.464	.16	.370	5.61	12.7	5.60	2.97	0	-3.04	1.15	6.56	10.0	4.968	2.74	4.80	4.66	6.82	10.42
=	14	B	N	3.8	12.3	.765	.396	.16	3.93	6.07	12.8	4.63	3.39	0	.583	5.59	8.60	10.3	4.968	2.10	3.27	6.42	8.85	10.67
=	15	C	P	3.5	12.6	.763	.412	.15	2.54	7.46	19.6	7.02	3.37	.083	-1.62	5.48	8.74	6.77	4.585	1.83	7.26	6.43	9.54	7.05
=	16	D	Q	1.8	9.0	.463	.440	.19	7.01	14.0	48.9	12.11	3.06	.10	4.42	7.14	11.9	13.3	3.886	1.77	16.78	8.00	12.22	13.77
=	17	E	R	3.0	11.2	.689	.463	.18	2.82	5.96	14.1	5.26	2.83	0	-1.23	3.92	7.24	11.9	4.355	2.32	4.03	4.82	7.33	12.17
=	18	F	S	3.0	11.9	.691	.466	.17	1.36	5.77	13.8	5.61	2.71	0	-3.23	2.77	6.04	11.7	4.340	2.64	4.74	3.54	6.74	11.93
	19	F	E	33.2	9.5	7.65	.372	.17	8.35	9.86	20.6	5.26	2.52	.133	11.0	6.77	5.79	6.50	4.340	3.05	12.51	7.94	6.83	6.82

TABLE X (CON'T)

Best Design	Tape No.	Design	Field Shape	L_1/a	L_2/a	L_1/λ_{c1}	L_2/λ_{c2}	B_2/B_o	Avg. Angle	Rms Angle	Max. Angle	Std. Dev.	Avg. R/a	Fraction $> 15^o$	Avg. Angle vs. Energy Class				λ_{co}/a	$J \approx J_o \left(\frac{R_o \text{ avg}}{R \text{ avg}}\right)^2$	RMS Angle vs. Energy Class			
															Low	2	3	High			Low	2	3	High
									Deg.	Deg.	Deg.	Deg.			Deg.	Deg.	Deg.	Deg.		A/cm^2	Deg.	Deg.	Deg.	Deg.
=	22	G	T	7.0	22.5	.951	.458	.15	2.10	2.70	6.48	1.68	2.91	0	.783	1.75	3.71	4.52	7.364	1.04	0.90	1.95	3.89	4.72
	23	G	P	4.0	14.1	.543	.287	.15	7.21	7.54	11.5	2.23	3.00	0	7.21	7.01	7.41	7.33	7.364	.979	7.53	7.35	7.81	7.61
	24	G	E	33.8	9.5	4.59	.219	.17	4.81	5.21	9.83	1.98	2.19	0	5.31	4.56	4.39	4.56	7.364	1.84	5.66	5.00	4.86	4.75
	25	C	E	33.7	9.4	7.35	.349	.17	6.24	10.6	26.6	8.58	2.65	.183	6.22	6.82	5.21	6.86	4.585	2.95	10.45	12.09	9.43	7.25
<	26	C	A	13.8	18.3	3.01	.679	.17	6.05	9.51	29.2	7.33	2.12	.133	9.25	4.24	2.75	2.96	4.585	4.61	11.85	9.02	4.09	3.20
<	27	G	A	13.7	18.3	1.86	.422	.17	2.35	2.90	6.17	1.70	1.71	0	3.50	.514	3.15	1.89	7.364	3.01	3.72	1.29	3.34	1.97
	28	C	T	7.0	22.0	1.53	.720	.15	1.32	9.05	31.4	8.95	1.48	.10	3.43	-1.71	-.787	4.69	4.585	9.46	10.23	9.61	2.15	4.81
	29	A	P	4.0	14.0	.869	.456	.15	2.06	10.0	39.7	9.83	3.17	.05	-.479	2.01	8.65	9.66	4.604	2.19	11.71	6.30	9.08	9.95
	30	B	P	4.0	14.0	.805	.423	.15	1.31	5.67	13.3	5.51	3.40	0	-2.89	2.88	7.71	10.3	4.968	2.09	4.45	4.22	7.97	10.72
	31	D	P	4.0	14.0	1.03	.540	.15	5.27	14.4	47.1	13.4	3.02	.15	8.03	-1.59	6.65	10.7	3.886	1.82	19.16	5.61	7.18	10.87
	32	E	P	4.0	14.0	.918	.482	.15	.206	5.87	13.2	5.87	3.06	0	-4.25	1.09	4.50	10.7	4.355	1.98	5.77	4.44	4.74	10.97
	33	F	P	4.0	14.0	.922	.484	.15	-.773	6.07	15.4	6.02	2.54	.017	-4.87	-.065	4.05	9.18	4.340	3.00	6.91	3.88	4.53	9.42
<	34	F	A	13.7	18.3	3.16	.717	.17	3.00	5.48	16.9	4.58	1.80	.017	4.79	1.94	.306	3.50	4.340	5.97	7.07	4.57	2.20	3.77
<	35	E	A	13.7	18.3	3.15	.714	.17	5.08	7.80	22.9	5.91	1.58	.083	7.55	4.70	.883	3.19	4.355	7.44	10.13	6.74	3.44	3.62
<	36	D	A	13.7	18.3	3.53	.801	.17	7.48	11.0	33.1	8.01	2.36	.117	11.4	4.85	3.32	4.56	3.886	2.98	14.97	7.02	4.25	5.01
<	37	B	A	13.7	18.3	2.76	.626	.17	2.63	7.52	15.4	7.05	1.47	.067	4.43	1.01	1.05	1.13	4.968	11.2	8.72	7.96	3.61	1.25
	38	B	E	33.7	9.4	6.78	.322	.17	6.44	7.79	16.5	4.37	2.43	.05	6.96	6.93	5.49	3.83	4.968	4.09	8.20	8.54	6.50	4.17
	39	D	E	33.7	9.4	8.67	.411	.17	6.82	10.5	23.3	7.99	1.89	.183	7.80	7.55	4.91	2.12	3.886	4.64	11.85	11.19	6.65	2.34
	40	E	E	33.7	9.4	7.74	.367	.17	5.62	6.56	15.2	3.38	2.20	.017	5.87	5.60	4.90	5.87	4.355	3.84	6.86	7.00	5.17	6.15
	41	D	U	Multi-Step	8.8	-	.430	.19	8.94	12.9	46.7	9.36	2.70	.15	7.29	11.4	9.49	9.26	3.886	2.27	14.59	12.09	10.19	9.46
	42	A	U	"	8.8	-	.363	.19	5.45	11.2	47.6	9.76	1.87	.067	5.90	6.17	2.15	6.76	4.604	6.30	13.69	8.86	3.30	7.04
														Avg.	8.62F 1.71P	7.13F 3.30P	6.66F 5.31P	7.20F 7.47P						

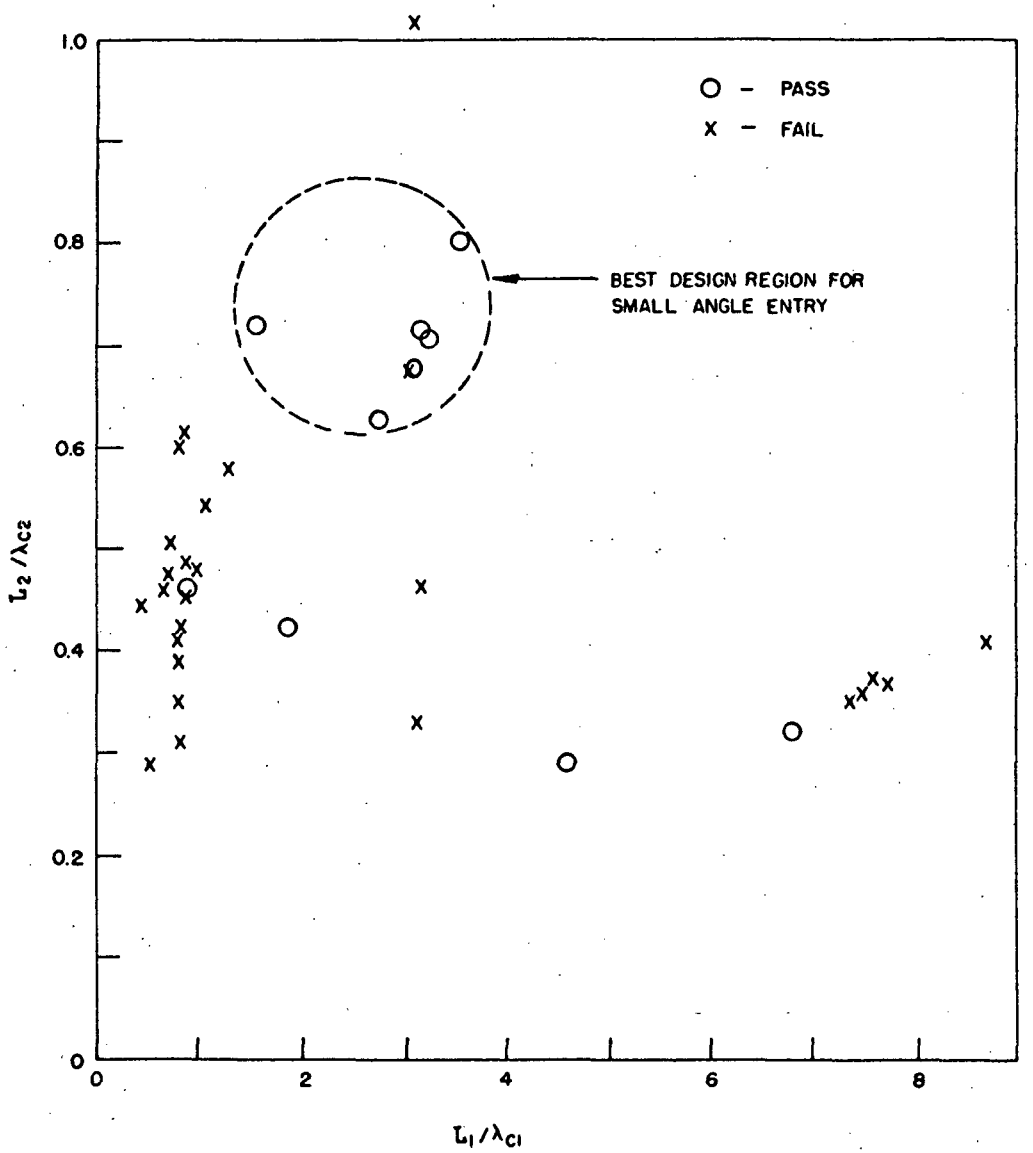

Figure 37 - Refocusing Field Configurations Rated for Producing Final Beam Recollimations with Angles of Fast and Slow Electrons Less Than 5 and 10 Degrees, Respectively, for Maximum Energy Recovery.

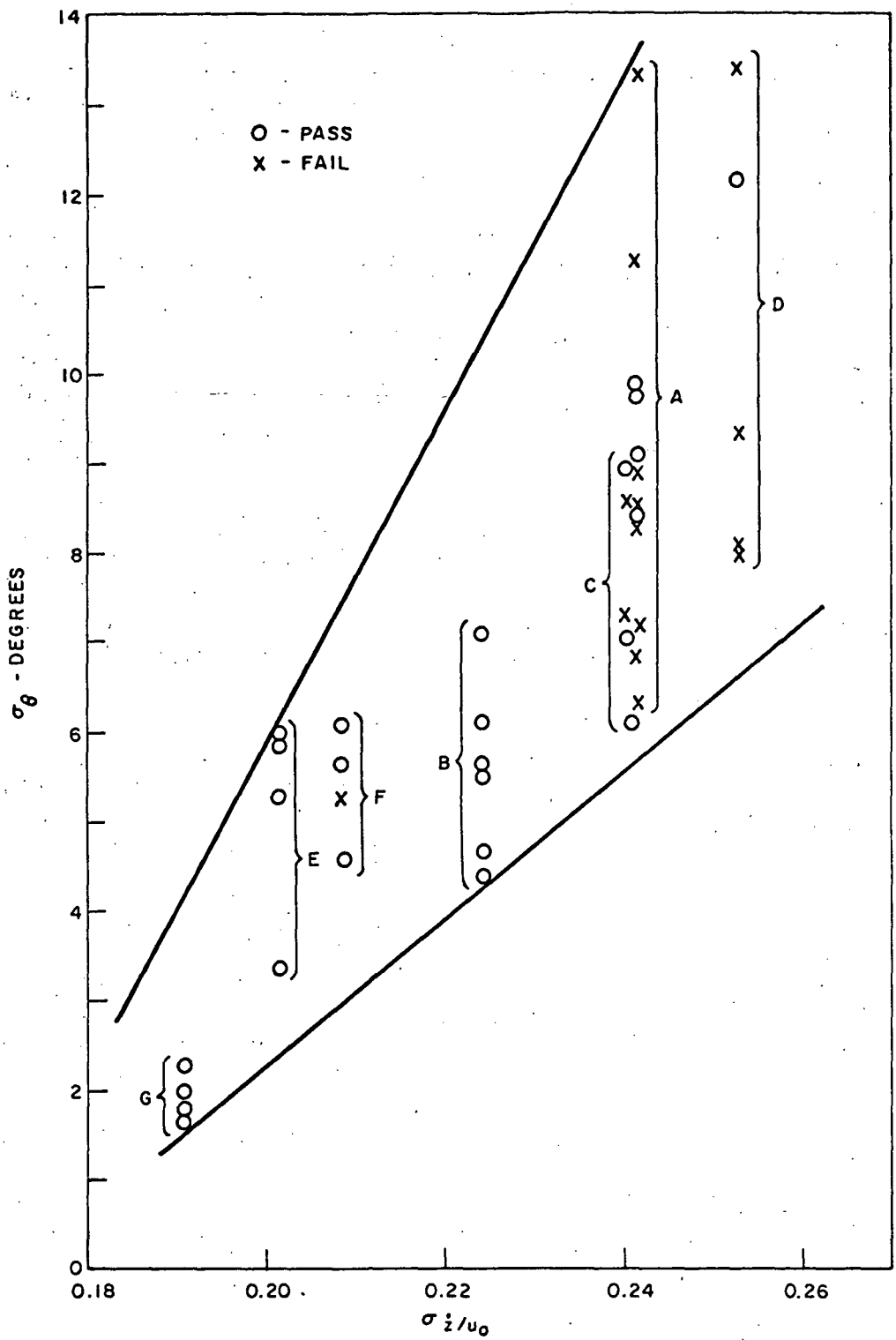

Figure 38 - Standard Deviation of Angles of Refocused Electrons versus Velocity Spread (Standard Deviation of Axial Component of Velocity) at Output Gap Exit Plane (Pass-Fail Test Based on Minimum Average Angle Refocusing)

of the standard deviation of the normalized axial velocities before refocusing. Again, the symbols o and x denote either passage or failure of the refocusing system, as determined by the criteria for producing a slightly expanding beam at the collector. Here it can be seen that designs having low axial velocity dispersion could be easily refocused with practically any reasonable field shape e.g., Designs B, E, F, and G. Refocusing of Designs A, C, and D is clearly more difficult and greater angular dispersion of the refocused beam results. From this figure it can be concluded that beams having a standard deviation below 0.23 of the normalized axial velocities are easily refocused while those having greater axial velocity dispersion are not. This is again illustrated in Figure 39 where efficiency and angular standard deviation for the optimum refocusing field for the seven klystrons are plotted versus the velocity spread in the spent beam. It may be seen that excessive velocity spread reduces the klystron conversion efficiency and increases the angular spread after optimum refocusing.

The average angle of the trajectories with respect to the axis of the acceptably refocused beams showed a strong relationship to the length of the plateau region of the magnetic field profile as indicated in Figure 40. In particular, Design B was studied with three refocusing fields in which the only difference was the length of the plateau. These points, shown encircled in Figure 40, are seen to lie on a steep line. It can also be seen from this figure that most of the other acceptably refocused beams tend to cluster around this line. From this study it can be concluded that if the average output angle after refocusing is to be from 2 to 5 degrees, the value of L_2/λ_{c2} should be between 0.35 and 0.4. For an average collector entrance angle of zero degrees, L_2/λ_{c2} should be approximately 0.5.

The average angle of the trajectories after refocusing showed a linear relationship with electron energy for the acceptable refocused beams as shown in Figure 41. The average angle of the low energy electrons was near 2 degrees while being near 7 degrees for the highest energy electrons. The average angle as a function of energy for the failing beams showed a much different behavior as indicated by the dashed line in Figure 40. In the latter case it appears that the average angle is almost independent of electron energy. The increase of the average angle with energy in the acceptable beams should be considered in a depressed collector design. It may eliminate the need for the central spike in certain cases. For these cases an average angle between 2 and 5 degrees was sought.

A summary of the results of the statistical analysis for optimum refocusing of the seven basic klystron designs considered is given in Table XI for both Minimum Average Angle and Maximum Energy Recovery refocusing.

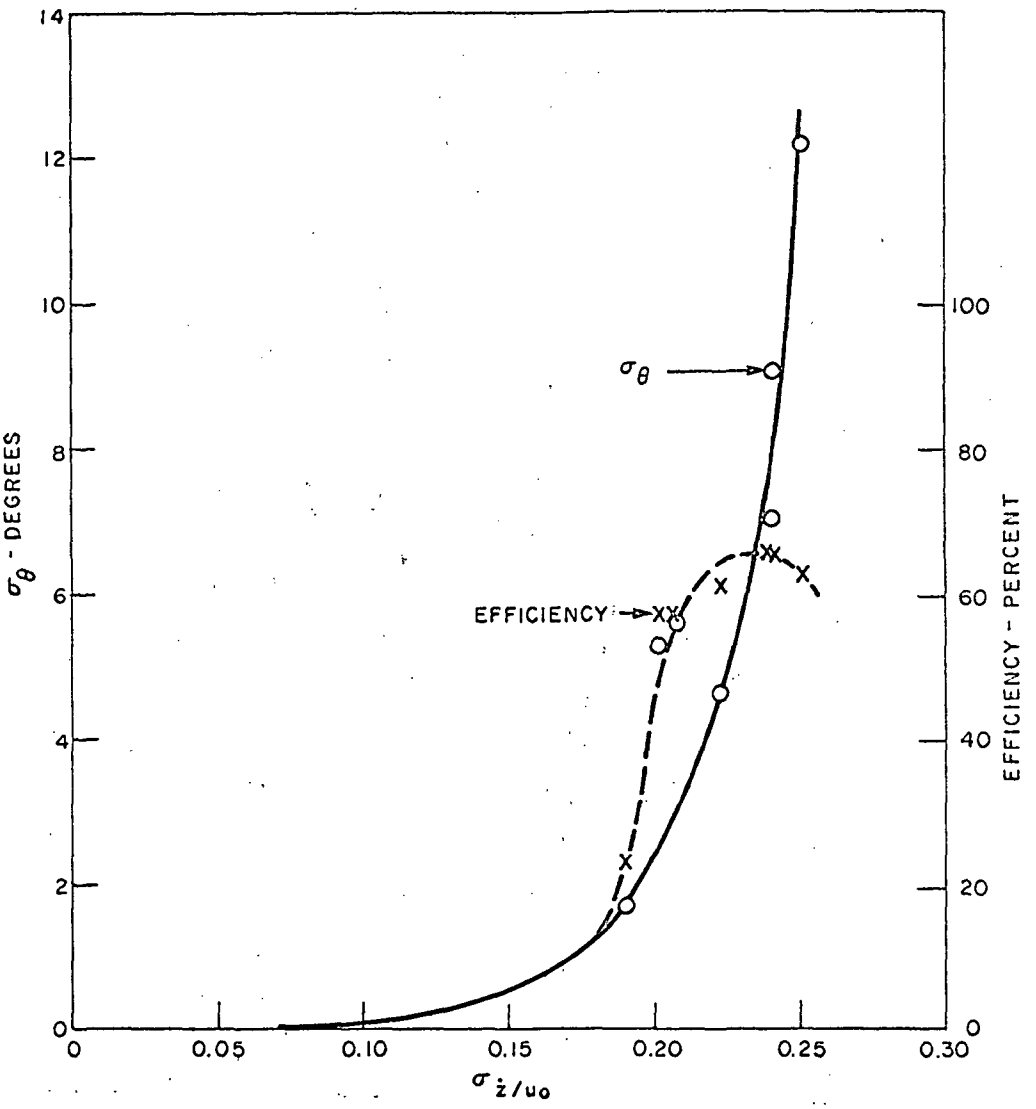

Figure 39 - Angular Spread (Standard Deviation) and Efficiency versus Velocity Spread (Standard Deviation of Axial Component of Spent-Beam Velocity) for the Seven Klystrons with Optimum Refocusing Field Distributions

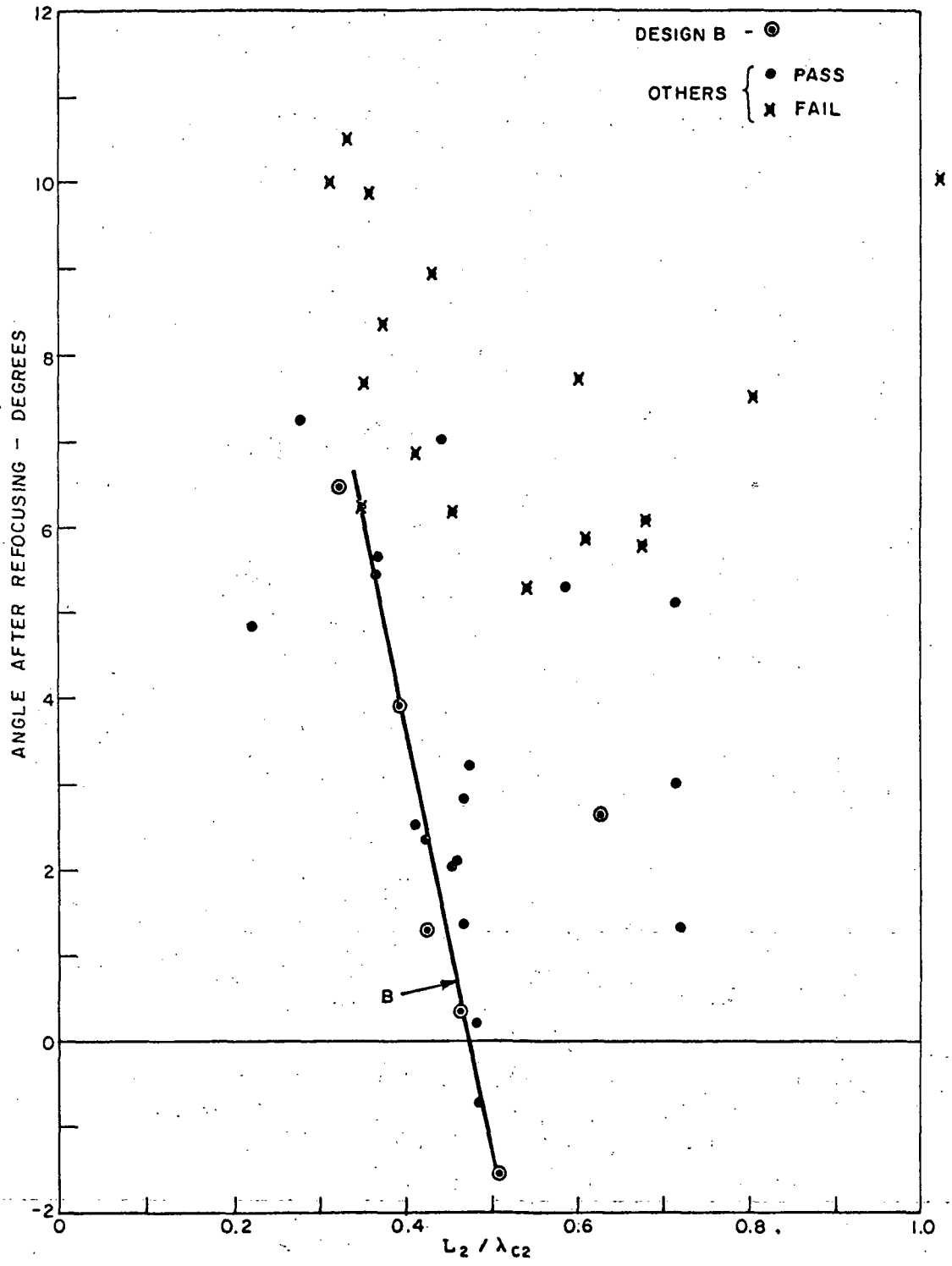

Figure 40 - Average Angle After Refocusing versus Normalized Length of Beam Stabilization Region L_2/λ_{c2} (Pass-Fail Test Based on Minimum Average Angle Criterion)

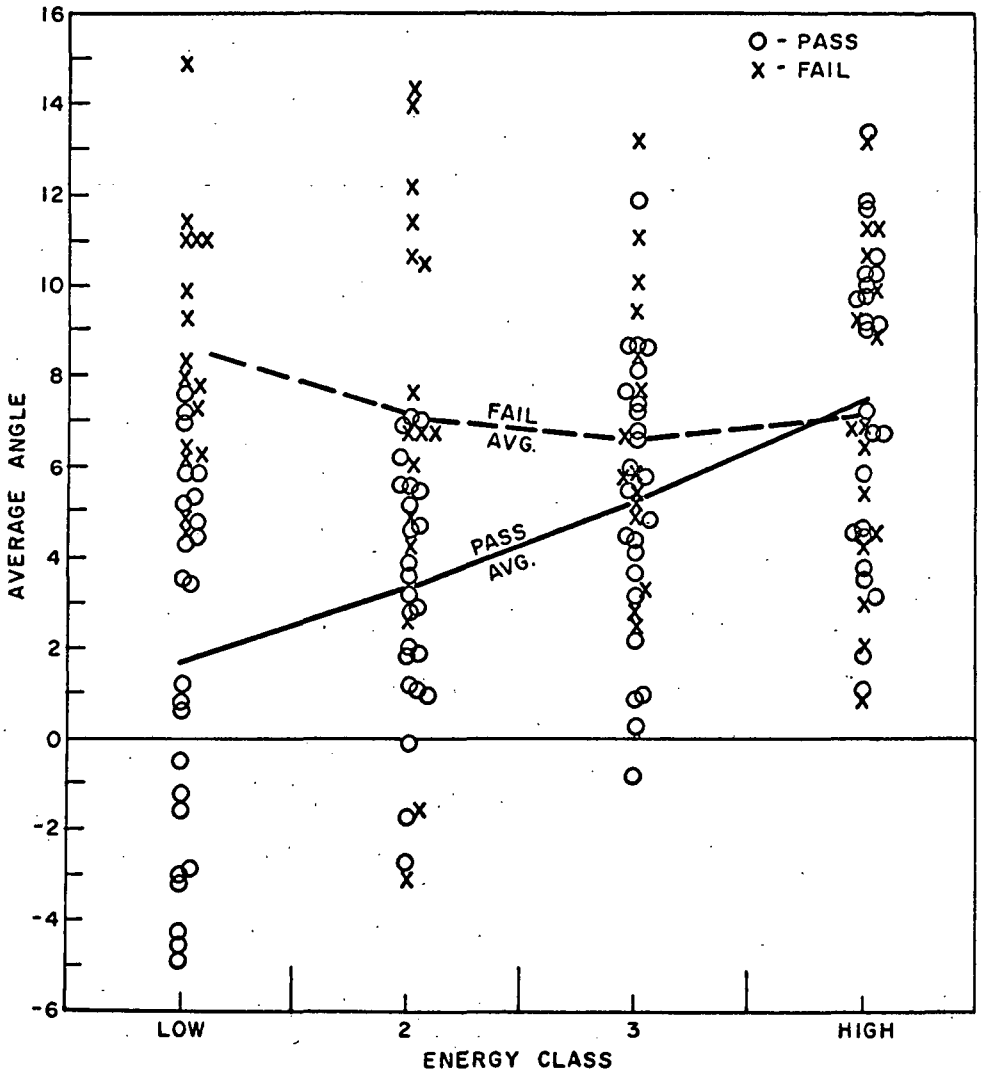

Figure 41 - Average Angle as Determined by the Energy Class of the Spent-Beam Electrons. A Common Design Objective in the Selection of Refocusing Parameters for the Above Cases was an Overall Average Angle Between 2 to 5 Degrees.

TABLE XI - STATISTICAL SUMMARY OF OPTIMUM, REFOCUSING FIELD DISTRIBUTION

Minimum Average Angle Criterion

Klystron Design	L_1/λ_{c1}	L_2/λ_{c2}	$\bar{\theta}$	θ_{rms}	σ_θ	θ_{max}
A	0.87	0.47	3.2	9.6	9.1	46.2
B	0.76	0.40	3.9	6.1	4.6	12.8
C	0.76	0.41	2.5	7.5	7.0	19.6
D	0.46	0.44	7.0	14.0	12.1	48.9
E	0.69	0.46	2.8	6.0	5.3	14.1
F	0.69	0.47	1.4	5.8	5.6	13.8
G	0.95	0.46	2.1	2.7	1.7	6.5

Maximum Energy Recovery Criterion

A	3.11	0.68	5.8	9.2	7.1	24.2
B	2.76	0.63	2.6	7.5	7.0	15.4
C	3.01	0.68	6.0	9.5	7.3	29.2
D	3.53	0.80	7.5	11.0	8.0	33.1
E	3.15	0.71	5.1	7.8	5.9	22.9
F	3.16	0.72	3.0	5.5	4.6	16.9
G	1.86	0.42	2.4	2.9	1.7	6.2

A comparison of the design parameters of klystrons C and G shows them to be very similar. The relatively low efficiency obtained for Design G results from the deliberate choice of a very low rf voltage in the output cavity. When Design G was refocused with the optimum Design C field, the refocusing action was good (Tapes 15 and 23). Consequently, it may be concluded that a refocusing field distribution designed according to the above specifications for a high efficiency klystron will in general yield acceptable refocusing when that klystron is operated at low efficiency. If the klystron is driven above saturation, however, an excessive velocity spread is generated with a consequent reduction in conversion efficiency and less effective refocusing will result.

CONCLUSIONS

For improved efficiency of conversion of prime power to rf power in communications or radar systems using linear-beam power amplifiers such as a klystron or a traveling-wave tube, it is desirable to collect the spent beam from the amplifier in an energy-recovering multistage depressed potential collector. Because energy recovery in such collectors is enhanced by a prior dilution of space charge and recollimation of the spent beam, methods for expanding and refocusing the spent beam in klystrons were investigated.

Good beam expansion and recollimation with reduced radial velocities can be attained with a tapered axial field distribution followed either by a short axial field plateau or a short region containing a circumferential magnetic field. Physical methods of generating the two types of refocusing field distributions with pole pieces and permanent magnets are proposed.

An extensive statistical study was made of the refocusing properties of magnetic field distributions containing only axial and radial field components. For both high and low efficiency klystrons with power outputs ranging from 1 to 4 kW, general design principles were found that yield acceptable refocusing for all cases considered. For optimum entrance conditions into a multistage depressed potential collector for maximum energy recovery, it is desirable to favor the recollimation of the fast electrons in the spent electron beam at the expense of the slow electrons while limiting the angle of entry of the slow electrons to less than 10 degrees and prohibiting as far as possible a negative angle for any electron. The optimum field profile for diluting the beam space charge and refocusing the beam with small angles at a larger diameter was found to be a rapid decrease of the main collimating magnetic field in a distance of approximately 2 to 3 cyclotron wavelengths as computed for the electron of average velocity in the spent beam, the main collimating field strength falling to a reduced amplitude sufficiently low to yield the required dilution of beam space charge, followed by a beam stabilization region of extent between 0.6 and 0.8 cyclotron wavelengths computed in terms of the reduced field amplitude.

Because of similarities in the spent beams of klystrons and traveling-wave tubes, these results are generally applicable to TWT's when amplifiers of equal efficiency are compared.

Since more definitive results could be achieved by the computation of complete electron trajectories from the output interaction gap of the klystron through the beam expansion and recollimation region and into the multistage collector until the trajectory ends on a collector electrode, it is recommended that additional evaluation of refocusing field distributions be made from a statistical analysis of the entire electron trajectories. Also, since a reversed or negative plateau field could more readily be achieved in periodic permanent magnet beam collimation structures, design studies should be carried out for refocusing field profiles with a field reversal between the last main field segment and the beam stabilization plateau.

Appendix A

CALCULATION OF THE SPACE-CHARGE FORCES IN A KLYSTRON BEAM

Dr. E. J. Craig

In order to obtain an acceptable model of the electron beam in a klystron certain simplifying assumptions are made:

(1) the beam and the rf circuit have cylindrical symmetry;

(2) before the beam interacts with any rf fields it is cylindrical in shape and the charge density is everywhere a constant.

Let the radius of the cylindrical beam be represented by b and the tunnel radius by a.

The electron beam will be approximated by a set of toroids or rings of charge of rectangular cross-section. These rings are obtained by slicing the beam into disks w meters thick, as shown in Figure 1 and by cutting each disk into N_r concentric cylinders of equal volumes.

Each ring will be identified by its radius of gyration and the axial position of its center of mass. All linear dimensions hereafter will be normalized to the radius, a, of the drift tube, and so, for the kth ring its location will be denoted by (r_k, z_k) whereas the actual coordinates in meters will be (ar_k, az_k).

If the normalized radius of the beam initially is b, and N_r is the number of the rings radially, then the initial radii of the rings are

$$r_k = b \sqrt{\frac{k - \frac{1}{2}}{N_r}} \qquad k = 1, 2, \ldots, N_r \tag{37}$$

For any ring with nominal radius r the inner (r_i) and outer (r_o) radii are related to r by

$$r^2 = \frac{r_o^2 + r_i^2}{2} \tag{38}$$

The innermost ring has an inner radius of zero, thus constituting a disk, and the square of the outer radius of this disk is $2r_m^2$, where r_m is the radius gyration of the disk. Since the quantity $2r_m^2$ occurs frequently, it will be useful to call it RR:

$$RR = 2r_m^2 = b^2/N_r \tag{39}$$

The area of each ring is $2\pi r_m^2 = \pi RR$ so that $r_o^2 - r_i^2 = RR$ and the difference in the squares of the radii of two rings that overlap must be less than or equal to RR.

SPACE-CHARGE FORCES

The most time-consuming part of a digital computer program for the simulation of an electron-beam device has always been the calculation of the space-charge forces. The obvious procedure at this point is to obtain an expression for the electric field due to a ring of charge. Once this is obtained the expression can be integrated over the volume of another ring to obtain an expression for the force of one ring on another.

Unfortunately, the expression for the field of the ring involves an infinite series similar to but a little more complicated than Equation (40) below. Such a series converges slowly when the field is required near a ring, and this region is the one of primary interest. Experience has indicated that a compromise between speed and accuracy is necessary, and so the toroidal ring with charge of uniform density is replaced by a thin ring that passes through the axial center of the toroidal and has a radius equal to the radius of gyration of the original ring. Figure 29a shows such a ring and Figure 29b the thin ring used to approximate it.

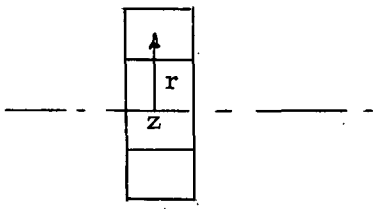

Figure 29a - A Ring

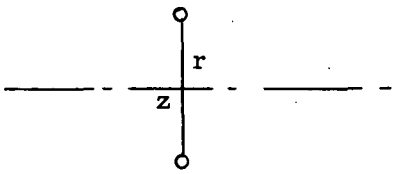

Figure 29b - Its Approximation

The potential within a cylinder of radius a of a ring at z = 0 and normalized radius r_1 at a point (r_2, z) can be deduced from the Green's function for a charge in a metal cylinder.[9] This function is

$$\phi = \frac{Q}{2\pi\epsilon_o a} \sum_{n=1}^{\infty} \frac{J_0(\lambda_n r_1) J_0(\lambda_n r_2)}{\lambda_n J_1^2(\lambda_n)} \exp(-\lambda_n |z|) \tag{40}$$

where λ_n is the nth root of the equation $J_0(x) = 0$, starting with the smallest. Q is the total charge on the ring. J_0 and J_1 are Bessel functions of the first kind, orders zero and one.

If Equation (40) is differentiated with respect to r_2 and z then the field components can be shown to be

$$E_r = \frac{Q}{2\pi\epsilon_o a^2} \sum_{n=1}^{\infty} \frac{J_0(\lambda_n r_1) J_1(\lambda_n r_2)}{J_1^2(\lambda_n)} \exp(-\lambda_n |z|) \tag{41}$$

$$E_z = \frac{Q}{2\pi\epsilon_o a^2} \sum_{n=1}^{\infty} \frac{J_0(\lambda_n r_1) J_0(\lambda_n r_2)}{J_1^2(\lambda_n)} \exp(-\lambda_n |z|) \tag{42}$$

The sign of Equation (42) must be changed if z is negative.

The series in Equations (41) and (42) converge slowly when z is small (requiring, for example, 74 terms to obtain four-place accuracy when z = 0.04). There are other disadvantages: the Bessel functions are time consuming to calculate and the zeroes of J_0 must either be calculated or in storage. If one recognizes that the ring model is good only if there are many rings, and that the space-charge forces will require time proportional to the square of the total number of rings, then it is not surprising that Equations (41) and (42) are rarely used to calculate the space-charge forces.

THE METHOD OF IMAGES

Attempts to find simpler expressions for the fields of rings of charge led to the method of images. If a ring should have an image in the wall of the cylinder, one could conceptually remove the cylindrical boundary and calculate fields due to the ring and its image, thus, accounting for the effect of the tunnel walls. Unfortunately, the only geometrical object to have a unique image in a cylindrical wall is a line charge parallel to the cylinder's axis. This may be verified by examining the optical image of objects within a cylindrical mirror. Objects close to the mirror have a fairly well-defined image, but this image gets fuzzy as the object approaches the axis. This observation poses the following question: what is the shape of the conducting body that most nearly represents a cylinder in the vicinity of the ring for which the ring does indeed see a clear image?

Specifically: Let a ring of charge be centered at the origin with radius r_1 (normalized, hence less than unity). Let its charge be $-Q$ and let another ring, also centered at the origin, in the same plane as the first, have a charge of qQ and radius b (greater than unity). Assuming that no metal boundaries exist at all, what must the constants q and b be so the zero-potential surface between the two rings looks like a cylinder? In particular, what must q and b be if the potential at $r_2 = 1$ is zero both when $z = 0$ and when $|z| = 2$? The choice of 2 for $|z|$ is arbitrary, but it is based on the fact that the expressions for the fields in Equations (41) and (42) are relatively small this far from the ring.

A digital computer was used to obtain a relation between q, b, and r_1. For a given value of r_1, b was found to be related to r_1 by

$$b = 1.3617 - 0.3205\, r_1^2 - 0.0412\, r_1^4 \tag{43}$$

and q is related to both b and r_1 by

$$q = \sqrt{b}\left[1 - 0.08\sqrt{r_1}(1 - r_1)\right] \tag{44}$$

With these two constants it is now possible to calculate the field by computing the field due to two rings only, the original and its image.

Before leaving this point, it is useful to sketch the $\phi = 0$ equipotential due to a ring and its image and to compare it to the cylinder it is supposed

to approximate. This equipotential varies a little as r_1 is varied, but because it must go through the points $r_2 = \pm 1$, $z = 0$ or ± 2, this variation is slight. Figure 2 shows this equipotential for a choice of $r_1 = 0.5$. While this figure is interesting, it does not give the reader a clear picture of how well the image model approximates the actual situation. It is clear that the image approach will not be very accurate when the magnitude of z is near 2.5.

The accuracy of the method of images may be demonstrated by a calculation of the fields from the ring and its image and by comparing the results with the values obtained from Equations (41) and (42). The potential due to a ring of radius r_1 centered on the origin at a point whose coordinates are (r_2, z) is given by

$$\phi = \frac{Q}{2\pi^2 \epsilon_o a} \cdot \frac{kK(k^2)}{2\sqrt{r_1 r_2}} \tag{45}$$

where

$$k^2 = \frac{4r_1 r_2}{(r_1 + r_2)^2 + z^2} \tag{46}$$

and $K(k^2)$ is the complete elliptic integral of the first kind. The field components obtained from this function are

$$E_r = \frac{Q}{2\pi^2 \epsilon_o a^2} \cdot \frac{2r_1 H(k^2) - r_2 E(k^2)}{\sqrt{(r_1+r_2)^2 + z^2}\left[(r_1 - r_2)^2 + z^2\right]} \tag{47}$$

$$E_z = \frac{Q}{2\pi^2 \epsilon_o a^2} \cdot \frac{zE(k^2)}{\sqrt{(r_1+r_2)^2 + z^2}\left[(r_1 - r_2)^2 + z^2\right]} \tag{48}$$

where $E(k^2)$ is the complete elliptic integral of the second kind and

$$H(k^2) = \frac{1}{k^2}\left[(1 - k^2/2)E(k^2) - (1 - k^2)K(k^2)\right] \tag{49}$$

Note that the computation of the approximate field within the cylinder requires two evaluations of Equations (47) and (49), one for r_1 and Q and one for b and qQ substituted for r_1 and Q, respectively.

SUBROUTINE EH

The functions $E(k^2)$ and $H(k^2)$ (Equation (13)) are evaluated by a subroutine called EH. If we let

$$m = 1 - k^2 \tag{50}$$

the expressions for E(m) and K(m) can be found[10]

$$E(m) = 1 + c_1 m + c_2 m^2 + c_3 m^3 + c_4 m^4 + m \cdot \ln(1/m)(d_1 + d_2 m + d_3 m^2 + d_4 m^3) \tag{51}$$

with

$c_1 = 0.44325\ 1411463$ $\quad$ $d_1 = 0.24998\ 368310$

$c_2 = 0.06260\ 601220$ $\quad$ $d_2 = 0.09200\ 180037$

$c_3 = 0.04757\ 383546$ $\quad$ $d_3 = 0.04069\ 697526$

$c_4 = 0.01736\ 506451$ $\quad$ $d_4 = 0.00526\ 449639$

and

$$H(m) = 0.5 + a_1 m + a_2 m^2 + a_3 m^3 + a_4 m^4 - z(b_1 + b_2 m + b_3 m^2 + b_4 m^3 + b_5 m^4) \tag{52}$$

where

$$z = \frac{m \cdot \ln(1/m)}{1 - m} \quad \text{for } m \neq 1$$

and

$$z = 1 \quad \text{when } m = 1$$

and

$$a_1 = -0.16466\ 865380 \qquad b_1 = 0.37500\ 815845$$
$$a_2 = -0.00840\ 338298 \qquad b_2 = -0.04600\ 680577$$
$$a_3 = 0.01078\ 561702 \qquad b_3 = 0.00245\ 309795$$
$$a_4 = 0.00582\ 942987 \qquad b_4 = 0.01030\ 281763$$
$$b_5 = 0.00178\ 562192$$

SUBROUTINE EH(M,E,H) was thoroughly checked both by comparing with tables of elliptic integrals and by writing another separate routine for the elliptic integrals using the arithmetic-geometric mean principle.

Appendix B

TABLE OF FINAL RADII, VELOCITIES, ANGLES AND ENERGIES
OF RINGS AT Z/A = 60

CASE NUMBER 1

R/A	Z DOT / U	R DOT / U	ANGLE (DEG)	POTENTIAL
3.577	.47	.08	9.65	.227
4.408	.55	.008	.91	.303
4.778	.746	.114	8.72	.571
5.576	.452	.091	11.48	.213
4.034	.563	.063	6.38	.321
3.77	.547	.04	4.22	.301
1.053	1.283	.037	1.69	1.649
1.745	.789	.03	2.2	.623
1.927	.869	.048	3.21	.758
1.547	.733	.015	1.22	.538
1.368	.667	.022	1.9	.446
1.833	.654	.02	1.78	.429
1.787	.621	.024	2.28	.387
3.376	.613	.028	2.66	.376
3.402	.583	.021	2.08	.34
2.99	.56	.064	6.51	.318
4.034	.577	.07	6.92	.338
4.125	.543	.05	5.34	.298
3.629	.446	.091	11.55	.207
3.854	.438	.049	6.45	.194
3.863	.537	.001	.16	.288
5.2	.722	.095	7.55	.531
4.044	.54	.086	9.11	.299
3.964	.509	.069	7.79	.264
1.909	1.293	.07	3.11	1.679
2.388	.757	.054	4.11	.576
2.362	.838	.052	3.6	.705
3.712	.705	.057	4.68	.5
2.775	.648	.019	1.74	.421
2.434	.624	.037	3.41	.391
2.628	.576	.068	6.77	.336
3.623	.587	.033	3.28	.345
3.143	.545	.077	8.11	.303
2.78	.527	.042	4.56	.279
3.833	.54	.083	8.73	.299
4.389	.491	.079	9.13	.247
3.458	.414	.048	6.73	.173
4.993	.711	.08	6.47	.512
3.145	.543	.027	2.87	.296
4.171	.489	.086	9.97	.247
2.539	1.299	.094	4.17	1.698
3.152	.718	.072	5.73	.521
3.148	.806	.067	4.79	.654
5.114	.688	.086	7.17	.48
4.986	.625	.051	4.68	.393
3.133	.621	.037	3.47	.387
3.296	.552	.085	8.82	.313
3.506	.534	.092	9.84	.294
3.355	.514	.089	9.87	.272
4.675	.488	.1	11.61	.249
3.421	.5	.001	.13	.25
2.557	.465	.054	6.68	.219

MAX R/A = 5.57612 RMS R/A = 3.51501
AVG ANG = 5.50506 DEG MAX ANG = 11.6136 DEG
STD DEV = 3.12679 DEG
AVG ANG MAG = 5.50506 DEG
NUMBER OF TRAJECTORIES = 52

TABLE OF FINAL RADII, VELOCITIES, ANGLES AND ENERGIES
OF RINGS AT Z/A = 60

CASE NUMBER 2

R/A	Z DOT / U	R DOT / U@	ANGLE (DEG)	POTENTIAL
1.895	.597	.02	1.97	.357
1.712	.534	.009	1.01	.285
.847	.439	.019	2.48	.193
1.593	.494	.002	.29	.244
1.578	.484	.002	.29	.234
.961	.369	.005	.78	.136
2.939	.282	.006	1.36	.079
3.461	.33	.03	5.24	.11
2.02	.44	.054	7.04	.197
1.123	.643	-.021	-1.81	.414
1.068	1.298	.018	.8	1.686
1.095	.962	.027	1.65	.927
.961	.822	.017	1.24	.677
.868	.935	.019	1.16	.876
.83	.899	.015	.96	.808
.982	.854	.018	1.2	.73
1.762	.728	.045	3.53	.532
1.797	.686	.039	3.33	.472
1.925	.644	.031	2.82	.416
3.736	.585	.055	5.39	.345
3.111	.519	.034	3.75	.27
3.364	.437	.077	10.09	.197
2.83	.497	.039	4.51	.248
2.692	.486	.04	4.75	.238
5.015	.409	.071	9.88	.172
3.09	.394	.01	1.59	.155
1.649	.461	.019	2.36	.213
.055	.638	.002	.21	.407
1.376	1.306	.005	.25	1.706
.443	.92	.009	.61	.848
1.122	.744	.034	2.68	.555
1.053	.873	.016	1.08	.763
2.341	.865	.036	2.4	.75
3.245	.798	.085	6.13	.644
2.876	.714	.069	5.59	.515
2.997	.667	.07	6.01	.45
3.748	.639	.073	6.5	.414
5.027	.568	.071	7.13	.327
4.3	.519	.045	5.04	.272
3.535	.475	.055	6.61	.229
4.564	.543	.055	5.81	.298
4.166	.53	.044	4.77	.283
5.242	.401	.075	10.61	.166
5.228	.335	.019	3.31	.112
4.597	.397	.032	4.68	.158
4.828	.423	.091	12.22	.187
3.48	.554	.043	4.5	.309
.328	.661	-.011	-.88	.437
1.658	1.305	-.008	-.34	1.703
1.232	.763	.064	4.83	.586
3.535	.715	.039	3.18	.513
3.551	.812	.057	4.07	.663
4.233	.784	.08	5.88	.622
4.28	.748	.065	4.98	.564
3.248	.688	.071	5.91	.478
3.82	.64	.088	7.88	.417
4.77	.616	.087	8.02	.387

MAX R/A = 5.24278 RMS R/A = 3.00239
AVG ANG = 3.81815 DEG MAX ANG = 12.2288 DEG
STD DEV = 3.03213 DEG
AVG ANG MAG = 3.92377 DEG
NUMBER OF TRAJECTORIES = 57

TABLE OF FINAL RADII, VELOCITIES, ANGLES AND ENERGIES
OF RINGS AT Z/A = 60

CASE NUMBER 3

R/A	Z DOT / U	R DOT / U	ANGLE (DEG)	POTENTIAL
2.106	.943	.051	3.13	.893
2.141	.968	.053	3.18	.941
2.122	.923	.052	3.24	.855
1.8	.776	.036	2.66	.603
2.221	.719	.055	4.38	.52
2.531	.588	.056	5.48	.349
1.951	.39	.052	7.65	.155
5.791	.219	.136	31.87	.066
2.171	.413	.051	7.09	.173
2.263	.736	.056	4.4	.546
3.073	.413	.068	9.4	.175
1.761	1.363	.063	2.67	1.864
2.04	.912	.047	2.97	.834
2.891	.334	.039	6.81	.113
2.733	.379	.057	8.62	.146
1.814	.751	.041	3.15	.566
4.418	.907	.085	5.38	.83
4.562	.936	.091	5.6	.885
4.157	.805	.061	4.37	.651
4.893	.738	.055	4.31	.547
3.72	.67	.039	3.36	.451
3.849	.588	.012	1.24	.346
5.131	.372	.134	19.86	.156
3.687	.279	.065	13.18	.082
4.097	.528	.1	10.78	.289
3.906	.872	.07	4.59	.765
3.194	.442	.068	8.82	.2
2.992	1.375	.108	4.49	1.904
2.846	.832	.064	4.4	.697
3.353	.634	.019	1.73	.402
5.263	.749	.062	4.75	.565
4.639	.835	.08	5.53	.704
4.418	.725	.055	4.41	.529
3.896	.653	.081	7.07	.433
4.804	.609	.02	1.96	.371
3.772	.597	.02	1.98	.357
5.24	.466	.04	5	.219
5.043	.289	.166	29.91	.111
7.481	.29	.176	31.28	.115
3.96	.707	.063	5.12	.504
4.619	.926	.096	5.96	.867
3.566	.471	.045	5.51	.223
3.964	1.384	.142	5.87	1.936
4.094	.892	.098	6.33	.805
5.061	.331	-.002	-.3	.109

MAX R/A = 7.48163 RMS R/A = 3.85812
AVG ANG = 7.09802 DEG MAX ANG = 31.8746 DEG
STD DEV = 7.20026 DEG
AVG ANG MAG = 7.11098 DEG
NUMBER OF TRAJECTORIES = 45

TABLE OF FINAL RADII, VELOCITIES, ANGLES AND ENERGIES
OF RINGS AT Z/A = 60

CASE NUMBER 4

R/A	Z DOT / U	R DOT / U	ANGLE (DEG)	POTENTIAL
7.274	.496	-.001	-.1	.246
7.22	.572	.021	2.17	.327
2.956	.749	.05	3.82	.564
3.939	.569	.012	1.28	.324
5.538	.559	.023	2.44	.313
.345	1.282	-.013	-.58	1.645
.353	.786	.003	.22	.618
.401	.866	.013	.89	.751
3.526	.614	-.001	-.08	.378
4.066	.586	.001	.16	.344
4.318	.571	-.014	-1.39	.326
4.044	.584	.013	1.32	.341
5.017	.553	.02	2.14	.306
7.459	.473	-.014	-1.68	.224
9.465	.476	-.025	-2.94	.227
.998	.732	-.024	-1.81	.537
1.094	.667	-.028	-2.41	.446
2.461	.657	-.017	-1.46	.432
2.616	.625	-.02	-1.75	.391
5.624	.452	.004	.51	.204
7.892	.561	.014	1.49	.315
4.028	.729	.063	4.99	.535
6.049	.558	-.006	-.56	.311
6.019	.526	0	.07	.277
1.416	1.294	.004	.2	1.675
1.699	.757	-.001	-.04	.573
1.702	.837	.004	.28	.702
6.225	.559	-.007	-.7	.313
5.817	.51	-.008	-.82	.26
5.639	.43	.003	.44	.185
2.556	.698	.094	7.72	.496
3.65	.651	.009	.87	.424
5.203	.636	-.007	-.61	.405
4.998	.589	-.02	-1.94	.348
7.085	.603	.034	3.23	.364
8.152	.571	-.004	-.31	.327
8.669	.554	.018	1.91	.307
4.439	.718	.054	4.3	.519
7.87	.564	.004	.47	.319
6.45	.508	-.012	-1.3	.259
2.248	1.302	.025	1.12	1.697
2.834	.721	.009	.73	.52
3.082	.809	.013	.94	.655
4.66	.698	.033	2.76	.489
4.757	.629	.084	7.62	.403
7.699	.641	.017	1.53	.411
7.818	.577	-.006	-.57	.333
7.956	.559	-.01	-.94	.313
8.395	.542	-.009	-.95	.293
7.177	.508	-.024	-2.6	.259
8.774	.524	.023	2.54	.275
7.795	.491	.054	6.35	.244

MAX R/A = 9.46588 RMS R/A = 5.55131
AVG ANG = .754749 DEG MAX ANG = 7.72505 DEG
STD DEV = 2.35154 DEG
AVG ANG MAG = 1.73285 DEG
NUMBER OF TRAJECTORIES = 52

TABLE OF FINAL RADII, VELOCITIES, ANGLES AND ENERGIES
OF RINGS AT Z/A = 60

CASE NUMBER 5

R/A	Z DOT / U	R DOT / U	ANGLE (DEG)	POTENTIAL
.72	.591	.05	4.85	.352
.597	.528	.036	3.96	.28
.623	.44	-.009	-1.17	.193
.618	.488	.012	1.44	.239
1.018	.48	-.006	-.65	.231
1.128	.365	.052	8.21	.136
2.49	.261	.102	21.29	.078
1.5	.32	.006	1.17	.102
.828	.44	-.036	-4.63	.194
.335	.64	.02	1.85	.41
.311	1.297	-.042	-1.84	1.684
.196	.96	.046	2.77	.924
1.223	.819	.075	5.26	.677
1.266	.937	.074	4.55(	.884
1.311	.9	.075	4.78	.816
.968	.851	.074	4.96	.73
.498	.724	.046	3.64	.527
.5	.68	.053	4.51	.466
.715	.638	.059	5.35	.41
3.165	.588	.019	1.91	.347
3.711	.522	.017	1.86	.272
5.48	.454	-.017	-2.05	.206
4.098	.502	.01	1.23	.252
4.318	.495	.005	.68	.245
10.111	.433	-.02	-2.59	.187
5.195	.394	-.049	-7.03	.157
.644	.64	.023	2.09	.41
1.144	1.305	-.055	-2.41	1.707
.103	.919	.05	3.11	.847
.702	.745	-.032	-2.4	.556
.751	.873	-.037	-2.37	.764
1.368	.864	-.004	-.25	.747
1.734	.794	.082	5.9	.637
2.614	.718	.004	.36	.516
2.597	.67	.006	.59	.449
2.929	.642	.017	1.56	.412
5.333	.582	.028	2.76	.339
5.948	.535	.026	2.88	.287
6.998	.498	.021	2.42	.249
4.979	.554	.024	2.52	.307
5.114	.541	.024	2.54	.293
7.82	.423	-.02	-2.58	.179
5.282	.334	.047	8.12	.113
8.628	.454	-.012	-1.47	.206
3.238	.556	.018	1.9	.31
4.052	.754	.032	2.49	.57
4.919	.701	.007	.63	.492
4.792	.654	.004	.41	.427
5.118	.632	.027	2.48	.4
1.129	.665	.034	2.97	.444
1.719	1.305	-.049	-2.12	1.705
.426	.761	.074	5.56	.585
2.744	.813	.03	2.13	.661
3.023	.779	.119	8.7	.621
14.227	.438	.009	1.18	.192
3.001	.467	-.019	-2.21	.219

MAX R/A = 14.227 RMS R/A = 4.07194
AVG ANG = 2.00179 DEG MAX ANG = 21.2968 DEG
STD DEV = 4.07743 DEG
AVG ANG MAG = 3.27645 DEG
NUMBER OF TRAJECTORIES = 56

TABLE OF FINAL RADII, VELOCITIES, ANGLES AND ENERGIES
OF RINGS AT Z/A = 60

CASE NUMBER 6

R/A	Z DOT / U	R DOT / U	ANGLE (DEG)	POTENTIAL
1.425	.943	-.003	-.13	.889
1.426	.968	-.001	-.05	.937
1.434	.922	-.003	-.15	.851
1.229	.775	-.011	-.81	.602
1.396	.718	-.006	-.44	.516
1.488	.587	-.008	-.71	.345
2.069	.394	.008	1.19	.155
8.066	.256	-.051	-11.21	.068
2.805	.42	-.006	-.76	.176
1.67	.737	-.004	-.27	.543
3.814	.421	-.026	-3.46	.178
.688	1.363	.002	.09	1.858
1.339	.912	-.005	-.3	.832
2.643	.334	-.012	-2	.111
2.683	.383	-.018	-2.55	.147
1.16	.751	-.009	-.64	.564
5.295	.918	.045	2.82	.844
5.182	.946	.053	3.21	.899
5.87	.817	.034	2.38	.669
6.635	.755	.041	3.16	.571
7.616	.689	.024	2.01	.476
9.104	.615	.025	2.37	.378
10.217	.421	-.011	-1.38	.177
7.481	.306	.008	1.67	.093
6.139	.546	-.024	-2.5	.298
4.581	.879	.031	2.03	.774
6.658	.467	.006	.74	.218
2.325	1.378	.041	1.72	1.901
3.076	.836	.009	.63	.699
7.174	.65	.023	2.1	.423
7.467	.769	.051	3.79	.595
6.194	.849	.046	3.15	.724
7.586	.744	.038	2.94	.555
7.459	.674	.017	1.5	.455
9.539	.637	.048	4.38	.408
9.811	.625	.035	3.23	.392
5.759	.482	.004	.58	.233
6.737	.335	.052	8.89	.114
13.02	.356	-.026	-4.07	.127
7.45	.726	.029	2.31	.528
5.572	.937	.053	3.26	.882
6.888	.493	.026	3.1	.244
3.435	1.389	.073	3	1.935
5.17	.903	.039	2.53	.818
9.59	.346	.02	3.42	.12

MAX R/A = 13.021 RMS R/A = 6.02852
AVG ANG = .911022 DEG MAX ANG = 11.2012 DEG
STD DEV = 2.96407 DEG
AVG ANG MAG = 2.30358 DEG
NUMBER OF TRAJECTORIES = 45

TABLE OF FINAL RADII, VELOCITIES, ANGLES AND ENERGIES
OF RINGS AT Z/A = 60

CASE NUMBER 7

R/A	Z DOT / U	R DOT / U	ANGLE (DEG)	POTENTIAL
1.062	.536	.021	2.24	.288
.547	.494	.029	3.37	.245
1.022	.38	.078	11.66	.15
3.438	.3	.098	18.2	.1
1.334	.452	.017	2.19	.205
1.003	1.299	.048	2.11	1.69
.459	.824	.005	.35	.68
.461	.9	.008	.51	.811
1.236	.732	.025	2.03	.536
.612	.645	.05	4.51	.419
1.423	.523	.048	5.3	.276
1.759	.505	.027	3.11	.255
4.492	.431	.153	19.55	.21
2.692	.473	.111	13.27	.237
1.099	1.306	.036	1.58	1.706
.96	.748	.069	5.31	.565
1.202	.867	.014	.95	.752
.923	.719	.026	2.14	.518
2.041	.645	.124	10.94	.432
2.125	.534	.032	3.46	.287
1.842	.554	.051	5.26	.31
4.951	.444	.131	16.49	.214
3.696	.443	.06	7.81	.2
1.744	.563	.047	4.84	.319
1.311	1.304	.04	1.78	1.703
1.17	.718	.09	7.15	.523
1.103	.791	.013	1.01	.626
1.692	.696	.123	10.08	.499
3.28	.634	.138	12.27	.421

MAX R/A = 4.95144 RMS R/A = 2.09801
AVG ANG = 6.19321 DEG MAX ANG = 19.5546 DEG
STD DEV = 5.453 DEG
AVG ANG MAG = 6.19321 DEG
NUMBER OF TRAJECTORIES = 29

TABLE OF FINAL RADII, VELOCITIES, ANGLES AND ENERGIES
OF RINGS AT Z/A = 60

CASE NUMBER 8

R/A	Z DOT / U	R DOT / U	ANGLE (DEG)	POTENTIAL
1.856	.553	.063	6.5	.309
2.228	.522	.073	7.95	.277
2.396	.394	.035	5.2	.156
1.366	.301	0	.16	.09
2.772	.469	.081	9.85	.227
1.695	1.305	.087	3.82	1.711
3.234	.864	.14	9.21	.766
2.026	.924	.138	8.53	.873
1.737	.743	.063	4.91	.556
1.69	.663	.079	6.82	.446
3.417	.554	.129	13.11	.324
3.351	.537	.136	14.26	.307
3.164	.426	.065	8.75	.186
3.946	.534	.166	17.28	.313
1.284	1.306	.042	1.85	1.707
5.272	.865	.202	13.18	.789
3.174	.915	.185	11.45	.872
2.984	.745	.12	9.15	.57
2.875	.668	.119	10.13	.461
4.225	.571	.185	18.02	.361
4.055	.594	.184	17.26	.387
3.629	.425	.087	11.62	.188
2.874	.411	.076	10.52	.175
4.597	.648	.195	16.8	.459
1.528	1.303	.047	2.09	1.702
4.44	.802	.158	11.16	.668
4.35	.866	.212	13.77	.796
4.098	.756	.18	13.38	.605
3.804	.667	.152	12.9	.468

MAX R/A = 5.27297
AVG ANG = 9.99325 DEG
STD DEV = 4.69518 DEG
AVG ANG MAG = 9.99325 DEG
NUMBER OF TRAJECTORIES = 29

RMS R/A = 3.22363
MAX ANG = 18.0282 DEG

TABLE OF FINAL RADII, VELOCITIES, ANGLES AND ENERGIES
OF RINGS AT Z/A = 60

CASE NUMBER 9

R/A	Z DOT / U	R DOT / U	ANGLE (DEG)	POTENTIAL
2.507	.581	.135	13.11	.356
2.384	.517	.129	14.02	.284
.765	.431	.091	11.93	.194
1.308	.479	.108	12.71	.241
.274	.474	.03	3.72	.225
.874	.354	.097	15.43	.135
7.282	.238	.152	32.62	.08
.587	.313	.019	3.63	.098
.011	.433	.035	4.66	.189
2.078	.631	.124	11.13	.413
.572	1.292	.129	5.74	1.686
1.671	.952	.135	8.11	.924
1.22	.81	.057	4.04	.66
.573	.927	.023	1.42	.861
.738	.889	.031	1.99	.791
1.397	.842	.074	5.05	.715
2.076	.715	.144	11.42	.532
2.427	.67	.136	11.52	.468
2.37	.627	.126	11.4	.41
2.782	.584	.006	.62	.342
3.619	.521	.014	1.61	.271
6.437	.456	.024	3.1	.209
4.402	.503	.02	2.36	.253
4.72	.496	.02	2.37	.246
12.211	.432	.072	9.46	.192
6.335	.4	-.004	-.46	.16
3.077	.467	-.018	-2.15	.219
.513	.637	.025	2.31	.406
.625	1.302	-.105	-4.57	1.708
1.345	.91	.146	9.12	.851
.081	.738	.063	4.87	.55
.146	.867	.083	5.51	.759
.618	.861	-.042	-2.8	.743
.678	.793	.053	3.84	.632
2.178	.716	-.018	-1.41	.513
2.233	.669	-.015	-1.23	.448
2.686	.641	.007	.67	.411
5.944	.583	.054	5.31	.343
6.745	.535	.064	6.83	.291
8.022	.498	.07	8.11	.253
5.421	.554	.046	4.74	.309
5.531	.541	.046	4.87	.295
9.16	.424	.048	6.55	.182
6.003	.334	.067	11.47	.116
15.99	.428	.107	14.13	.195
10.119	.453	.061	7.72	.209
3.072	.556	.011	1.23	.309
.738	.656	.035	3.08	.432
1.367	1.303	-.085	-3.73	1.706
2.342	.75	.163	12.26	.589
3.896	.719	.015	1.22	.517
2.366	.795	.008	.59	.633
2.065	.783	.042	3.13	.616
4.028	.754	.03	2.31	.569
5.35	.701	.031	2.53	.492
5.169	.654	.027	2.42	.428
5.425	.631	.048	4.36	.4

MAX R/A = 15.9908 RMS R/A = 4.67484
AVG ANG = 5.54891 DEG MAX ANG = 32.6227 DEG
STD DEV = 6.05045 DEG
AVG ANG MAG = 6.12127 DEG
NUMBER OF TRAJECTORIES = 57

TABLE OF FINAL RADII, VELOCITIES, ANGLES AND ENERGIES
OF RINGS AT Z/A = 60

CASE NUMBER 10

R/A	Z DOT / U	R DOT / U	ANGLE (DEG)	POTENTIAL
.665	.534	.031	3.32	.286
.981	.498	-.008	-.88	.248
2.625	.393	-.037	-5.32	.155
1.4	.296	-.006	-1.14	.088
1.286	.445	.076	9.77	.204
.683	1.296	.084	3.71	1.687
1.759	.82	.086	6.02	.68
1.712	.896	.087	5.59	.812
.333	.73	.019	1.53	.533
.893	.643	.066	5.88	.418
5.53	.544	.015	1.63	.296
5.601	.526	-.004	-.43	.276
6.707	.455	.016	2.05	.207
2.587	.481	-.018	-2.03	.232
.497	1.307	-.059	-2.56	1.712
.942	.748	.042	3.23	.561
.633	.864	.042	2.81	.749
2.194	.723	.048	3.79	.526
3.272	.654	.052	4.56	.43
8.451	.57	.017	1.77	.326
8.258	.587	.035	3.48	.346
10.097	.473	.026	3.15	.225
10.518	.47	.007	.86	.221
5.667	.546	.187	18.95	.333
.114	1.302	.085	3.76	1.704
2.608	.722	.057	4.57	.525
2.003	.791	.054	3.91	.629
4.043	.708	.069	5.62	.506
6.17	.654	.057	4.99	.431

MAX R/A = 10.5184 RMS R/A = 4.5472
AVG ANG = 3.19707 DEG MAX ANG = 18.9531 DEG
STD DEV = 4.24427 DEG
AVG ANG MAG = 4.04754 DEG
NUMBER OF TRAJECTORIES = 29

TABLE OF FINAL RADII, VELOCITIES, ANGLES AND ENERGIES
OF RINGS AT Z/A = 60

CASE NUMBER 11

R/A	Z DOT / U	R DOT / U	ANGLE (DEG)	POTENTIAL
3.875	.568	.058	5.88	.326
3.759	.522	.035	3.83	.274
2.678	.38	.005	.83	.144
8.013	.263	.183	34.75	.103
4.322	.479	.007	.86	.23
1.57	1.305	.037	1.64	1.705
5.313	.866	.055	3.64	.753
3.186	.92	.053	3.32	.85
3.125	.747	.032	2.46	.56
3.194	.668	.036	3.1	.448
5.937	.566	.049	5.01	.323
6.666	.553	.047	4.92	.308
4.834	.439	-.003	-.27	.193
9.36	.572	.056	5.65	.33
.09	1.303	.082	3.61	1.705
11.024	.869	.128	8.4	.772
5.826	.913	.104	6.5	.845
5.545	.724	.087	6.91	.533
5.993	.652	.064	5.64	.43
10.182	.555	.087	8.99	.315
10.177	.573	.092	9.11	.337
6.311	.417	.017	2.35	.174
5.779	.437	.02	2.71	.191
6.485	.612	.09	8.35	.383
.041	1.301	.086	3.78	1.7
7.454	.766	.094	7.03	.596
7.322	.844	.107	7.22	.725
10.454	.789	.131	9.48	.64
8.417	.684	.104	8.64	.479

MAX R/A = 11.0249 RMS R/A = 6.44557
AVG ANG = 6.01658 DEG MAX ANG = 34.7579 DEG
STD DEV = 6.0636 DEG
AVG ANG MAG = 6.03476 DEG
NUMBER OF TRAJECTORIES = 29

Appendix C

STATISTICAL ANALYSIS OF POST OUTPUT GAP ELECTRONS

DATA TAPE NO. 43
NASA KLYSTRON DESIGN A

OUTPUT GAP EXIT LOCATION Z/A = 14.69

RING	R/A	ANGLE (DEG)	POTENTIAL
1	.29	3.59	.276
2	.26	3.65	.268
3	.24	3.07	.234
4	.22	.62	.209
5	.22	-2.73	.195
6	.24	-6.21	.181
7	.34	-6.6	.205
8	.32	-7.34	.192
9	.3	-7.26	.189
10	.3	-5.72	.232
11	.27	-3.33	.304
12	.24	-4.01	.597
13	.3	-.39	1.774
14	.28	-.6	.748
15	.32	-.48	.525
16	.31	-.59	.466
17	.31	.23	.538
18	.31	.84	.374
19	.31	1.11	.317
20	.32	2.43	.267
21	.57	9.71	.202
22	.47	11.56	.168
23	.43	11.03	.161
24	.37	8.28	.13
25	.36	3.87	.087
26	.39	-.48	.132
27	.39	-9.83	.132
28	.4	-13.97	.136
29	.4	-12.05	.147
30	.41	-9.97	.182
31	.36	-.35	.246
32	.39	-6.72	.579
33	.55	-.43	1.784
34	.49	-.88	.717
35	.55	-.91	.402
36	.57	1.29	.38
37	.57	1.14	.425
38	.6	3.37	.277
39	.61	3.66	.251
40	.62	6.78	.224
41	.76	11.79	.153
42	.67	18.7	.111
43	.56	21.18	.05
44	.56	14.96	.065
45	.47	16.64	.04
46	.45	4.66	.054
47	.48	.53	.104
48	.46	-5.5	.098
49	.44	-6.64	.091
50	.48	-2.21	.172

51	.5	5.66	.266
52	.47	-5.17	.571
53	.67	-.69	1.79
54	.62	-1.59	.689
55	.72	-.79	.264
56	.72	.95	.29
57	.72	1.1	.327
58	.76	3.05	.22
59	.78	2.84	.214
60	.83	6.61	.173

AVG R/A = .4602 AVG ANG = 1.02928
RMS R/A = .487808 RMS ANG = 7.13733
MAX R/A = .835 MAX ANG = 21.1843
STD DEV = .161779 STD DEV = 7.06273

ENERGY WTD AVG ANGLE =-.207376 DEGREES
ENERGY WTD RMS ANGLE = 4.54099 DEGREES
FRACTION OF RINGS WITH ANGLE GREATER THAN 15 DEG = .05
AUXILIARY REFOCUSING COIL NOT NEEDED

LOWEST ENERGY CLASS
AVG R/A = .464
RMS R/A = .492124
AVG ANG = 1.86043 DEGREES
RMS ANG = 9.44536 DEGREES
NUMBER OF ELECTRONS = 32

SECOND ENERGY CLASS
AVG R/A = .484875
RMS R/A = .51295
AVG ANG = 1.46843 DEGREES
RMS ANG = 2.60751 DEGREES
NUMBER OF ELECTRONS = 16

THIRD ENERGY CLASS
AVG R/A = .385222
RMS R/A = .241
AVG ANG =-2.19674 DEGREES
RMS ANG = 3.19777 DEGREES
NUMBER OF ELECTRONS = 9

HIGHEST ENERGY CLASS
AVG R/A = .513
RMS R/A = .535682
AVG ANG =-.500365 DEGREES
RMS ANG = .517418 DEGREES
NUMBER OF ELECTRONS = 3

TAPE NO. 43

```
STATISTICAL ANALYSIS OF POST OUTPUT GAP ELECTRONS

DATA TAPE NO. 43
NASA KLYSTRON DESIGN A

OUTPUT GAP EXIT LOCATION Z/A = 14.69


MIN ZDOT/U = .194
AVG ZDOT/U = .53275
MAX ZDOT/U = 1.338
STD DEV = .241091


TIME:  00 MINS. 02 SECS.



LIST  500

 STDB      12:11   MON   6-12-72

500 DATA 43,14.69,60,1,1,1
501 DATA .297,.033,.525,.261,.033,.517,.249,.026,.484
502 DATA .222,.005,.458,.222,-.021,.442,.241,-.046,.423
503 DATA .344,-.052,.45,.327,-.056,.435,.302,-.055,.432
504 DATA .301,-.048,.48,.28,-.032,.551,.247,-.054,.771
505 DATA .308,-.009,1.332,.281,-.009,.865,.322,-.006,.725
506 DATA .318,-.007,.683,.315,.003,.734,.315,.009,.612
507 DATA .315,.011,.563,.324,.022,.517,.572,.076,.444
508 DATA .478,.087,.425,.433,.077,.395,.372,.052,.357
509 DATA .367,.02,.295,.4,-.003,.364,.397,-.062,.358
510 DATA .405,-.089,.358,.41,-.08,.375,.415,-.074,.421
511 DATA .37,-.003,.496,.393,-.089,.756,.551,-.01,1.336
512 DATA .491,-.013,.847,.552,-.01,.634,.571,.014,.617
513 DATA .571,.013,.652,.604,.031,.526,.611,.032,.5
514 DATA .63,.056,.471,.763,.08,.383,.671,.107,.316
515 DATA .567,.081,.209,.561,.066,.247,.472,.058,.194
516 DATA .459,.019,.233,.486,.003,.323,.462,-.03,.312
517 DATA .444,-.035,.301,.49,-.016,.415,.51,.051,.514
518 DATA .472,-.068,.753,.68,-.016,1.338,.628,-.023,.83
519 DATA .73,-.007,.514,.723,.009,.539,.724,.011,.572
520 DATA .767,.025,.469,.784,.023,.463,.835,.048,.414
999 END
```

STATISTICAL ANALYSIS OF POST OUTPUT GAP ELECTRONS

DATA TAPE NO. 44
NASA KLYSTRON DESIGN B

OUTPUT GAP EXIT LOCATION Z/A = 14.24

RING	R/A	ANGLE (DEG)	POTENTIAL
1	.24	3	.285
2	.23	1.67	.262
3	.24	0	.235
4	.27	-3.5	.21
5	.3	-5.06	.205
6	.35	-4.6	.201
7	.29	-4.72	.202
8	.28	-4.26	.21
9	.3	-3.48	.228
10	.3	-1.61	.286
11	.31	-2.85	.498
12	.32	-.44	1.428
13	.19	0	1.366
14	.31	1.12	.504
15	.3	1.34	.591
16	.3	2.34	.405
17	.3	2.16	.51
18	.29	2.41	.443
19	.27	2.79	.329
20	.26	4.1	.296
21	.44	7.04	.223
22	.41	3.58	.2
23	.39	.13	.19
24	.4	-2.28	.182
25	.41	-4.71	.171
26	.45	-12.79	.169
27	.44	-12.98	.164
28	.46	-9.44	.176
29	.46	-10.49	.188
30	.42	-6.16	.263
31	.49	-7.97	.479
32	.58	-.53	1.44
33	.35	-.3	1.352
34	.51	2.71	.35
35	.53	5.01	.455
36	.53	8.51	.345
37	.54	7.78	.394
38	.52	9.05	.334
39	.52	10.55	.269
40	.5	9.76	.245
41	.58	10.07	.183
42	.52	7.28	.161
43	.52	4.51	.155
44	.52	1.57	.16
45	.48	-3.33	.144
46	.51	-9.59	.152
47	.52	-10.26	.145
48	.54	-9.02	.161
49	.5	-5.25	.191
50	.47	2.06	.277

51	.54	-7.5	.475
52	.69	-1.48	1.448
53	.45	-.35	1.334
54	.67	5.39	.26
55	.67	9.34	.307
56	.72	13.3	.228
57	.72	11.92	.278
58	.71	12.56	.251
59	.72	14.21	.215
60	.64	12.73	.201

AVG R/A = .4504 AVG ANG = .755511
RMS R/A = .471977 RMS ANG = 6.91552
MAX R/A = .724 MAX ANG = 14.2159
STD DEV = .141075 STD DEV = 6.87413

ENERGY WTD AVG ANGLE = .69654 DEGREES
ENERGY WTD RMS ANGLE = 5.45152 DEGREES
FRACTION OF RINGS WITH ANGLE GREATER THAN 15 DEG = 0
AUXILIARY REFOCUSING COIL NOT NEEDED

LOWEST ENERGY CLASS
AVG R/A = .459103
RMS R/A = .475052
AVG ANG =-1.08415 DEGREES
RMS ANG = 8.01507 DEGREES
NUMBER OF ELECTRONS = 29

SECOND ENERGY CLASS
AVG R/A = .459556
RMS R/A = .488373
AVG ANG = 4.91651 DEGREES
RMS ANG = 6.8433 DEGREES
NUMBER OF ELECTRONS = 18

THIRD ENERGY CLASS
AVG R/A = .4095
RMS R/A = .356
AVG ANG =-1.12474 DEGREES
RMS ANG = 4.48315 DEGREES
NUMBER OF ELECTRONS = 8

HIGHEST ENERGY CLASS
AVG R/A = .4324
RMS R/A = .469506
AVG ANG =-.545683 DEGREES
RMS ANG = .738694 DEGREES
NUMBER OF ELECTRONS = 5

TAPE NO. 44

```
STATISTICAL ANALYSIS OF POST OUTPUT GAP ELECTRONS

DATA TAPE NO. 44
NASA KLYSTRON DESIGN B

OUTPUT GAP EXIT LOCATION Z/A = 14.24


MIN ZDOT/U = .376
AVG ZDOT/U = .57465
MAX ZDOT/U = 1.203
STD DEV = .224142



LIST 500

 STDB    14:02   MON   6-12-72

500 DATA 44,14.24,60,1,1,1
501 DATA .249,.028,.534,.238,.015,.512,.241,0,.485
502 DATA .273,-.028,.458,.304,-.04,.452,.356,-.036,.448
503 DATA .294,-.037,.449,.286,-.034,.457,.309,-.029,.477
504 DATA.301,-.015,.535,.311,-.035,.705,.323,-.009,1.195
505 DATA .199,0,1.169,.32,.014,.71,.305,.018,.769
506 DATA .305,.026,.636,.304,.027,.714,.299,.028,.665
507 DATA .277,.028,.573,.27,.039,.543,.449,.058,.469
508 DATA .414,.028,.447,.394,.001,.436,.405,-.017,.427
509 DATA .419,-.034,.413,.458,-.091,.401,.443,-.091,.395
510 DATA .466,-.069,.415,.467,-.079,.427,.423,-.055,.51
511 DATA .497,-.096,.686,.585,-.011,1.2,.355,-.006,1.163
512 DATA .516,.028,.591,.535,.059,.672,.535,.087,.581
513 DATA .545,.085,.622,.522,.091,.571,.527,.095,.51
514 DATA .5,.084,.488,.585,.075,.422,.528,.051,.399
515 DATA .521,.031,.393,.522,.011,.401,.49,-.022,.379
516 DATA .52,-.065,.385,.523,-.068,.376,.547,-.063,.397
517 DATA .505,-.04,.436,.475,.019,.526,.547,-.09,.684
518 DATA .7,-.031,1.203,.457,-.007,1.155,.677,.048,.508
519 DATA .679,.09,.547,.724,.11,.465,.721,.109,.516
520 DATA .713,.109,.489,.723,.114,.45,.648,.099,.438
999 END
```

STATISTICAL ANALYSIS OF POST OUTPUT GAP ELECTRONS

DATA TAPE NO. 45
NASA KLYSTRON DESIGN C

OUTPUT GAP EXIT LOCATION Z/A = 12.59

RING	R/A	ANGLE (DEG)	POTENTIAL
1	.2	.23	.239
2	.2	-2.34	.217
3	.25	-5.92	.19
4	.3	-7.76	.19
5	.36	-5.81	.189
6	.31	-5.27	.171
7	.29	-5.06	.186
8	.27	-5.69	.206
9	.23	-3.76	.238
10	.26	-1.71	.363
11	.33	.73	.874
12	.25	1.17	1.853
13	.23	2.9	.397
14	.19	2.37	.392
15	.2	1.96	.274
16	.18	.85	.36
17	.18	.17	.412
18	.18	-1.05	.505
19	.19	.57	.351
20	.2	1.47	.254
21	.36	6.74	.173
22	.33	1.8	.145
23	.33	-4.17	.138
24	.35	-11.7	.14
25	.43	-23.67	.125
26	.45	-17.67	.141
27	.46	-14.29	.157
28	.4	-15.91	.149
29	.34	-4.48	.201
30	.45	-9.42	.33
31	.6	.67	.859
32	.45	2.34	1.869
33	.42	5.8	.363
34	.34	3.57	.314
35	.4	13.18	.207
36	.31	8.43	.29
37	.29	4.11	.31
38	.29	-1.58	.43
39	.32	8.42	.276
40	.42	11.89	.194
41	.48	15.69	.118
42	.46	13.68	.097
43	.41	6.45	.076
44	.41	-3.45	.089
45	.43	-15.43	.09
46	.48	-21.48	.107
47	.48	-17.31	.113
48	.43	-5.07	.131
49	.44	7.07	.206
50	.51	-10.28	.346

```
 51              .73             -.5             .846
 52              .58              2.88           1.884
 53              .57              8.55            .326
 54              .55             13.91            .209
 55              .62             21.77            .144
 56              .58             17.66            .2
 57              .52             14.39            .252
 58              .42              5.59            .353
 59              .54             16.3             .211
 60              .56             19.65            .138

AVG R/A = .384783               AVG ANG = .374806
RMS R/A = .406276               RMS ANG = 10.0419
MAX R/A = .732 MAX ANG = 23.6665
STD DEV = .130391               STD DEV = 10.0349

ENERGY WTD AVG ANGLE = 1.21625 DEGREES
ENERGY WTD RMS ANGLE = 7.07721 DEGREES
FRACTION OF RINGS WITH ANGLE GREATER THAN 15 DEG = .183
AUXILIARY REFOCUSING COIL NEEDED

LOWEST ENERGY CLASS
     AVG R/A = .416844
     RMS R/A = .428076
     AVG ANG =-.829232  DEGREES
     RMS ANG = 12.8459  DEGREES
     NUMBER OF ELECTRONS = 32

SECOND ENERGY CLASS
     AVG R/A = .334588
     RMS R/A = .357093
     AVG ANG = 2.28554  DEGREES
     RMS ANG = 6.57843  DEGREES
     NUMBER OF ELECTRONS = 17

THIRD ENERGY CLASS
     AVG R/A = .34575
     RMS R/A = .337
     AVG ANG = .470288  DEGREES
     RMS ANG = 1.53957  DEGREES
     NUMBER OF ELECTRONS = 8

HIGHEST ENERGY CLASS
     AVG R/A = .431333
     RMS R/A = .451539
     AVG ANG = 2.13577  DEGREES
     RMS ANG = 2.25102  DEGREES
     NUMBER OF ELECTRONS = 3


TAPE NO. 45
```

```
STATISTICAL ANALYSIS OF POST OUTPUT GAP ELECTRONS

DATA TAPE NO. 45
NASA KLYSTRON DESIGN C

OUTPUT GAP EXIT LOCATION Z/A = 12.59


MIN ZDOT/U = .274
AVG ZDOT/U = .530167
MAX ZDOT/U = 1.371
STD DEV = .24028




LIST  500

 STDB

500 DATA 45,12.59,60,1,1,1
501 DATA .204,.002,.489,.208,-.019,.466,.26,-.045,.434
502 DATA .306,-.059,.433,.364,-.044,.433,.319,-.038,.412
503 DATA .298,-.038,.43,.279,-.045,.452,.238,-.032,.487
504 DATA .262,-.018,.603,.336,0.012,.935,.258,.028,1.361
505 DATA .239,.032,.63,.195,.026,.626,.204,.018,.524
506 DATA .188,.009,.6,.186,.002,.642,.183,-.013,.711
507 DATA .194,.006,.593,.203,.013,.504,.37,.049,.414
508 DATA .339,.012,.381,.337,-.027,.371,.359,-.076,.367
509 DATA .437,-.142,.324,.457,-.114,.358,.465,-.098,.385
510 DATA .401,-.106,.372,.346,-.035,.447,.459,-.094,.567
511 DATA .602,.011,.927,.453,.056,1.366,.422,.061,.6
512 DATA .343,.035,.56,.409,.104,.444,.319,.079,.533
513 DATA .296,.04,.556,.293,-.018,.656,.322,.077,.52
514 DATA .43,.091,.432,.486,.093,.331,.461,.074,.304
515 DATA .418,.031,.274,.419,-.018,.299,.434,-.08,.29
516 DATA .485,-.12,.305,.484,-.1,.321,.431,-.032,.361
517 DATA .45,.056,.451,.518,-.105,.579,.732,-.008,.92
518 DATA .583,.069,1.371,.571,.085,.565,.559,.11,.444
519 DATA .623,.141,.353,.589,.136,.427,.521,.125,.487
520 DATA .424,.058,.592,.548,.129,.441,.568,.125,.35
999 END
```

STATISTICAL ANALYSIS OF POST OUTPUT GAP ELECTRONS

DATA TAPE NO. 46
NASA KLYSTRON DESIGN D

OUTPUT GAP EXIT LOCATION Z/A = 9.5

RING	R/A	ANGLE (DEG)	POTENTIAL
1	.22	3.4	.29
2	.21	.44	.269
3	.22	-1.96	.248
4	.24	-3.63	.21
5	.27	-4.55	.184
6	.3	-5.38	.155
7	.34	-4.06	.245
8	.41	-2.13	.289
9	.37	-3.41	.254
10	.37	-3.35	.264
11	.37	-3.39	.37
12	.32	-2.97	.596
13	.3	.52	1.703
14	.26	-1.67	.998
15	.29	.07	.625
16	.29	1.47	.542
17	.29	2.26	.467
18	.28	3.67	.388
19	.28	4.72	.339
20	.25	5.28	.306
21	.42	11.06	.214
22	.38	5.56	.13
23	.37	-4.73	.107
24	.36	-18	.06
25	.38	-9.95	.087
26	.42	-12.55	.095
27	.47	-7.38	.176
28	.52	-9.54	.25
29	.53	-10.39	.212
30	.53	-9.79	.221
31	.47	-8.7	.316
32	.51	-7.99	.559
33	.54	1.13	1.724
34	.46	-2.69	.966
35	.51	.94	.533
36	.51	3.69	.445
37	.51	5.48	.394
38	.52	9.71	.31
39	.51	11.94	.267
40	.47	13.3	.241
41	.55	19.57	.09
42	.51	13.57	.058
43	.45	-1.45	.025
44	.46	-2.79	.051
45	.46	-9.28	.039
46	.47	-16.73	.044
47	.55	-7.73	.127
48	.59	-11.83	.21
49	.58	-14.23	.185
50	.59	-13.06	.204

51	.54	-7.1	.285
52	.58	-9.19	.546
53	.66	.82	1.742
54	.58	-3.28	.924
55	.66	1.31	.429
56	.66	5.11	.353
57	.64	6.76	.323
58	.69	11.71	.252
59	.68	15.52	.218
60	.65	20.13	.172

AVG R/A = .452433 AVG ANG =-.924105
RMS R/A = .471592 RMS ANG = 8.60857
MAX R/A = .691 MAX ANG = 20.1363
STD DEV = .133051 STD DEV = 8.55882

ENERGY WTD AVG ANGLE =-.310012 DEGREES
ENERGY WTD RMS ANGLE = 6.12744 DEGREES
FRACTION OF RINGS WITH ANGLE GREATER THAN 15 DEG = .083
AUXILIARY REFOCUSING COIL NOT NEEDED

LOWEST ENERGY CLASS
AVG R/A = .457515
RMS R/A = .474221
AVG ANG =-1.90287 DEGREES
RMS ANG = 10.7721 DEGREES
NUMBER OF ELECTRONS = 33

SECOND ENERGY CLASS
AVG R/A = .4448
RMS R/A = .468656
AVG ANG = 2.00898 DEGREES
RMS ANG = 5.38033 DEGREES
NUMBER OF ELECTRONS = 15

THIRD ENERGY CLASS
AVG R/A = .448
RMS R/A = .472
AVG ANG =-2.95116 DEGREES
RMS ANG = 4.71678 DEGREES
NUMBER OF ELECTRONS = 8

HIGHEST ENERGY CLASS
AVG R/A = .448
RMS R/A = .477482
AVG ANG = .205785 DEGREES
RMS ANG = 1.11908 DEGREES
NUMBER OF ELECTRONS = 4

TAPE NO. 46

```
STATISTICAL ANALYSIS OF POST OUTPUT GAP ELECTRONS

DATA TAPE NO. 46
NASA KLYSTRON DESIGN D

OUTPUT GAP EXIT LOCATION Z/A = 9.5


MIN ZDOT/U = .159
AVG ZDOT/U = .552
MAX ZDOT/U = 1.32
STD DEV = .252364




LIST  500

 STDB      16:57  MON   6-12-72

500 DATA 46,9.5,60,1,1,1
501 DATA .224,.032,.538,.219,.004,.519,.23,-.017,.498
502 DATA .243,-.029,.458,.275,-.034,.428,.303,-.037,.393
503 DATA .349,-.035,.494,.412,-.02,.538,.374,-.03,.504
504 DATA .373,-.03,.513,.371,-.036,.608,.326,-.04,.771
505 DATA .31,.012,1.305,.269,-.029,.999,.292,.001,.791
506 DATA .295,.019,.736,.294,.027,.683,.289,.04,.622
507 DATA .282,.048,.581,.258,.051,.551,.424,.089,.455
508 DATA .384,.035,.359,.374,-.027,.327,.362,-.076,.234
509 DATA .385,-.051,.291,.428,-.067,.301,.472,-.054,.417
510 DATA .528,-.083,.494,.534,-.083,.453,.533,-.08,.464
511 DATA .473,-.085,.556,.515,-.104,.741,.544,.026,1.313
512 DATA .468,-.046,.982,.514,.012,.73,.512,.043,.666
513 DATA .512,.06,.625,.527,.094,.549,.518,.107,.506
514 DATA .477,.113,.478,.556,.101,.284,.512,.057,.236
515 DATA .455,-.004,.159,.468,-.011,.226,.47,-.032,.196
516 DATA .48,-.061,.203,.559,-.048,.354,.591,-.094,.449
517 DATA .587,-.106,.418,.595,-.102,.44,.543,-.066,.53
518 DATA .586,-.118,.73,.669,.019,1.32,.588,-.055,.96
519 DATA .661,.015,.655,.666,.053,.592,.648,.067,.565
520 DATA .691,.102,.492,.69,.125,.45,.659,.143,.39
999 END
```

STATISTICAL ANALYSIS OF POST OUTPUT GAP ELECTRONS

DATA TAPE NO. 47
NASA KLYSTRON DESIGN E

OUTPUT GAP EXIT LOCATION Z/A = 9.58

RING	R/A	ANGLE (DEG)	POTENTIAL
1	.24	2.08	.364
2	.24	1.29	.33
3	.24	-.52	.304
4	.25	-2.19	.276
5	.27	-4.34	.239
6	.29	-5.2	.236
7	.28	-3.91	.279
8	.27	-4.08	.27
9	.3	-3.61	.309
10	.28	-3.46	.3
11	.29	-2.89	.484
12	.31	-1.82	1.224
13	.27	-1.01	1.426
14	.28	-.42	.687
15	.29	.73	.6
16	.29	.92	.654
17	.28	1.8	.446
18	.29	1.33	.533
19	.27	2.24	.403
20	.26	3.24	.381
21	.42	5.22	.289
22	.41	3.85	.27
23	.41	-.35	.242
24	.41	-2.34	.216
25	.42	-4.01	.184
26	.44	-6.94	.192
27	.46	-8.24	.232
28	.46	-6.97	.244
29	.45	-7.05	.255
30	.44	-4.81	.301
31	.42	-7.76	.454
32	.54	-3.53	1.223
33	.47	-1.45	1.421
34	.5	.15	.524
35	.51	3.51	.468
36	.52	3.69	.509
37	.52	6.85	.373
38	.52	5.99	.424
39	.51	8.62	.328
40	.48	7.52	.302
41	.55	6.64	.225
42	.53	5.26	.199
43	.53	4.36	.187
44	.53	1.15	.158
45	.53	-1.7	.138
46	.54	-4.81	.174
47	.54	-8.68	.209
48	.55	-8.82	.227
49	.54	-5.53	.238
50	.51	-1.41	.28

```
 51              .46             -4.62            .433
 52              .66             -4.99            1.243
 53              .6              -1.88            1.422
 54              .64              1.46            .389
 55              .68              6.91            .328
 56              .68              5.99            .374
 57              .69             10.11            .286
 58              .68              8.37            .324
 59              .65             10.83            .266
 60              .61              9.77            .256

AVG R/A = .4468                  AVG ANG = 3.07498E-02
RMS R/A = .467234                RMS ANG = 5.15459
MAX R/A = .695 MAX ANG = 10.831
STD DEV = .136665                STD DEV = 5.1545

ENERGY WTD AVG ANGLE =-.283638 DEGREES
ENERGY WTD RMS ANGLE = 4.44451 DEGREES
FRACTION OF RINGS WITH ANGLE GREATER THAN 15 DEG = 0
AUXILIARY REFOCUSING COIL NOT NEEDED

LOWEST ENERGY CLASS
     AVG R/A = .470407
     RMS R/A = .484306
     AVG ANG =-1.08318  DEGREES
     RMS ANG = 6.02173  DEGREES
     NUMBER OF ELECTRONS = 27

SECOND ENERGY CLASS
     AVG R/A = .433444
     RMS R/A = .463118
     AVG ANG = 2.57937  DEGREES
     RMS ANG = 5.11  DEGREES
     NUMBER OF ELECTRONS = 18

THIRD ENERGY CLASS
     AVG R/A = .3974
     RMS R/A = .66
     AVG ANG =-.421216  DEGREES
     RMS ANG = 3.32162  DEGREES
     NUMBER OF ELECTRONS = 10

HIGHEST ENERGY CLASS
     AVG R/A = .4662
     RMS R/A = .490915
     AVG ANG =-2.22512  DEGREES
     RMS ANG = 2.63775  DEGREES
     NUMBER OF ELECTRONS = 5


TAPE NO. 47
```

```
STATISTICAL ANALYSIS OF POST OUTPUT GAP ELECTRONS

DATA TAPE NO. 47
NASA KLYSTRON DESIGN E

OUTPUT GAP EXIT LOCATION Z/A = 9.58


MIN ZDOT/U = .372
AVG ZDOT/U = .61845
MAX ZDOT/U = 1.194
STD DEV = .20325



EDIT DELETE 100-130,140-254,999
READY.


LIST

 STDB       15:26   THURS.  6-15-72

135 PRINT "NASA KLYSTRON DESIGN E"
500 DATA 47,9.58,60,1,1,1
501 DATA .245,.022,.603,.243,.013,.575,.244,-.005,.552
502 DATA .254,-.02,.525,.271,-.037,.488,.3,-.044,.484
503 DATA .288,-.036,.527,.278,-.037,.519,.303,-.035,.555
504 DATA .29,-.033,.547,.296,-.035,.695,.318,-.035,1.106
505 DATA .271,-.021,1.194,.285,-.006,.829,.294,.01,.775
506 DATA .293,.013,.809,.283,.021,.668,.292,.017,.73
507 DATA .278,.036,.634,.265,.035,.617,.428,.049,.536
508 DATA .417,.035,.519,.415,-.003,.492,.417,-.019,.465
509 DATA .423,-.03,.429,.443,-.053,.436,.461,-.069,.477
510 DATA .467,-.06,.491,.46,-.062,.502,.444,-.046,.547
511 DATA .421,-.091,.668,.548,-.068,1.104,.473,-.03,1.192
512 DATA .502,.002,.724,.516,.042,.683,.527,.046,.712
513 DATA .522,.073,.607,.526,.068,.648,.513,.086,.567
514 DATA .484,.072,.545,.553,.055,.472,.535,.041,.445
515 DATA .536,.033,.432,.537,.008,.398,.534,-.011,.372
516 DATA .543,-.035,.416,.542,-.069,.452,.559,-.073,.471
517 DATA .548,-.047,.486,.519,-.013,.529,.468,-.053,.656
518 DATA .662,-.097,1.111,.607,-.039,1.192,.642,.016,.624
519 DATA .681,.069,.569,.684,.064,.609,.695,.094,.527
520 DATA .687,.083,.564,.66,.097,.507,.618,.086,.499
```

STATISTICAL ANALYSIS OF POST OUTPUT GAP ELECTRONS

DATA TAPE NO. 48
NASA KLYSTRON DESIGN F

OUTPUT GAP EXIT LOCATION Z/A = 9.38

RING	R/A	ANGLE (DEG)	POTENTIAL
1	.23	1.12	.371
2	.23	.57	.355
3	.23	-.52	.305
4	.24	-2.58	.261
5	.26	-5.02	.241
6	.3	-5.95	.251
7	.26	-4.6	.249
8	.27	-4.12	.265
9	.29	-4.74	.271
10	.28	-3.26	.358
11	.32	-2.34	.578
12	.31	.51	1.498
13	.24	1.73	1.193
14	.23	2.48	.615
15	.22	2.72	.574
16	.21	2.63	.578
17	.23	2.96	.432
18	.22	2.83	.499
19	.23	3.53	.4
20	.23	2.98	.378
21	.42	5.12	.276
22	.39	2.75	.249
23	.38	-.59	.237
24	.4	-2.37	.211
25	.41	-3.77	.181
26	.42	-8.47	.188
27	.44	-8.08	.213
28	.43	-7.65	.217
29	.43	-7.6	.234
30	.41	-4.32	.341
31	.51	-7.3	.547
32	.55	.97	1.51
33	.43	2.73	1.184
34	.43	4.76	.487
35	.4	6.19	.458
36	.39	7.13	.457
37	.44	8.93	.373
38	.4	8.31	.413
39	.48	8.31	.329
40	.46	6.93	.317
41	.54	7.03	.224
42	.54	6.16	.208
43	.52	5.55	.162
44	.53	1.6	.153
45	.52	-1.42	.133
46	.52	-5.19	.158
47	.52	-9.38	.195
48	.52	-7.72	.199
49	.53	-4.6	.236
50	.49	1.08	.335

```
 51              .58             -9.15            .542
 52              .68              1.11           1.528
 53              .54              3.55           1.166
 54              .59              6.01            .372
 55              .62              9.54            .335
 56              .59             10.49            .364
 57              .68              9.32            .281
 58              .63             11.27            .316
 59              .66             10.06            .265
 60              .61              9.36            .241

AVG R/A = .423283               AVG ANG = .964288
RMS R/A = .445197               RMS ANG = 5.81728
MAX R/A = .687 MAX ANG = 11.27
STD DEV = .137956               STD DEV = 5.73681

ENERGY WTD AVG ANGLE = 1.46188 DEGREES
ENERGY WTD RMS ANGLE = 5.06738 DEGREES
FRACTION OF RINGS WITH ANGLE GREATER THAN 15 DEG = 0
AUXILIARY REFOCUSING COIL NOT NEEDED

LOWEST ENERGY CLASS
     AVG R/A = .443143
     RMS R/A = .460298
     AVG ANG =-1.3322   DEGREES
     RMS ANG = 6.06261  DEGREES
     NUMBER OF ELECTRONS = 28

SECOND ENERGY CLASS
     AVG R/A = .413471
     RMS R/A = .437611
     AVG ANG = 4.80397  DEGREES
     RMS ANG = 6.61455  DEGREES
     NUMBER OF ELECTRONS = 17

THIRD ENERGY CLASS
     AVG R/A = .3733
     RMS R/A = .267
     AVG ANG = .641539  DEGREES
     RMS ANG = 4.94523  DEGREES
     NUMBER OF ELECTRONS = 10

HIGHEST ENERGY CLASS
     AVG R/A = .4454
     RMS R/A = .472683
     AVG ANG = 1.4152   DEGREES
     RMS ANG = 1.60986  DEGREES
     NUMBER OF ELECTRONS = 5


TAPE NO. 48
```

```
STATISTICAL ANALYSIS OF POST OUTPUT GAP ELECTRONS

DATA TAPE NO. 48
NASA KLYSTRON DESIGN F

OUTPUT GAP EXIT LOCATION Z/A = 9.38


MIN ZDOT/U = .365
AVG ZDOT/U = .615683
MAX ZDOT/U = 1.236
STD DEV = .20808




LIST 500

 STDB       10:31    TUES.  6-12-72

500 DATA 48,9.38,60,1,1,1
501 DATA .233,.012,.609,.236,.006,.596,.239,-.005,.553
502 DATA .242,-.023,.511,.267,-.043,.49,.303,-.052,.499
503 DATA .263,-.04,.498,.275,-.037,.514,.292,-.043,.519
504 DATA .289,-.034,.598,.324,-.031,.76,.311,.011,1.224
505 DATA .248,.033,1.092,.238,.034,.784,.224,.036,.757
506 DATA .218,.035,.76,.233,.034,.657,.227,.035,.706
507 DATA .238,.039,.632,.24,.032,.614,.429,.047,.524
508 DATA .397,.024,.499,.39,-.005,.487,.402,-.019,.46
509 DATA .414,-.028,.425,.425,-.064,.43,.442,-.065,.458
510 DATA .438,-.062,.462,.437,-.064,.48,.411,-.044,.583
511 DATA .52,-.094,.734,.553,.021,1.229,.432,.052,1.087
512 DATA .437,.058,.696,.405,.073,.673,.4,.084,.671
513 DATA .442,.095,.604,.408,.093,.636,.482,.083,.568
514 DATA .467,.068,.559,.547,.058,.47,.541,.049,.454
515 DATA .529,.039,.401,.532,.011,.392,.528,-.009,.365
516 DATA .523,-.036,.397,.524,-.072,.436,.529,-.06,.443
517 DATA .533,-.039,.485,.497,.011,.579,.59,-.117,.727
518 DATA .683,.024,1.236,.55,.067,1.078,.597,.064,.607
519 DATA .621,.096,.571,.599,.11,.594,.687,.086,.524
520 DATA .636,.11,.552,.666,.09,.507,.614,.08,.485
999 END
```

STATISTICAL ANALYSIS OF POST OUTPUT CAP ELECTRONS

DATA TAPE NO. 49
NASA LOW EFFICIENCY KLYSTRON

OUTPUT GAP EXIT LOCATION Z/A =-5

RING	R/A	ANGLE (DEG)	POTENTIAL
1	.24	-2.26	.49
2	.25	-2.04	.476
3	.25	-1.85	.473
4	.27	V1.77	.483
5	.27	-1.49	.503
6	.28	-1.09	.536
7	.28	-.75	.589
8	.28	-.21	.703
9	.27	.23	.868
10	.26	.7	1.119
11	.25	.84	1.428
12	.23	.9	1.582
13	.23	.65	1.454
14	.23	-.24	1.21
15	.23	-.27	.982
16	.23	-.64	82
17	.23	-1.1	.707
18	.23	-1.51	.618
19	.23	-1.66	.551
20	.24	-2.21	.516
21	.42	-4.12	.482
22	.43	-3.86	.467
23	.44	-30.84	.627
24	.47	-3.34	.473
25	.47	-2.87	.491
26	.48	-2.25	.523
27	.49	-1.38	.588
28	.49	-.32	.697
29	.48	4.72	.867
30	.46	1.12	1.119
31	.43	1.51	1.433
32	.41	1.46	1.583
33	.4	1.01	1.454
34	.39	-.41	1.21
35	.39	-.45	.98
36	.4	-1.22	.819
37	.4	-2.09	.706
38	.4	-2.69	.616
39	.4	-3.16	.547
40	.41	-3.89	.509
41	.54	-5.43	.476
42	.55	-5	.459
43	.56	-4.84	.452
44	.6	-4.59	.462
45	.6	-4.06	.466
46	.62	-3.26	.512
47	.64	-2.02	.578
48	.64	-.7	.688
49	.63	1.08	.857
50	.6	1.41	1.122

51	.55	1.82	1.439
52	.53	1.91	1.586
53	.51	1.45	1.482
54	.51	-.53	1.205
55	.51	-.62	.978
56	.51	-1.56	.819
57	.52	-2.75	.702
58	.52	-3.6	.612
59	.52	-4.25	.543
60	.53	-5.34	.504

AVG R/A = .419833 AVG ANG =-1.82385
RMS R/A = .440319 RMS ANG = 4.69622
MAX R/A = .646 MAX ANG = 30.8397
STD DEV = .132744 STD DEV = 4.32759

ENERGY WTD AVG ANGLE =-.983192 DEGREES
ENERGY WTD RMS ANGLE = 4.10921 DEGREES
FRACTION OF RINGS WITH ANGLE GREATER THAN 15 DEG = .017
AUXILIARY REFOCUSING COIL NOT NEEDED

LOWEST ENERGY CLASS
AVG R/A = .434167
RMS R/A = .455652
AVG ANG =-3.18863 DEGREES
RMS ANG = 3.44143 DEGREES
NUMBER OF ELECTRONS = 24

SECOND ENERGY CLASS
AVG R/A = .428353
RMS R/A = .44741
AVG ANG =-2.67559 DEGREES
RMS ANG = 7.73646 DEGREES
NUMBER OF ELECTRONS = 17

THIRD ENERGY CLASS
AVG R/A = .3914
RMS R/A = .42
AVG ANG = .097637 DEGREES
RMS ANG = .703121 DEGREES
NUMBER OF ELECTRONS = 10

HIGHEST ENERGY CLASS
AVG R/A = .397111
RMS R/A = .415386
AVG ANG = 1.28941 DEGREES
RMS ANG = 1.35737 DEGREES
NUMBER OF ELECTRONS = 9

TAPE NO. 49

```
STATISTICAL ANALYSIS OF POST OUTPUT GAP ELECTRONS

DATA TAPE NO. 49
NASA LOW EFFICIENCY KLYSTRON

OUTPUT GAP EXIT LOCATION Z/A =-5


MIN ZDOT/U = .67
AVG ZDOT/U = .8739
MAX ZDOT/U = 1.259
STD DEV = .190841



EDIT DELETE 100-130,140-254
READY.

999
LIST

135 PRINT "NASA LOW EFFICIENCY KLYSTRON"
500 DATA 49,-5,60,1,1,1
501 DATA .248,-.0276,.7,.252,-.0245,.69,.26,-.0222,.688
502 DATA .275,-.0214,.695,.275,-.0184,.709,.284,-.0138,.732
503 DATA .286,-.01,.768,.287,-.00305,.839,.279,.0038,.932
504 DATA .269,.013,1.058,.25,.0176,1.195,.24,.0199,1.258
505 DATA .232,.0138,1.206,.231,-.0046,1.1,.231,-.0046,.991
506 DATA .234,-.01,.906,.237,-.0161,.841,.237,-.0207,.786
507 DATA .238,-.0215,.742,.243,-.0276,.718,.427,-.0498,.693
508 DATA .433,-.046,.682,.443,-.406,.68,.475,-.04,.687
509 DATA .475,-.035,.7,.489,-.0284,.723,.497,-.0184,.767
510 DATA .499,-.0046,.835,.49,.0767,.928,.468,.0207,1.058
511 DATA .432,.0316,1.197,.412,.0322,1.258,.401,.0214,1.206
512 DATA .398,-.0077,1.1,.4,-.0077,.99,.405,-.0192,.905
513 DATA .406,-.0306,.84,.41,-.0368,.784,.41,-.0407,.739
514 DATA .42,-.0483,.712,.547,-.0652,.687,.551,-.059,.675
515 DATA .566,-.0567,.67,.609,-.0544,.678,.609,-.0483,.681
516 DATA .63,-.0407,.715,.642,-.0268,.76,.646,-.01,.83
517 DATA .636,.0176,.926,.606,.0261,1.059,.56,.0383,1.199
518 DATA .531,.0422,1.259,.516,.0306,1.205,.515,-.01,1.098
519 DATA .517,-.0107,.989,.52,-.0245,.905,.524,-.0402,.837
520 DATA .525,-.0491,.781,.526,-.0545,.735,.536,-.066,.707
```

STATISTICAL ANALYSIS OF REFOCUSED TRAJECTORIES

ANALOG COMPUTER TAPE NO. 7
NASA KLYSTRON DESIGN A, FIELD G, PLOT 4-18-72-1

COLLECTOR ENTRANCE LOCATION Z/A = 43.71

RING	R/A	ANGLE (DEG)	POTENTIAL
1	2.13	1.44	.226
2	1.85	1.02	.215
3	1.66	1.21	.183
4	1.36	.79	.161
5	1.14	-2.81	.156
6	1.02	.17	.146
7	2.67	-7.07	.218
8	1.87	-5.72	.198
9	1.45	-3.19	.172
10	2.62	-4.69	.213
11	2.76	4.36	.243
12	2.06	3.89	.485
13	1.85	6.41	1.55
14	2.83	7.07	.63
15	3.33	6.64	.44
16	3.31	5.66	.392
17	3.35	7.05	.452
18	3.02	3.41	.316
19	2.61	1.96	.267
20	2.13	2.65	.219
21	4.39	1.21	.183
22	3.3	-7.57	.169
23	2.2	-12.37	.158
24	1.07	-7.28	.13
25	1.22	2.6	.069
26	1.09	-8.2	.105
27	.99	-10.76	.103
28	1.05	-14.7	.118
29	1.88	-9.11	.114
30	2.07	3	.151
31	2.47	-1.77	.205
32	2.8	5.92	.466
33	3	10.52	1.588
34	4.55	11.11	.628
35	4.92	6.76	.37
36	5.17	6.65	.359
37	5.48	8.48	.397
38	4.09	5.09	.269
39	3.85	7.27	.235
40	4.61	8.21	.202
41	3.68	-7.46	.253
42	2.89	-2.93	.102
43	4.2	46.21	.113
44	2.08	11.82	.089
45	2.41	18.4	.079
46	2	14.73	.059
47	1.59	6.28	.092
48	1.66	9.25	.089
49	1.85	8.18	.074
50	2.27	-3.24	.124

```
 51              3.68            .75             .247
 52              3.79            9.45            .467
 53              3.66            12.49           1.611
 54              5.87            13.8            .629
 55              4.25            8.89            .235
 56              4.23            6.57            .268
 57              4.74            5.45            .314
 58              5.09            4.54            .191
 59              5.17            2.19            .189
 60              5.55           -9.19            .272

AVG R/A = 2.94006               AVG ANG = 3.1968
RMS R/A = 3.23048               RMS ANG = 9.61096
MAX R/A = 5.87487               MAX ANG = 46.2189
STD DEV = 1.33866               STD DEV = 9.06372

ENERGY WTD AVG ANGLE = 5.48196 DEGREES
ENERGY WTD RMS ANGLE = 8.91434 DEGREES
FRACTION OF RINGS WITH ANGLE GREATER THAN 15 DEG = .033
AUXILIARY REFOCUSING COIL NOT NEEDED
```

```
LIST--500
```

```
500 DATA 7,5415,60,123.875,495.5,5931
501 DATA 1060,71,2823,920,49,2751,824,54,2543,675,33,2383
502 DATA 568,-115,2347,508,7,2267,1323,-341,2752,929,-263,2629
503 DATA 719,-137,2459,1301,-224,2731,1370,223,2921,1025,281,4122
504 DATA 919,825,7338,1405,580,4675,1653,456,3912,1643,367,3697
505 DATA 1660,490,3958,1501,199,3332,1297,105,3065,1059,129,2777
506 DATA 2180,54,2537,1638,-322,2424,1095,-505,2304,535,-271,2124
507 DATA 609,71,1558,542,-275,1909,494,-357,1879,522,-519,1979
508 DATA 933,-318,1984,1029,121,2305,1225,-83,2688,1391,418,4028
509 DATA 1490,1365,7349,2258,907,4615,2440,425,3583,2566,412,3531
510 DATA 2717,552,3698,2028,273,3064,1909,365,2858,2289,381,2639
511 DATA 1824,-387,2959,1436,-97,1900,2082,1440,1380,1035,363,1734
512 DATA 1198,528,1587,992,369,1403,791,197,1789,826,286,1756
513 DATA 919,230,1599,1129,-118,2086,1925,39,2950,1880,666,4001
514 DATA 1815,1629,7351,2911,1123,4569,2107,445,2842,2100,352,3055
515 DATA 2350,316,3311,2525,206,2590,2563,99,2580,2751,-494,3055
999 END
```

STATISTICAL ANALYSIS OF REFOCUSED TRAJECTORIES

ANALOG COMPUTER TAPE NO. 7
NASA KLYSTRON DESIGN A, FIELD G, PLOT 4-18-72-1

COLLECTOR ENTRANCE LOCATION Z/A = 43.71

AVG R/A = 2.94006	AVG ANG = 3.1968
RMS R/A = 3.23048	RMS ANG = 9.61096
MAX R/A = 5.87487	MAX ANG = 46.2189
STD DEV = 1.33866	STD DEV = 9.06372

ENERGY WTD AVG ANGLE = 5.48196 DEGREES
ENERGY WTD RMS ANGLE = 8.91434 DEGREES
FRACTION OF RINGS WITH ANGLE GREATER THAN 15 DEG = .033
AUXILIARY REFOCUSING COIL NOT NEEDED

LOWEST ENERGY CLASS
AVG R/A = 2.29276
RMS R/A = 2.58291
AVG ANG = 1.20489 DEGREES
RMS ANG = 11.2177 DEGREES
NUMBER OF ELECTRONS = 32

SECOND ENERGY CLASS
AVG R/A = 3.77523
RMS R/A = 3.90895
AVG ANG = 3.1468 DEGREES
RMS ANG = 5.7955 DEGREES
NUMBER OF ELECTRONS = 16

THIRD ENERGY CLASS
AVG R/A = 3.78966
RMS R/A = 4.74269
AVG ANG = 8.16342 DEGREES
RMS ANG = 8.62838 DEGREES
NUMBER OF ELECTRONS = 9

HIGHEST ENERGY CLASS
AVG R/A = 2.84157
RMS R/A = 2.93823
AVG ANG = 9.81063 DEGREES
RMS ANG = 10.1323 DEGREES
NUMBER OF ELECTRONS = 3

TAPE NO. 7

STATISTICAL ANALYSIS OF REFOCUSED TRAJECTORIES

ANALOG COMPUTER TAPE NO. 14
NASA KLYSTRON DESIGN B, FIELD N, PLOT 5-1-72-1

COLLECTOR ENTRANCE LOCATION Z/A = 40.76

RING	R/A	ANGLE (DEG)	POTENTIAL
1	2.47	2.53	.25
2	2.25	1.79	.228
3	2.05	1.56	.202
4	2.26	3.38	.181
5	2.6	3.53	.182
6	3.09	5.36	.186
7	2.59	1.69	.182
8	2.57	2.23	.187
9	2.49	5.71	.2
10	2.22	4.01	.252
11	3.02	6.21	.446
12	1.89	6.67	1.285
13	1.59	5.67	1.382
14	2.81	7.98	.446
15	2.43	7.31	.52
16	2.94	7.32	.36
17	2.53	7.39	.447
18	2.71	7.37	.389
19	2.77	5.14	.291
20	2.76	3.32	.265
21	3.27	1.18	.216
22	2.85	.06	.191
23	2.67	-1.3	.181
24	2.67	-2.05	.173
25	2.65	-3.01	.166
26	2.9	-5.04	.183
27	2.64	-4.54	.178
28	3.23	-3.93	.183
29	3.57	-2.72	.191
30	3.69	6.97	.232
31	4.47	8.42	.453
32	3.19	11.44	1.33
33	2.76	9.89	1.399
34	4.89	9.49	.331
35	4.62	12.76	.419
36	5.38	10.54	.324
37	5.18	12.64	.367
38	5.34	9.71	.315
39	4.93	3.99	.275
40	4.09	2.14	.25
41	3.59	3.24	.188
42	3.12	2.82	.16
43	3.05	2.03	.155
44	3.06	.83	.162
45	2.57	1.09	.144
46	2.73	-2.56	.163
47	2.62	-1.49	.156
48	3.21	-3.85	.18
49	3.62	-2.65	.199
50	4.71	3.76	.259

```
 51              4.63            9.22            .442
 52              3.67            12.73           1.332
 53              3.62            12.77           1.41
 54              5.07            4.14            .275
 55              5.96            6.67            .312
 56              4.34            1.73            .256
 57              5.66            3.81            .302
 58              5.02            2.25            .282
 59              3.91            2.5             .239
 60              3.73            3.94            .211

AVG R/A = 3.38667               AVG ANG = 3.93458
RMS R/A = 3.54213               RMS ANG = 6.07286
MAX R/A = 5.9615                MAX ANG = 12.7776
STD DEV = 1.03786               STD DEV = 4.62587

ENERGY WTD AVG ANGLE = 6.47372 DEGREES
ENERGY WTD RMS ANGLE = 7.96521 DEGREES
FRACTION OF RINGS WITH ANGLE GREATER THAN 15 DEG = 0
AUXILIARY REFOCUSING COIL NOT NEEDED
```

```
LIST  500

 STDA

500 DATA 14,5824,60,142.875,571.5,5931
501 DATA 1417,131,2963,1286,89,2833,1172,73,2667,1295,149,2521
502 DATA 1490,156,2527,1766,239,2547,1482,75,2530,1474,100,2564
503 DATA 1427,264,2640,1274,209,2975,1728,429,3940,1081,781,6678
504 DATA 913,689,6939,1606,550,3923,1390,545,4245,1681,454,3532
505 DATA 1446,511,3936,1551,475,3672,1587,287,3189,1579,177,3051
506 DATA 1869,57,2759,1632,3,2593,1526,-57,2527,1531,-88,2469
507 DATA 1519,-127,2420,1662,-223,2529,1511,-198,2499,1848,-174,2537
508 DATA 2042,-123,2590,2109,347,2838,2558,585,3950,1825,1358,6705
509 DATA 1580,1206,6912,2799,563,3366,2646,849,3747,3080,619,3324
510 DATA 2962,787,3507,3054,562,3284,2818,217,3106,2343,111,2964
511 DATA 2057,146,2572,1786,117,2371,1745,83,2336,1751,35,2390
512 DATA 1471,43,2256,1562,-107,2399,1499,-61,2347,1837,-169,2512
513 DATA 2071,-122,2645,2696,198,3012,2648,632,3893,2099,1509,6679
514 DATA 2073,1558,6870,2902,225,3104,3407,385,3291,2482,91,3005
515 DATA 3237,217,3253,2873,124,3151,2238,127,2900,2136,188,2723
999 END
```

STATISTICAL ANALYSIS OF REFOCUSED TRAJECTORIES

ANALOG COMPUTER TAPE NO. 14
NASA KLYSTRON DESIGN B, FIELD N, PLOT 5-1-72-1

COLLECTOR ENTRANCE LOCATION Z/A = 40.76

AVG R/A = 3.38667	AVG ANG = 3.93458
RMS R/A = 3.14213	RMS ANG = 6.07286
MAX R/A = 5.9615	MAX ANG = 12.7776
STD DEV = 1.03786	STD DEV = 4.62587

ENERGY WTD AVG ANGLE = 6.47372 DEGREES
ENERGY WTD RMS ANGLE = 7.96521 DEGREES
FRACTION OF RINGS WITH ANGLE GREATER THAN 15 DEG = 0
AUXILIARY REFOCUSING COIL NOT NEEDED

LOWEST ENERGY CLASS
AVG R/A = 2.9441
RMS R/A = 2.98297
AVG ANG = .583483 DEGREES
RMS ANG = 3.26626 DEGREES
NUMBER OF ELECTRONS = 29

SECOND ENERGY CLASS
AVG R/A = 4.25216
RMS R/A = 4.42118
AVG ANG = 5.59094 DEGREES
RMS ANG = 6.42394 DEGREES
NUMBER OF ELECTRONS = 18

THIRD ENERGY CLASS
AVG R/A = 3.29114
RMS R/A = 3.27034
AVG ANG = 8.60446 DEGREES
RMS ANG = 8.85138 DEGREES
NUMBER OF ELECTRONS = 9

HIGHEST ENERGY CLASS
AVG R/A = 2.91557
RMS R/A = 3.03489
AVG ANG = 10.2692 DEGREES
RMS ANG = 10.6708 DEGREES
NUMBER OF ELECTRONS = 4

TAPE NO. 14

TIME: 00 MINS. 11 SECS.

STATISTICAL ANALYSIS OF REFOCUSED TRAJECTORIES

ANALOG COMPUTER TAPE NO. 15
NASA KLYSTRON DESIGN C, FIELD P,OPLOT 5-3-72-1

COLLECTOR ENTRANCE LOCATION Z/A = 36.78

RING	R/A	ANGLE (DEG)	POTENTIAL
1	2.5	1.94	.219
2	2.41	1.66	.2
3	2.64	2.17	.177
4	3.17	3.58	.183
5	3.4	6.78	.186
6	3.22	1.87	.17
7	3.01	3.26	.179
8	2.82	4.44	.193
9	2.25	4.56	.214
10	2.29	5.07	.329
11	2.57	8.99	.802
12	1.23	4.18	1.701
13	2.67	6.41	.36
14	2.42	5.82	.352
15	2.53	3.09	.252
16	2.41	5.4	.323
17	2.08	5.67	.366
18	1.61	4.98	.446
19	2.29	5.14	.314
20	2.51	2.39	.233
21	3.02	-1.64	.181
22	2.33	-1.95	.153
23	2.24	-2.46	.148
24	2.39	-3.55	.156
25	2.56	5.89	.143
26	3.27	-3.27	.181
27	4.22	-3.73	.19
28	3.18	-4.21	.182
29	3.91	-.33	.203
30	3.44	9.43	.306
31	4.61	15.56	.839
32	2.07	7.09	1.729
33	4.73	9.82	.345
34	4.31	7.33	.294
35	4.05	.24	.224
36	4.71	5.18	.279
37	4.51	6.46	.292
38	3.33	9.3	.388
39	4.59	4.14	.267
40	3.87	.16	.21
41	3.49	-6.39	.119
42	2.51	-16.74	.119
43	1.91	-14.62	.122
44	1.98	-17.28	.11
45	1.88	-19.58	.109
46	3.34	-6.56	.11
47	3.42	3.08	.125
48	2.87	1.19	.143
49	4.74	.12	.225
50	4.35	11.74	.311

```
 51              5.28            15.68           .832
 52              2.64            9.02            1.75
 53              6.36            11.08           .328
 54              5.21            2.34            .235
 55              4.57            7.22            .153
 56              5.15            2.57            .237
 57              5.92            4.48            .27
 58              5.45            10.31           .327
 59              5.14            1.9             .237
 60              4.26            5.43            .146

AVG R/A = 3.36913               AVG ANG = 2.53641
RMS R/A = 3.56723               RMS ANG = 7.46299
MAX R/A = 6.36715               MAX ANG = 19.5774
STD DEV = 1.17222               STD DEV = 7.01875

ENERGY WTD AVG ANGLE = 5.5073  DEGREES
ENERGY WTD RMS ANGLE = 7.9887  DEGREES
FRACTION OF RINGS WITH ANGLE GREATER THAN 15 DEG = .083
AUXILIARY REFOCUSING COIL NOT NEEDED
```

```
LIST  500

500 DATA 15,5955,60,161.925,647.7,5931
501 DATA 1623,94,2775,1561,77,2652,1714,95,2497,2056,159,2535
502 DATA 2208,303,2545,2089,80,2449,1951,143,2508,1832,202,2598
503 DATA 1461,219,2741,1489,301,3390,1666,831,5249,801,564,7716
504 DATA 1731,398,3538,1570,357,3501,1644,161,2973,1563,318,3358
505 DATA 1349,355,3572,1047,344,3946,1488,298,3311,1627,120,2866
506 DATA 1958,-72,2527,1513,-79,2322,1457,-98,2287,1549,-145,2342
507 DATA 1661,231,2236,2121,-144,2523,2735,-168,2580,2063,-186,2528
508 DATA 2537,-15,2676,2231,538,3239,2989,1458,5234,1344,963,7740
509 DATA 3064,595,3434,2792,411,3191,2627,12,2809,3055,283,3121
510 DATA 2927,361,3188,2161,598,3650
511 DATA 2978,222,3060,2508,8,2720,2265,-228,2039,1627,-591,1966
512 DATA 1239,-523,2005,1288,-585,1881,1223,-659,1853,2166,-225,1959
513 DATA 2221,113,2098,1865,47,2248,3075,6,2816,2819,674,3241
514 DATA 3421,1463,5209,1711,1231,7749,4124,654,3337,3380,118,2878
515 DATA 2963,292,2302,3339,130,2889,3839,241,3073,3530,608,3339
516 DATA 3334,96,2889,2762,215,2261
999 END
```

STATISTICAL ANALYSIS OF REFOCUSED TRAJECTORIES

ANALOG COMPUTER TAPE NO. 15
NASA KLYSTRON DESIGN C, FIELD P, PLOT 5-3-72-1

COLLECTOR ENTRANCE LOCATION Z/A = 36.78

AVG R/A = 3.36913	AVG ANG = 2.53641
RMS R/A = 3.56723	RMS ANG = 7.46299
MAX R/A = 6.36715	MAX ANG = 19.5774
STD DEV = 1.17222	STD DEV = 7.01875

ENERGY WTD AVG ANGLE = 5.5073 DEGREES
ENERGY WTD RMS ANGLE = 7.9887 DEGREES
FRACTION OF RINGS WITH ANGLE GREATER THAN 15 DEG = .083
AUXILIARY REFOCUSING COIL NOT NEEDED

LOWEST ENERGY CLASS
AVG R/A = 3.02831
RMS R/A = 3.11368
AVG ANG =-1.62243 DEGREES
RMS ANG = 7.25502 DEGREES
NUMBER OF ELECTRONS = 30

SECOND ENERGY CLASS
AVG R/A = 4.33616
RMS R/A = 4.50666
AVG ANG = 5.48244 DEGREES
RMS ANG = 6.43082 DEGREES
NUMBER OF ELECTRONS = 17

THIRD ENERGY CLASS
AVG R/A = 3.16304
RMS R/A = 2.2495
AVG ANG = 8.7357 DEGREES
RMS ANG = 9.54157 DEGREES
NUMBER OF ELECTRONS = 10

HIGHEST ENERGY CLASS
AVG R/A = 1.98446
RMS R/A = 2.06668
AVG ANG = 6.76645 DEGREES
RMS ANG = 7.05349 DEGREES
NUMBER OF ELECTRONS = 3

TAPE NO. 15

STATISTICAL ANALYSIS OF REFOCUSED TRAJECTORIES

ANALOG COMPUTER TAPE NO. 17
NASA KLYSTRON DESIGN E, FIELD R, PLOT 5-4-72-2

COLLECTOR ENTRANCE LOCATION Z/A = 33.94

RING	R/A	ANGLE (DEG)	POTENTIAL
1	1.83	1.45	.318
2	1.71	.91	.289
3	1.83	.52	.267
4	1.79	-1.31	.246
5	1.43	-3.66	.221
6	1.56	-3.78	.227
7	2.1	-1.83	.263
8	1.87	-2.34	.253
9	2.49	.83	.283
10	2.4	.75	.274
11	1.87	5.88	.42
12	2.43	7.74	1.116
13	1.9	6.85	1.291
14	2.44	6.75	.609
15	2.57	6.61	.533
16	2.55	7.22	.581
17	2.4	4.08	.4
18	2.57	5.79	.475
19	2.18	2.62	.36
20	1.96	2.11	.337
21	2.67	3.7	.255
22	2.53	2.56	.239
23	2.29	-.09	.217
24	2.04	-.81	.195
25	1.87	-.15	.161
26	1.9	.29	.177
27	2.29	-2.17	.228
28	2.6	-3.15	.244
29	2.82	-2.88	.257
30	3.29	0	.287
31	3.81	8.86	.401
32	4.09	12.99	1.161
33	3.25	11.34	1.316
34	4.09	8.78	.494
35	4.3	7.97	.451
36	4.54	9.41	.492
37	3.64	4.59	.369
38	4.23	6.21	.421
39	3.03	5.53	.311
40	2.88	5.53	.274
41	3.1	-4.66	.211
42	2.54	-8.17	.195
43	2.25	-9.28	.188
44	1.61	-7.67	.158
45	1.25	-2.09	.134
46	2.15	-3.47	.154
47	2.67	1.67	.187
48	2.77	.45	.214
49	2.94	-.78	.234
50	3.2	-.14	.268

51	4.63	5.82	.404
52	4.63	14.05	1.18
53	4.1	14.08	1.335
54	4.2	6.8	.374
55	3.68	7.27	.304
56	3.96	5.8	.365
57	4	8.6	.252
58	3.58	7.62	.3
59	4.05	4.62	.237
60	3.92	2.65	.23

AVG R/A = 2.82596 AVG ANG = 2.8199
RMS R/A = 2.97093 RMS ANG = 5.96452
MAX R/A = 4.63708 MAX ANG = 14.0869
STD DEV = .916714 STD DEV = 5.25583

ENERGY WTD AVG ANGLE = 5.65843 DEGREES
ENERGY WTD RMS ANGLE = 7.8758 DEGREES
FRACTION OF RINGS WITH ANGLE GREATER THAN 15 DEG = 0
AUXILIARY REFOCUSING COIL NOT NEEDED

LOWEST ENERGY CLASS
AVG R/A = 2.40648
RMS R/A = 2.51441
AVG ANG =-1.22517 DEGREES
RMS ANG = 4.0262 DEGREES
NUMBER OF ELECTRONS = 27

SECOND ENERGY CLASS
AVG R/A = 3.05225
RMS R/A = 3.16604
AVG ANG = 3.91735 DEGREES
RMS ANG = 4.82 DEGREES
NUMBER OF ELECTRONS = 18

THIRD ENERGY CLASS
AVG R/A = 3.16478
RMS R/A = 2.94774
AVG ANG = 7.24215 DEGREES
RMS ANG = 7.33485 DEGREES
NUMBER OF ELECTRONS = 10

HIGHEST ENERGY CLASS
AVG R/A = 3.59885
RMS R/A = 3.72385
AVG ANG = 11.868 DEGREES
RMS ANG = 12.171 DEGREES
NUMBER OF ELECTRONS = 5

TAPE NO. 17

STATISTICAL ANALYSIS OF REFOCUSED TRAJECTORIES

ANALOG COMPUTER TAPE NO. 16
NASA KLYSTRON DESIGN D, FIELD Q, PLOT 5-4-72-1

COLLECTOR ENTRANCE LOCATION Z/A = 29.29

RING	R/A	ANGLE (DEG)	POTENTIAL
1	2.1	1.54	.243
2	2	.32	.221
3	1.98	.34	.201
4	1.85	-2.78	.18
5	1.84	-5.06	.171
6	1.63	-6.91	.166
7	2.95	7.62	.207
8	2.58	12.39	.246
9	3.1	10.22	.217
10	2.99	10.75	.224
11	2.25	8.62	.314
12	2.53	8.72	.517
13	1.37	7.49	1.481
14	1.84	8.74	.857
15	2.27	9.8	.526
16	2.39	9.93	.455
17	2.59	9.63	.395
18	2.81	7.9	.335
19	2.73	5.51	.297
20	2.42	3.05	.266
21	2.49	4.06	.183
22	1.77	-12.29	.149
23	1.37	-14.59	.147
24	1.94	41.37	.114
25	1.27	-13.05	.155
26	1.23	-14.27	.133
27	3.37	-2.71	.232
28	4.52	6.99	.266
29	4.46	2.35	.277
30	4.5	3.41	.274
31	3.87	11.05	.281
32	3.58	11.5	.524
33	2.38	12.68	1.537
34	3.15	14.37	.864
35	4.16	15.74	.499
36	4.46	14.86	.434
37	4.64	13.24	.403
38	4.53	8.32	.363
39	3.78	5.44	.309
40	2.92	4.22	.241
41	2.16	1.45	.123
42	1.54	-12.65	.153
43	2.77	42.27	.069
44	1.45	-9.88	.153
45	3.43	48.9	.088
46	1.91	27.77	.066
47	2.53	-4.61	.141
48	4.65	2.48	.308
49	4.1	.88	.285
50	4.64	2.44	.315

```
 51              4.81            7.52            .325
 52              3.81            13.42           .494
 53              3               14.25           1.571
 54              4.19            17.91           .859
 55              5.16            14.69           .463
 56              5.38            11.93           .427
 57              5.17            10.31           .399
 58              4               6.5             .296
 59              3.89            10.15           .197
 60              4.26           -5.65            .227

AVG R/A = 3.06173               AVG ANG = 7.01457
RMS R/A = 3.27252               RMS ANG = 13.9986
MAX R/A = 5.38222               MAX ANG = 48.9026
STD DEV = 1.15549               STD DEV = 12.1143

ENERGY WTD AVG ANGLE = 8.72926 DEGREES
ENERGY WTD RMS ANGLE = 11.8117 DEGREES
FRACTION OF RINGS WITH ANGLE GREATER THAN 15 DEG = .1
AUXILIARY REFOCUSING COIL NOT NEEDED



LIST 500

500 DATA 16,4464,60,152.4,609.6,5931
501 DATA 1285,79,2924,1220,16,2792,1208,16,2665,1129,-122,2516
502 DATA 1127,-216,2444,994,-291,2402,1802,359,2681,1576,632,2875
503 DATA 1893,491,2723,1827,524,2759,1372,499,3291,1544,647,4218
504 DATA 840,942,7158,1122,835,5429,1385,733,4241,1461,691,3945
505 DATA 1580,624,3677,1713,473,3405,1669,311,3219,1479,163,3057
506 DATA 1518,180,2532,1079,-488,2241,838,-574,2206,1184,1325,1504
507 DATA 780,-527,2275,753,-535,2104,2055,-135,2857,2756,373,3040
508 DATA 2719,128,3119,2747,185,3103,2364,603,3086,2188,857,4209
509 DATA 1452,1615,7175,1921,1369,5343,2539,1138,4036,2721,1003,3779
510 DATA 2829,863,3666,2765,518,3539,2310,313,3283,1782,215,2909
511 DATA 1319,53,2087,942,-509,2268,1690,1050,1155,888,-399,2291
512 DATA 2092,1331,1161,1165,713,1354,1546,-179,2224,2839,143,3293
513 DATA 2504,49,3169,2829,142,3326,2938,443,3355,2328,968,4056
514 DATA 1830,1831,7207,2556,1691,5232,3151,1024,3906,3281,802,3795
515 DATA 3153,671,3686,2439,366,3208,2372,465,2597,2598,-278,2813
999 END
```

STATISTICAL ANALYSIS OF REFOCUSED TRAJECTORIES

ANALOG COMPUTER TAPE NO. 16
NASA KLYSTRON DESIGN D, FIELD Q, PLOT 5-4-72-1

COLLECTOR ENTRANCE LOCATION Z/A = 29.29

AVG R/A = 3.06173	AVG ANG = 7.01457
RMS R/A = 3.27252	RMS ANG = 13.9986
MAX R/A = 5.38222	MAX ANG = 48.9026
STD DEV = 1.15549	STD DEV = 12.1143

ENERGY WTD AVG ANGLE = 8.72926 DEGREES
ENERGY WTD RMS ANGLE = 11.8117 DEGREES
FRACTION OF RINGS WITH ANGLE GREATER THAN 15 DEG = .1
AUXILIARY REFOCUSING COIL NOT NEEDED

LOWEST ENERGY CLASS
- AVG R/A = 2.49584
- RMS R/A = 2.66253
- AVG ANG = 4.41707 DEGREES
- RMS ANG = 16.7752 DEGREES
- NUMBER OF ELECTRONS = 30

SECOND ENERGY CLASS
- AVG R/A = 4.02969
- RMS R/A = 4.13545
- AVG ANG = 7.13776 DEGREES
- RMS ANG = 7.99633 DEGREES
- NUMBER OF ELECTRONS = 16

THIRD ENERGY CLASS
- AVG R/A = 3.36086
- RMS R/A = 3.37107
- AVG ANG = 11.9376 DEGREES
- RMS ANG = 12.2234 DEGREES
- NUMBER OF ELECTRONS = 9

HIGHEST ENERGY CLASS
- AVG R/A = 2.82119
- RMS R/A = 2.96967
- AVG ANG = 13.3439 DEGREES
- RMS ANG = 13.7671 DEGREES
- NUMBER OF ELECTRONS = 5

TAPE NO. 16

STATISTICAL ANALYSIS OF REFOCUSED TRAJECTORIES

ANALOG COMPUTER TAPE NO. 18
NASA KLYSTRON DESIGN F, FIELD S, PLOT 5-5-72-1

COLLECTOR ENTRANCE LOCATION Z/A = 34.59

RING	R/A	ANGLE (DEG)	POTENTIAL
1	1.88	.82	.342
2	1.87	.52	.328
3	1.71	-.71	.283
4	1.51	-3.07	.248
5	1.46	-3.82	.236
6	1.83	-4.14	.255
7	1.47	-3.18	.243
8	1.76	-3.13	.259
9	2.03	-3.28	.269
10	2.5	3.7	.335
11	2.03	5.7	.534
12	2.27	7.55	1.402
13	1.99	6.5	1.098
14	2.46	4.9	.571
15	2.45	4.21	.534
16	2.44	4.23	.539
17	2.03	1.62	.404
18	2.25	2.87	.466
19	1.88	1.23	.372
20	1.81	1.17	.35
21	2.8	2.29	.258
22	2.41	.03	.233
23	2.23	-.21	.223
24	2.1	-1.09	.198
25	1.92	-2.49	.17
26	2.09	.43	.18
27	2.12	-.61	.214
28	2.12	-.89	.222
29	2.32	-3.2	.245
30	3.41	.43	.331
31	3.56	11.03	.51
32	3.86	12.7	1.467
33	3.37	10.68	1.109
34	3.72	5.21	.469
35	3.6	3.64	.442
36	3.54	3.35	.443
37	2.96	2.53	.359
38	3.22	2.1	.4
39	2.96	3.74	.319
40	2.92	4.38	.303
41	3.04	-7.91	.227
42	2.71	-9.8	.219
43	1.82	-8.67	.191
44	1.67	-7.48	.176
45	1.38	-3.28	.152
46	1.51	-10.75	.172
47	2.47	-6.21	.182
48	2.59	-4	.187
49	2.91	-1.34	.234
50	3.59	.65	.332
51	4.87	12.31	.495
52	4.44	13.78	1.485
53	4.45	13.74	1.11
54	4.05	5.36	.36
55	3.88	6	.32
56	3.86	5.34	.354
57	4.25	3.87	.262
58	3.83	7.31	.296
59	4.17	-.57	.249
60	3.8	-4.89	.238

AVG R/A = 2.70772 AVG ANG = 1.35938
RMS R/A = 2.85551 RMS ANG = 5.77128
MAX R/A = 4.87814 MAX ANG = 13.7883
STD DEV = .906721 STD DEV = 5.6089

ENERGY WTD AVG ANGLE = 4.58275 DEGREES
ENERGY WTD RMS ANGLE = 7.54658 DEGREES
FRACTION OF RINGS WITH ANGLE GREATER THAN 15 DEG = 0
AUXILIARY REFOCUSING COIL NOT NEEDED

STATISTICAL ANALYSIS OF REFOCUSED TRAJECTORIES

ANALOG COMPUTER TAPE NO. 18
NASA KLYSTRON DESIGN F, FIELD S, PLOT 5-5-72-1

COLLECTOR ENTRANCE LOCATION Z/A = 34.59

AVG R/A = 2.70772	AVG ANG = 1.35938
RMS R/A = 2.85551	RMS ANG = 5.77128
MAX R/A = 4.87814	MAX ANG = 13.7883
STD DEV = .906721	STD DEV = 5.6089

ENERGY WTD AVG ANGLE = 4.52275 DEGREES
ENERGY WTD RMS ANGLE = 7.54658 DEGREES
FRACTION OF RINGS WITH ANGLE GREATER THAN 15 DEG = 0
AUXILIARY REFOCUSING COIL NOT NEEDED

LOWEST ENERGY CLASS
- AVG R/A = 2.31994
- RMS R/A = 2.44434
- AVG ANG =-3.22911 DEGREES
- RMS ANG = 4.73931 DEGREES
- NUMBER OF ELECTRONS = 27

SECOND ENERGY CLASS
- AVG R/A = 2.89137
- RMS R/A = 3.00521
- AVG ANG = 2.77352 DEGREES
- RMS ANG = 3.54137 DEGREES
- NUMBER OF ELECTRONS = 18

THIRD ENERGY CLASS
- AVG R/A = 2.93638
- RMS R/A = 1.47857
- AVG ANG = 6.03521 DEGREES
- RMS ANG = 6.74274 DEGREES
- NUMBER OF ELECTRONS = 10

HIGHEST ENERGY CLASS
- AVG R/A = 3.68329
- RMS R/A = 3.77153
- AVG ANG = 11.6946 DEGREES
- RMS ANG = 11.93 DEGREES
- NUMBER OF ELECTRONS = 5

TAPE NO. 18

STATISTICAL ANALYSIS OF REFOCUSED TRAJECTORIES

ANALOG COMPUTER TAPE NO. 22
NASA LOW EFFICIENCY KLYSTRON, FIELD T, PLOT 5-18-72-1

COLLECTOR ENTRANCE LOCATION Z/A = 35.21

RING	R/A	ANGLE (DEG)	POTENTIAL
1	1.66	.77	.455
2	1.6	.69	.441
3	1.56	.74	.438
4	1.59	.96	.45
5	1.59	.87	.469
6	1.59	.58	.501
7	1.7	.39	.551
8	2.01	.79	.659
9	2.32	1.72	.813
10	2.36	2.86	1.044
11	1.94	2.92	1.327
12	1.75	2.8	1.47
13	1.74	2.6	1.351
14	1.77	2.17	1.123
15	1.76	1.91	.912
16	1.7	1.49	.761
17	1.59	1.12	.655
18	1.54	1.02	.572
19	1.55	.85	.511
20	1.57	.87	.479
21	2.91	.61	.455
22	2.81	.37	.44
23	2.78	.58	.439
24	2.87	1.19	.451
25	2.87	1.22	.467
26	2.8	1.15	.502
27	3	.97	.567
28	3.43	1.53	.67
29	4.49	3.61	.822
30	3.96	4.72	1.058
31	3.35	5.03	1.343
32	3	4.68	1.478
33	3	4.42	1.358
34	3	3.76	1.132
35	2.99	3.25	.917
36	2.93	2.57	.766
37	2.79	2.19	.66
38	2.75	1.76	.575
39	2.78	1.19	.513
40	2.82	.99	.478
41	3.75	-.29	.446
42	3.65	-.14	.43
43	3.63	.07	.427
44	3.72	.56	.442
45	3.6	1.06	.446
46	3.48	1.49	.495
47	3.59	.96	.563
48	4.13	1.47	.668
49	4.85	3.52	.816
50	5.08	5.94	1.062

```
 51              4.38            6.47            1.355
 52              3.96            6.1             1.488
 53              3.82            5.59            1.361
 54              3.91            4.75            1.133
 55              3.88            4.06            .917
 56              3.73            3.24            .767
 57              3.61            2.73            .658
 58              3.61            2.2             .574
 59              3.67            1.37            .51
 60              3.72            .91             .474

AVG R/A = 2.90531               AVG ANG = 2.10498
RMS R/A = 3.05904               RMS ANG = 2.69518
MAX R/A = 5.08462               MAX ANG = 6.47764
STD DEV = .957571               STD DEV = 1.68317

ENERGY WTD AVG ANGLE = 2.7494  DEGREES
ENERGY WTD RMS ANGLE = 3.29959 DEGREES
FRACTION OF RINGS WITH ANGLE GREATER THAN 15 DEG = 0
AUXILIARY REFOCUSING COIL NOT NEEDED


TIME:  00 MINS. 04 SECS.



LIST  500

 STDA       14:15   THURS.  5-18-72

500 DATA 22,5721,60,162.5,650,5931
501 DATA 1082,54,4001,1043,48,3940,1020,51,3929,1039,67,3979
502 DATA 1036,62,4063,1039,43,4198,1106,30,4406,1308,67,4815
503 DATA 1509,161,5346,1536,303,6055,1263,349,6825,1143,352,7183
504 DATA 1135,313,6887,1155,239,6283,1149,189,5661,1110,135,5173
505 DATA 1037,94,4801,1003,80,4485,1014,63,4241,1027,63,4106
506 DATA 1892,43,4001,1829,26,3938,1811,40,3930,1867,83,3983
507 DATA 1866,87,4056,1824,85,4204,1955,76,4466,2233,130,4855
508 DATA 2924,339,5369,2576,503,6081,2180,603,6847,1951,589,7187
509 DATA 1952,533,6892,1954,415,6298,1947,323,5671,1907,233,5187
510 DATA 1819,185,4816,1793,139,4499,1813,89,4249,1835,71,4103
511 DATA 2444,-20,3964,2374,-9,3892,2362,5,3879,2420,39,3947
512 DATA 2341,74,3964,2268,109,4175,2340,75,4451,2689,125,4848
513 DATA 3158,330,5350,3305,633,6081,2851,779,6861,2577,770,7196
514 DATA 2486,675,6888,2543,523,6293,2527,403,5668,2431,294,5189
515 DATA 2352,230,4808,2349,173,4494,2387,102,4237,2421,65,4083
999 END
```

STATISTICAL ANALYSIS OF REFOCUSED TRAJECTORIES

ANALOG COMPUTER TAPE NO. 22
NASA LOW EFFICIENCY KLYSTRON, FIELD T, PLOT 5-18-72-1

COLLECTOR ENTRANCE LOCATION Z/A = 35.21

AVG R/A = 2.90531	AVG ANG = 2.10498
RMS R/A = 3.05904	RMS ANG = 2.69518
MAX R/A = 5.08462	MAX ANG = 6.47764
STD DEV = .957571	STD DEV = 1.68317

ENERGY WTD AVG ANGLE = 2.7494 DEGREES
ENERGY WTD RMS ANGLE = 3.29959 DEGREES
FRACTION OF RINGS WITH ANGLE GREATER THAN 15 DEG = 0
AUXILIARY REFOCUSING COIL NOT NEEDED

LOWEST ENERGY CLASS
AVG R/A = 2.69577
RMS R/A = 2.82625
AVG ANG = .783111 DEGREES
RMS ANG = .896225 DEGREES
NUMBER OF ELECTRONS = 24

SECOND ENERGY CLASS
AVG R/A = 2.90489
RMS R/A = 3.05722
AVG ANG = 1.75054 DEGREES
RMS ANG = 1.94994 DEGREES
NUMBER OF ELECTRONS = 17

THIRD ENERGY CLASS
AVG R/A = 3.32554
RMS R/A = 2.82308
AVG ANG = 3.70872 DEGREES
RMS ANG = 3.88957 DEGREES
NUMBER OF ELECTRONS = 10

HIGHEST ENERGY CLASS
AVG R/A = 2.99795
RMS R/A = 3.14072
AVG ANG = 4.5175 DEGREES
RMS ANG = 4.72154 DEGREES
NUMBER OF ELECTRONS = 9

TAPE NO. 22

SYMBOLS

a	Tunnel radius
B_1	Main collimating magnetic field amplitude
B_2	Beam stabilization (plateau) field amplitude
B_r	Radial component of magnetic field
B_z	Axial component of magnetic field
B_θ	Azimuthal component of magnetic field
c	Velocity of light
e	Electron charge
E_r	Radial component of cavity gap electric field
E_z	Axial component of cavity gap electric field
f	Signal frequency
H	Magnetic excitation amplitude
I_o	DC beam current
I_1	Fundamental rf current amplitude
J	Number of electron rings per disk
J_o	Interaction gap length
ℓ	Interaction gap length
L_1	Length of beam expansion region
L_2	Length of beam stabilization region (plateau)
m	Electron rest mass
N	Number of electron disks per beam wavelength λ_e
Q	Cavity selectivity parameter $f/\Delta f$
Q_R	Charge associated with electron ring, $-2\pi I_o/JN\omega$
R	1) Cavity shunt impedance
	2) Normalized ring radius r/a
R_c	Normalized radius of electron ring at cathode
u_o	DC beam electron velocity
V_o	Electron beam voltage
$\bar{z}$	Average z component of velocity of spent-beam electrons

SYMBOLS (Continued)

β	Axial propagation constant ω/u_o
γ	Radial propagation constant $\beta\sqrt{1 - (u_o/c)^2}$
Δf	Bandwidth
ϵ_o	Vacuum permittivity
η	Klystron electronic conversion efficiency
θ	1) Transit angle
	2) Azimuthal angle in cylindrical coordinate system
	3) Electron trajectory angle with respect to axis
λ_c	Cyclotron wavelength $2\pi u_o/\omega_c$
λ_{c1}	Spent-beam cyclotron wavelength $2\pi m\bar{\dot{z}}/eB_1$
λ_{c2}	Plateau cyclotron wavelength $2\pi m\bar{\dot{z}}/eB_2$
λ_e	Electron beam wavelength u_o/f
λ_q	Plasma wavelength $2\pi u_o/\omega_q$
μ_o	Vacuum permeability
$\sigma_{\dot{z}/u_o}$	Standard deviation of spent-beam electron velocities
σ_θ	Standard deviation of electron trajectory angles
ω	Angular frequency $2\pi f$
ω_c	Cyclotron frequency eB/m
Ω_c	Normalized cyclotron frequency ω_c/ω
ω_p	Plasma frequency $(eJ_o/m\epsilon_o u_o)^{\frac{1}{2}}$
ω_q/ω_p	Plasma frequency reduction factor
Ω_r	Normalized radial magnetic field $eB_r/m\omega$
Ω_s	Normalized ring spin velocity $\dot{\theta}/\omega$
Ω_z	Normalized axial magnetic field $eB_z/m\omega$

REFERENCES

1. Mihran, T. G., and Neugebauer, W., "Analytic Study of a Depressed Collector for Linear Beam Microwave Amplifiers", NASA Document CR-72768, July 8, 1970

2. Neugebauer, W., and Mihran, T. G., "Multistage Depressed Electrostatic Collector for Magnetically Focused Space Borne Klystrons", NASA Document CR-72767, Sept. 14, 1970

3. Kosmahl, H. G., "A Novel Axisymmetric Collector for Linear Beam Microwave Tubes", NASA Document TND-6093, February 1971

4. Branch, G. M., and Mihran, T. G., "Analytical Designs of a Space-Borne Magnetically-Focused Klystron Amplifier", NASA Document CR-72461, October 25, 1968

5. Kosmahl, H. G., private communication

6. Smythe, W. R., "Static and Dynamic Electricity", McGraw-Hill, New York, p. 288, 1950

7. Pierce, J. R., "Theory and Design of Electron Beams", D. van Nostrand Co., New York, p. 36, 1954

8. Rawls, J. L., Ashley, J. R., and Kilb, W. P., "PPM Focusing of Convergent Beams Emerging from Partially Shielded Cathodes", IEEE Trans. ED-14, pp. 301-305, June 1967

9. Smythe, W. R., " Static and Dynamic Electricity", McGraw-Hill, New York, p. 175, 1939

10. Abramowitz, M., and Stegun, I. (eds) "Handbook of Mathematical Functions", National Bureau of Standards, Washington, D. C., pp. 591, 592, 1970

FINAL REPORT
MAILING LIST

		Copies
1.	National Aeronautics & Space Administration Headquarters Washington, D.C. 20546	
	Attn: ED/L. Jaffe	1
	ECC/A. M. G. Andrus	10
	EC/R. B. Marsten	1
2.	NASA-Lewis Research Center 21000 Brookpark Road Cleveland, Ohio 44135	
	Attn: H. W. Plohr (MS 54-1)	1
	R. E. Alexovich (MS 54-5)	1
	Dr. H. G. Kosmahl (MS 54-5)	1
	Tech. Utilization Officer (MS 3-19)	1
	Contract Section B (MS 500-313)	1
	Library (MS 60-3)	2
	Report Control Office (MS 5-5)	1
	N. T. Musial (MS 300-311)	1
	G. J. Chomos (MS 54-5)	50
3.	Communication Systems Inc. 5817 Columbia Pike Falls Church, Virginia 22046	
	Attn: J. Bisaga	1
4.	Rand Corporation 1700 Main Street Santa Monica, California 90404	
	Attn: Dr. J. Holt	1
5.	NASA-George C. Marshall Space Flight Center Huntsville, Alabama 35812	
	Attn: RASTR-A/E. C. Hamilton	1
	Library	1
6.	NASA-Goddard Space Flight Center Greenbelt, Maryland 20771	
	Attn: 733/R. Pickard	1
	Library	1

Copies

7. NASA-Ames Research Center
Moffett Field, California 94035

Attn: OART-MAO/E. Van Vleck (MS 202-6) 1
Library 1

8. NASA-Langley Research Center
Langley Station
Hampton, Virginia 23365

Attn: B. Kendall (MS-173) 1
Library (MS-185) 1

9. NASA-Manned Spacecraft Center
Houston, Texas 77001

Attn: Library 1

10. Jet Propulsion Laboratory
4800 Oak Grove Drive
Pasadena, California 91103

Attn: L. Derr 1
Library 1

11. NASA Scientific and Technical Information Facility
P.O. Box 33
College Park, Maryland 20740

Attn: NASA Representative 3

12. TRW Systems
One Space Park
Redondo Beach, California 90278

Attn: W.A. Finley/Space Vehicle Division 1
Alfred P. Fay 1

13. General Dynamics, Convair Division
P.O. Box 1128
San Diego, California 92112

Attn: F.J. Dore/Advanced Programs Laboratory 1

Copies

14. Hughes Aircraft Company
Space Systems Division
1194 W. Jefferson Boulevard
Culver City, California 90230

Attn: H. A. Rosen/Satellite Systems Laboratory 1

15. General Electric Company
Missile and Space Division
Valley Forge Space Technology Center
P. O. Box 8555
Philadelphia, Pennsylvania 19101

Attn: H. Collins 1
P. Nadler 1

16. Federal Communications Commission
521 12th Street
Washington, D. C. 20554

Attn: H. Fine 1

17. U. S. Information Agency
25M St. S. W.
Washington, D. C. 20547

Attn: IBS/EF/G. Jacobs 1

18. General Electric Company
Tube Department
Microwave Tube Operation
Schenectady, New York 12305

Attn: R. Dehn 1
Dr. T. Mihran 1
Dr. G. Branch 1
W. Neugebauer 1

19. Litton Industries
Electron Tube Division
960 Industrial Road
San Carlos, California 94070

Attn: Dr. G. Pokorney 1
J. Orr 1
W. Day 1
Dr. O. Sauseng 1
R. Cerko 1
B. D. McNary 1

Copies

20. Varian
Eastern Tube Division
Salem Road
Beverley, Massachusetts 01915

Attn: Dr. G. Farney 1

21. Hughes Aircraft Company
Electron Dynamics Division
P. O. Box 2999
Torrance, California 90509

Attn: Dr. J. Mendel 1
Dr. I. Tammaru 1
J. A. Christensen 1

22. Watkins Johnson Company
3333 Hillview Avenue
Palo Alto, California 94304

Attn: R. Espinosa 1

23. Varian Associates
611 Hansen Way
Palo Alto, California 94303

Attn: Dr. G. Caryotakis 1
Dr. J. Reutz 1
Dr. W. Ayers 1
Dr. W. Harmon 1

24. RCA
Industrial Tube Division
Lancaster, Pennsylvania

Attn: W. P. Bennett 1

25. Raytheon Company
Research Division
28 Seyon Street
Waltham, Massachusetts

Attn: W. Teich 1
Dr. J. M. Osepchuk 1

26. Mr. Lawrence Gasch 1
Aerospace Radar Branch
U. S. NRL
Washington, D. C. 20390

Copies

27. Mr. Robert Richardson — 1
Mail No. 1620
Martin-Marietta Corp.
Denver Division
P. O. Box 179
Denver, Colorado 90201

28. Mr. William E. Waters — 1
Sr. Engr. Staff Specialist
Philco Ford Corporation
3939 Fabian Way
MS C-70
Palo Alto, California 94303

29. Mr. George Orr — 1
Code 733
Goddard Space Flight Center
Greenbelt, Maryland 20771

30. Sperry
Electronic Tube Division
Gainesville, Florida 32601

Attn: H. H. Conners — 1

31. Lt. Commander L. Wardel — 1
Naval Electronic Systems Command
PME 116
Washington, D. C. 20360

32. Commanding Officer
Navy Space Systems Activity
Air Force Unit Post Office
Los Angeles, California 90045

Attn: Code 50 — 1

33. U. S. Air Force Liaison Officer (MS 501-3) — 1
c/o NASA-Lewis Research Center
21000 Brookpark Road
Cleveland, Ohio 44135

34. Department of the Air Force
Headquarters Aeronautical Systems Div. (AFSC)
Directorate of Avionics
Wright-Patterson Air Force Base, Ohio 45433

Attn: J. H. Sproule, Chief — 1
Analysis & Simulation Branch